Non-perturbative renormalization group beyond melonic sector

The Effective Vertex Expansion method for group fields theories

Vincent Lahoche[a1] and Dine Ousmane Samary[a,b2]

a) Commissariat à l'Énergie Atomique (CEA, LIST), 8 Avenue de la Vauve, 91120 Palaiseau, France

b) Faculté des Sciences et Techniques (ICMPA-UNESCO Chair), Université d'Abomey-Calavi, 072 BP 50, Benin

arXiv:1809.00247v2 [hep-th] 5 Sep 2018

Abstract

Tensor models admit the large N limit dominated by the graphs called melons. The melons are caracterized by the Gurau number $\varpi = 0$ and the amplitude of the Feynman graphs are proportional to $N^{-\varpi}$. Other leading order contributions i.e. $\varpi > 0$ called pseudo-melons can be taken into account in the renormalization program. The following paper deals with the renormalization group for a $U(1)$-tensorial group field theory model taking into account these two sectors (melon and pseudo-melon). It generalizes a recent work [arXiv:1803.09902], in which only the melonic sector have been studied. Using the power counting theorem the divergent graphs of the model are identified. Also, the effective vertex expansion is used to generate in detail the combinatorial analysis of these two leading order sectors. We obtained the structure equations, that help to improve the truncation in the Wetterich equation. The set of Ward-Takahashi identities is derived and their compactibility along the flow provides a non-trivial constraints in the approximation shemes. In the symmetric phase the Wetterich flow equation is given and the numerical solution is studied.

[1]vincent.lahoche@cea.fr

[2]dine.ousmanesamary@cipma.uac.bj

Contents

1 Introduction **2**

2 Flowing on tensorial group field theory space **5**

3 Melonic and pseudo-melonic sectors **11**
3.1 Renormalizable sectors 11
3.2 Pseudo-melonic sector 19

4 EVE for a mixing tensorial theory space **24**
4.1 Mixing melons and pseudo-melons 25
4.1.1 The quartic sector 26
4.1.2 Full non-branching sector 29
4.2 Structure equations for effective vertices 30
4.2.1 Two and four point effective vertices 30
4.2.2 Six and eight point effective vertices 43

5 Flow equations and their fixed points **53**
5.1 Flow for local couplings 53
5.2 Anomalous dimension 58
5.3 Investigations on the phase space structure 71
5.3.1 Vicinity of the non-Gaussian fixed point 71
5.3.2 Non Gaussian fixed points 73

6 Conclusion **74**

Appendices **74**

A Useful formulas **74**

B ϕ^6-truncation for mixing -$U(1)$ TGFT **76**
B.1 Truncation procedure 77
B.2 Fixed points in the UV regime 79

1 Introduction

The consistent formulation of the quantum theory of gravity (QG) is one of the fundamental and tedious problem of modern physics, which remains unsolved, and must probably intertwines between quantum mechanics (QM) and general relativity (GR). Its have evolved a lot since the last two decades due to the appearance of new background independent approaches such as loop quantum gravity, dynamical triangulations, noncommutative geometry (see [1]-[8] and references therein). Recently, tensors models (TMs) and group field theories (GFTs) are developed as new way to investigate this conundrum question [9]-[28]. TMs generalize matrix models and are considered as a convenient formalism for

studying random geometry in dimensions $D \geq 3$. Its provide a well-defined framework for addressing QG in higher dimensions and its cortege of consequences on integrable systems [19]. GFTs are quantum field theories over the group manifolds and are considered as a second quantization of loop quantum gravity [16]. GFT is characterised by a specific form of non-locality in their interactions, with the basis variable being a complex field, function of d-group elements [9], [27]. Recently TMs and GFTs are merged to provide the so called tensorial group field theory (TGFT) [29]-[58]. It can also be viewed as a new proposal for quantum field theories based on a Feynman path integral, which generates random graphs describing simplicial pseudo manifolds. It aims at providing a content to a phase transition called geometrogenesis scenario by relating a discrete quantum pregeometric phase of our spacetime to the classical continuum limit consistent with Einstein GR [44]-[46]. In short, within this approach, our spacetime and its geometry has to be reconstructed or must emerge from more fundamental and discrete degrees of freedom. Its very encouraging features such as renormalization of large class of models and asymptotic freedom on the one hand [47]-[50], and a coexistence with a Wilson-Fisher fixed point, on the other hand [51]-[57], ensure not only the quantum consistency at macroscopic scales but also, the possible existence of the condensate phase [67].

The renormalization of TGFT models started with the work given in [37]-[38]. The multiscale analysis and power counting theorem are used to prove that the $U(1)$- tensor models in three and four dimensions are just renormalizable. Very quickly several other interesting models is studied and have proved to be just and super renormalizable [29]-[43]. The classification of the renormalizable TGFT models framework are also investigated [32]. The computation of the β-functions to prove the asymptotic freedom and safety is also given [47]-[50]. Very recently the functional renormalization group (FRG) method is introduced in the context of TGFT and allowed to solve the flow equations of these various models [51]-[57]. The occurence of non-perturbative fixed points and their critical behavior in the UV and IR is studied. The confirmation of the asymptotic freedom and safety are also given. The FRG for TGFT [54] derived from the method using in the case of matrix models [69]-[78] can be simply applied when the dimension of tensors is not very high ($d = 3, d = 4, d = 5$). In the case where $d \geq 6$ due to the combinatoric, other technical methods require to be proposed. In [53] this question is solved and turned on a new way for investigating the FRG to higher dimensions tensors models [56]-[58]. FRG can be roughly described as a flow in a certain infinite dimensional functional space for actions, the theory space. The scale plays the role of time for this flow. Its allows the construction of a set of effective action Γ_s, $-\infty \leq s \leq +\infty$, which interpolate between the classical action S and the full effective action Γ such that this full effective action is obtained for the value $s = -\infty$ [70]. Γ is also called the generating functional of one-particle irreducible vertices. At the same time when s walks $\mathbb{R}$ the flow equations enable us to interpolate smoothly between the UV laws and the IR phenomena for our systems. The flow equations is describe by the Weterich equation in which the choice of IR regulator and the full effective action remain the only condition to provide solutions and probably maybe help to derive the fixed points.

The Feynman graphs of TM can be organized as a serie in $1/N$ and therefore the class of combinatorial objects can be selected. In the large N limit the dominant graphs are called melon [24]-[25]. This limit allows us to understand the statistical physics properties

such as continuum limits, phase transitions and critical exponents. Taking into account the Gurau $1/N$- expansion the amplitudes of the Feynman graphs are proportional to $N^{-\varpi}$, (ϖ is the Gurau degree), and the melonic contributions are caracterized by $\varpi = 0$. However, it might be possible to consider the non-melonic leading order contributions $\varpi \neq 0$, which we call in this work the pseudo-melonic graphs. The canonical dimension of the melons and the pseudo-melons is identified for the n-point graphes. The new leading order contributions (the pseudo-melons) modify dractically the power counting theorem and the renormalization properties of the class of models studied in this direction. In the non-perturbative analysis of the TGFT with melonic and pseudo-melonic graphs the FRG should be carefully use. There are several reason to consider the mixing melon and pseudo-melon see [65]-[66] for more explanation. The combinatorial analysis of these two sectors generated an intermediate sector between melon and pseudo-melon and should be taking into account in the renormalization program. This point will be discussed in detail throughout this work.

Recently one new breakthrough is done in the context of FRG of TGFT models, to improve the truncation and to choose the regulator in the appropriate way [59]. This is possible by adding in the Wetterich equation, the so called structure equations and the Ward-Takahashi identities. In the case of symmetric phase a nontrivial UV attractive fixed point is given. The WT identities is used to defined the nontrivial constraint on the flows and therefore the method proposed in [59] is totally different from the usual FRG method. Despite all the results in this recent contribution, a lot of questions need to be addressed. First the non-melonic Leading order contribution should been taken into account in the flow equations. The non–symmetric phase need also to be scrutinize using probably the intermediate field representation. The purpose of the following work is to provide the FRG by taking into account the leading order contribution (the melonic and pseudo-melonic graphs) in the flow equations. The new power counting theorem is derived and the classification of the graphs that contribute to these two sectors is given. The structure equations and the set of WT-identities are used to provide a nontrivial constraint on the reliability of the approximation schemes, especially on the truncation and the choice of the regulator. The comparisons between these new results and what we obtain in the case of usually truncation is also given.

The paper is organized as follows: In section (2) we provide the usefull definitions and notations, which will be used throughout the paper. Particularly we give the definition of our model and its symmetries, and then introduced the FRG method by giving the Wetterich equation. In section (3) the effective vertex expansion is studied. We identified the renormalization sector by using the power counting theorem. We also computed the canonical dimension of the n-point Feynman graphs that contribute to melons and pseudo-melons independently. In section (4) The same analysis as the previous section is given by mixing these two sectors. By contracting the elementary melon we generate the familly of six point vertices in which we considered only the non-branching sector. We identified one new leading order contribution that we called intermediate sector. The structure equations for melons pseudo-melons and intermediate graphs are also given carefully. Section (5) is devoted to the FRG analysis of the model using not only the structure equations but also the set of WT-identities as non-trivial constraints in the approximation shemes. The phase diagrams around the fixed points are also built and examinated. We then provide

discussion between our method and what we obtained in the case of ordinary truncation. In section (6) discussions and conclusion of our work is given. The set of two appendices is given. In appendix (A) the computation of the useful formulas concerning convergent sums that we used in the core of this paper are given. In appendix (B) the usual FRG analysis for a model is given. chosen the truncation in appropriate way and the regulator the flow of the couplings and mass are given. The proof of the asymtotically safety is also scrutinized.

2 Flowing on tensorial group field theory space

A tensorial group field theory (TGFT) is a field theory defined on a direct product of group manifolds. In this paper we focus on an Abelian group field theory, defined on d-copies of the unitary group $U(1)$ isomorphic to the complex numbers of module 1. We consider a pair of fields, say ϕ and $\bar{\phi}$ on $U(1)^d$

$$\phi, \bar{\phi} : U(1)^d \to \mathbb{C}\,. \tag{1}$$

The dynamics of the TGFT model is governed by the *classical action* $S(\phi, \bar{\phi})$ chosen to be of the form

$$S(\phi, \bar{\phi}) = \int d\mathbf{g}\, \bar{\phi}(\mathbf{g})(-\Delta_{\mathbf{g}} + m^2)\phi(\mathbf{g}) + S_{\rm int}(\phi, \bar{\phi})\,, \tag{2}$$

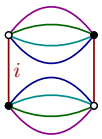
where $\Delta_{\mathbf{g}}$ denotes the Laplace–Beltrami operator on the torus $U(1)^d$ and $\mathbf{g} := (g_1, \cdots, g_d) \in U(1)^d$. For a tensorial theory, the interaction S_{int} is a sum of *connected tensorial invariants* $S_{\rm int}(\phi, \bar{\phi}) = \sum_n \mathcal{V}_n(\phi, \bar{\phi})$ made with an equal number n of fields ϕ and $\bar{\phi}$, whose arguments are identified and summed only between ϕ and $\bar{\phi}$. A generic interaction term in $\mathcal{V}_n$ is then of the form:

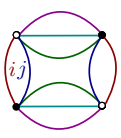
$$\upsilon_h(\phi, \bar{\phi}) = \lambda_h \int \prod_{p=1}^{n} d\mathbf{g}_p\, d\bar{\mathbf{g}}_p \prod_{p=1}^{n} \phi(\mathbf{g}_p)\bar{\phi}(\bar{\mathbf{g}}_p) \prod_{p=1}^{n}\prod_{i=1}^{d} \delta(g_{ip} - \bar{g}_{ih_i(p)})\,, \tag{3}$$

where δ denotes the Dirac delta distribution over $U(1)$ and λ_h denotes the *coupling constant*. The interaction as well as the coupling are indexed with a set of maps $h := \{h_i\,, i = 1, \cdots, d\}$ such that for any $p \in [\![1, n]\!]$; $h_i(p) \in [\![1, n]\!]$. We can then associate black and white nodes respectively for fields ϕ and $\bar{\phi}$, and a link between black and white nodes for each delta, labeled by a color index running from 1 to d. As a result, each interaction can be then labeled from an unique *colored bipartite regular graph* rather than with the map h; and $\mathcal{V}_n$ may be decomposed as a sum of terms indexed with such a graphs γ_n with n white nodes:

$$\mathcal{V}_n(\phi, \bar{\phi}) = \sum_{\gamma_n} \upsilon_{\gamma_n}(\phi, \bar{\phi})\,. \tag{4}$$

For the rest of this paper, we call *valence* the integer n. Such graphs are called *tensorial invariants bubbles*, or simply *bubbles*. As an example, for $n = 4$ and $d = 5$ we get:

$$\mathcal{V}_4(\phi, \bar{\phi}) = \sum_{i=1}^{d} \lambda_{4,i}$$ 

$$+ \sum_{j<i}^{d} \lambda_{4,ij}$$ 

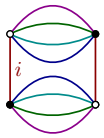
$$\,, \tag{5}$$

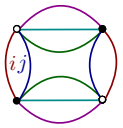
where each color on the graphs corresponds to one of the integer of the set $[\![1, d]\!]$, and $\lambda_{4,i}$, $\lambda_{4,ij}$ denote coupling constants. Note that in this representation we identified the diagram with the interaction itself. For convenience, in the rest of this paper, we do not work on $U(1)^d$ but on its Fourier dual space $\mathbb{Z}^d$. Fixing the group representation, any element $g \in U(1)$ can be uniquely represented as a complex number of module 1: $g = e^{i\theta}$ with $\theta \in [0, 2\pi[$. The fields can then be viewed as functions over the complex unit circle, depending on d–angular coordinates $\phi(\theta_1, \cdots, \theta_d)$ and $\bar{\phi}(\theta_1, \cdots, \theta_d)$, so that their Fourier decomposition writes as

$$\phi(\theta_1, \cdots, \theta_d) = \sum_{\vec{p} \in \mathbb{Z}^d} T_{\vec{p}}\, e^{i \sum_{j=1}^d \theta_j p_j}\,, \quad \bar{\phi}(\theta_1, \cdots, \theta_d) = \sum_{\vec{p} \in \mathbb{Z}^d} \bar{T}_{\vec{p}}\, e^{-i \sum_{j=1}^d \theta_j p_j}\,. \tag{6}$$

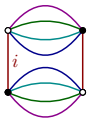
T and $\bar{T}$ are maps from $\mathbb{Z}^d$ to $\mathbb{C}$. They are *d-tensors* with infinite size. In Fourier components, the classical action (2) becomes, for $d = 5$:

$$S(T, \bar{T}) = \sum_{\vec{p}} \bar{T}_{\vec{p}}\,(\vec{p}^{\,2} + m^2)\,T_{\vec{p}} + \lambda_{4,1} \sum_{i=1}^{d} \quad + \lambda_{4,2} \sum_{j<i}^{d} \quad + \cdots\,, \tag{7}$$

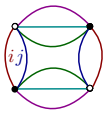




where we have chosen the same coupling for the two sets of interactions pictured above. In Fourier space, the Dirac delta occurring in the interactions like in (3) become discrete Kronecker delta. Because their explicit expressions shall be useful in the next sections, we give the decomposition of the following two diagrams:



$$=: \sum_{\{\vec{p}_i\}} \mathcal{V}^{(4,1)\,i}_{\vec{p}_1,\vec{p}_2,\vec{p}_3,\vec{p}_4} T_{\vec{p}_1} \bar{T}_{\vec{p}_2} T_{\vec{p}_3} \bar{T}_{\vec{p}_4}\,,$$



$$=: \sum_{\{\vec{p}_i\}} \mathcal{V}^{(4,2)\,ij}_{\vec{p}_1,\vec{p}_2,\vec{p}_3,\vec{p}_4} T_{\vec{p}_1} \bar{T}_{\vec{p}_2} T_{\vec{p}_3} \bar{T}_{\vec{p}_4}\,, \tag{8}$$

where:

$$\mathcal{V}^{(4,1)\,i}_{\vec{p}_1,\vec{p}_2,\vec{p}_3,\vec{p}_4} = \delta_{p_{1i} p_{4i}} \delta_{p_{2i} p_{3i}} \prod_{j \neq i} \delta_{p_{1j} p_{2j}} \delta_{p_{3j} p_{4j}}\,, \tag{9}$$

and:

$$\mathcal{V}^{(4,2)\,ij}_{\vec{p}_1,\vec{p}_2,\vec{p}_3,\vec{p}_4} = \prod_{l=i,j} \delta_{p_{1l} p_{4l}} \delta_{p_{2l} p_{3l}} \prod_{k \neq i,j} \delta_{p_{1k} p_{2k}} \delta_{p_{3k} p_{4k}}\,. \tag{10}$$

In the literature, the first diagrams are known as *melonics*. For our purpose, we then denote as *pseudo-melonics* the second ones with two weak edges rather than one. Because of their importance in the rest of this paper, we will denote by $\mathfrak{B}_i$ the 4-valent melonic diagrams and $\mathfrak{B}_{ij}$ the 4-valent pseudo-melonic ones. The indices i and ij referring to the *weak edges* in both cases.

Among their properties, the tensorial interactions have revealed a new and non-trivial notion of locality, said *traciality*, which is the only one appropriate to deals with non-local structure of the interactions over the group manifold. In particular, traciality allowed to renormalize the quantum field theory version of these classical theory, and it plays an important role in the building of their *renormalization group flow* [30]. Without additional gauge invariance like *closure constraint*, traciality reduce to tensoriality [39]. Then we retain the following definition:

Definition 1 *A connected tensorial invariant bubble interaction is said to be local. In the same footing, any interacting action expanded as a sum of such diagrams is said to be local.*

The quantum theory is then defined from the partition function[3]:

$$Z(J,\bar{J}) = \int dT d\bar{T}\, e^{-S(T,\bar{T})+J\bar{T}+\bar{J}T}\,, \tag{11}$$

where dT (resp. $d\bar{T}$) is the standard Lebesgue measure for path integration and $J\bar{T} := \sum_{\vec{p}} J_{\vec{p}}\bar{T}_{\vec{p}}$. Because of the ultraviolet (UV) divergences, we introduce a regularization which suppress the high momenta contributions. There are different choices of regularization functions. The most common for renormalization are Schwinger and sharp regularizations. For our purpose, it is suitable to consider the sharp regularization, such that the UV regularized free 2-point functions is:

$$C_\Lambda(\vec{p},\vec{p}\,') := \frac{\Theta(\Lambda^2-\vec{p}^{\,2})}{\vec{p}^{\,2}+m^2}\,\delta_{\vec{p}\vec{p}\,'}\,. \tag{12}$$

where Θ is the Heaviside step function. The presence of the Laplacian propagator in the classical action (2) generates a canonical notion of *scale* over the Feynman graphs. For TGFTs, these graphs are dual to simplicial topological manifold, and then generate discretization of topologial spaces from the pertubrative expansion itself. An example of such a Feynman graph is given in Figure (1), the dotted edges being Wick contractions between T and $\bar{T}$ fields. We conventionally attribute the color 0 to these edges.

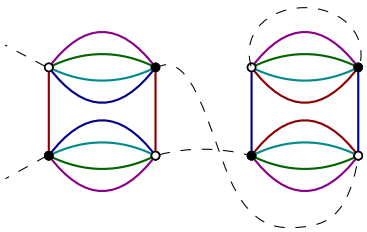


Figure 1: A typical Feynman graph contributing to the perturbative expansion of the connected 2-point functions. The dotted edges correspond to free propagator contractions between pair of fields.

An important notion for tensorial Feynman diagrams is the notion of *faces*, whose we recall in the following definition:

Definition 2 *A face is defined as a maximal and bicolored connected subset of lines, necessarily including the color 0. We distinguish two cases:*

- *The closed or internal faces, when the bicolored connected set correspond to a cycle.*

[3]Strictly speaking the term "quantum" is abusive, we should talk about statistical model, or quantum field theory in the euclidean time.

- *The open or external faces when the bicolored connected set does not close as a cycle.*

The boundary of a given face is then the subset of its dotted edges, and its length is defined as the number of internal dotted edges on its boundary.

To complete this definition, we provide what we call internal/external edges and interior/boundary vertices:

Definition 3 *On a given Feynman graph, the set of edges split into internal and external edges. External edges come from the Wick contraction with external fields and internal edges come from the Wick contractions between vertex fields. Moreover, a vertex is said to be a boundary vertex if at least one of the external edges is hooked to him. It is an interior vertex otherwise. Finally, we define the interior of a Feynman diagram as the set of internal vertices with dotted edges.*

The quantum fluctuation can then be integrated out from higher to lower scales, generating a sequence of effective theories which describes a curve into the theory space. Along the trajectories, all the coupling constant move from their initial definition, their running describing the *renormalization group flow*. The FRG is a specific method to build such a running, well adapted to the TGFT context. To parametrize the flow, we then introduce a real parameter $s \in]-\infty, +\infty[$ and a one parameter family of models Z_s such that:

$$Z_s[J, \bar{J}] := \int dT d\bar{T}\, e^{-S(T,\bar{T})-R_s(T,\bar{T})+\bar{J}T+\bar{T}J}\,. \tag{13}$$

The regulator term $R_s(T, \bar{T})$ depends on the running scale $k = e^s$ such that $\Lambda \geq k \geq 0$, and introduce a dynamical splitting into high and low scales. It act as a mass term which decouples the low scales contributions from long distance physics, allowing to build an effective action Γ_s for long distance observable, such that higher scales fluctuation have been integrated out and the coupling constants moved from their initial values to their effective values at the given scale k.

To make this more concrete, the regulator is chosen of the form [70]-[72].

$$R_s(T, \bar{T}) = \sum_{\vec{p}\in\mathbb{Z}^d} r_s(\vec{p}^{\,2})\bar{T}_{\vec{p}}\, T_{\vec{p}}\,, \tag{14}$$

so that the *regulator function* $r_s(\vec{p})$ may be suitably introduced in the kinetic part of the action, providing us the effective Gaussian propagator :

$$C_s(\vec{p}^{\,2}) = \frac{1}{\vec{p}^{\,2} + m^2 + r_s(\vec{p}^{\,2})}\,, \tag{15}$$

where we assumed $\Lambda \gg k$ so that the UV regulator disappears. The regulator function satisfy some properties ensuring that fluctuations are well integrated, among them (see [80] for more details):

- $r_s \geq 0$,

- $\lim_{s\to-\infty} r_s = 0$,
- $\lim_{s\to\infty} r_s = \infty$.

The last condition ensures that the initial conditions are those imposed by the classical action itself. Moreover, the second condition ensures that all the fluctuations are integrated out in the deep infrared (IR). The first condition finally protect the flow from singularities. Note that UV and IR correspond respectively to the ending points of the domain of s: $k = \infty$ in the UV sector and $k = 0$ in the IR. The central object in the FRG approach is the *averaged action* Γ_s, defined as the (slightly modified) Legendre transform of the free energy $W_s := \ln(Z_s)$:

$$\Gamma_s[M, \bar{M}] + R_s[M, \bar{M}] = \bar{J}M + \bar{M}J - W_s[J, \bar{J}] \,, \tag{16}$$

where M (resp. $\bar{M}$) is the means field:

$$M := \frac{\partial W_s}{\partial \bar{J}} \qquad \left(\text{resp. } \bar{M} = \frac{\partial W_s}{\partial J}\right) . \tag{17}$$

The presence of the regulator on the left hand side ensure the following initial conditions holds:

$$\Gamma_{s=-\infty} = \Gamma \,, \qquad \Gamma_{s=+\infty} = S \,, \tag{18}$$

where S is the classical action and Γ the full effective action for $r_s = 0$. The renormalization group flow is then described from an order one non-linear differential equation for Γ_s [73]:

$$\dot{\Gamma}_s = \sum_{\vec{p}} \dot{r}_s(\vec{p}^{\,2}) G_s(\vec{p}, \vec{p}) \,, \tag{19}$$

where the dot designates the derivative with respect to s i.e. $\dot{\Gamma}_s := \frac{\partial \Gamma_s}{\partial s}$ and

$$G_s^{-1} := \frac{\partial^2 \Gamma_s}{\partial M \partial \bar{M}} + r_s =: \Gamma_s^{(2)} + r_s \,, \tag{20}$$

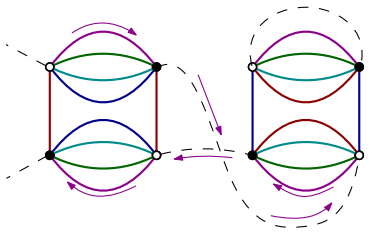
is the effective 2-point function. Moreover, the regulator is chosen such that only a finite windows of momenta contributes to the sum, ensuring that it is finite both in UV and IR. This equation is both simple and complicated. Simple, because it is of order one with respect to the flow parameter s. Moreover, it only involves a single effective loop rather than a multi-loop expansion as in standard Wilson-Polchinski approach, and is then well adapted to non-perturbative considerations. However, this equation is also highly non-linear, and except for very special cases, it is impossible to solve it exactly. Extracting from it a non-perturbative information on the renormalization group fow then requires approximations. The most popular for TGFT are truncations [51]-[57]. With this method, the flow in the full theory space is projected into a reduced dimensional subspace. Another method, already considered in [59] and that we will use in this paper may be called *effective vertex method*. Taking successive derivatives of Γ_s in flow equation (19), we then get an infinite hierarchical system, expressing $\dot{\Gamma}_s^{(n)}$ in terms of $\Gamma_s^{(n+2)}$ and $\Gamma_s^{(n+1)}$. The effective vertex method stop the infinite hierarchical tower of equation expressing $\Gamma_s^{(n+2)}$ and $\Gamma_s^{(n+1)}$

in terms of derivatives up to a certain n, so that the system of equation becomes closed. The importance of this new method comes from the fact that we keep the full momentum dependence on the effective vertex. We will compare the two methods in the last section, and point out the new behavior coming from the full momentum dependence.

Now let us give an important aspect about the construction of the flow and the difference between symmetric and non-symmetric phases. Usually, these terms refers to the value of the mean field M. For $M = 0$, the model is said to be in the symmetric phase. Otherwise the model is said to be in the non-symmetric phase. For tensorial group field theories, we adopt another definition, already considered in [59]:

Definition 4 ***Symmetric and non-symmetric phases*** *As long as the effective two-points function G_s remains diagonal: $G_s(\vec{p}, \vec{q}) \propto \delta_{\vec{p}\vec{q}}$, the theory is said to be in the symmetric or perturbative phase. If this is not the case the theory is said to be in the non-symmetric or non-perturbative regime.*

This definition comes from the fact that in a perturbative regime, all the 1PI correlations functions of the form $\Gamma_s^{(2n+1)}$ vanishes. Moreover, the conservation of the external momenta running along the boundaries of the external faces ensure the presence of a global conservation Kronecker delta $\delta_{\vec{p}\vec{q}}$. For instance, let us consider the violet external face on the Feynman graph given on Figure (1):

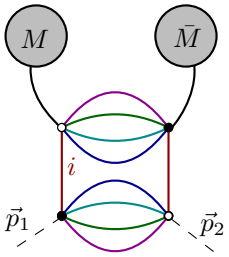


. (21)

The path of the boundary of the violet face in equation (21) is indicated with arrow. Each propagator share a Kronecker delta, as well as each colored edge. Then, the momentum is already conserved along the path. The same property is true for all colors. Now, let us consider $\Gamma^{(2)}_{s;\vec{p}\vec{q}}(M, \bar{M})$ for a non vanishing means fields. Expanding it in power of these fields, we get:

$$\Gamma^{(2)}_{s;\vec{p}\vec{q}}(M, \bar{M}) = \Gamma^{(2)}_{s;\vec{p}\vec{q}}(0,0) + \sum_{\vec{p}_1,\vec{p}_2} \Gamma^{(4)}_{s;\vec{p}\vec{q};\vec{p}_1,\vec{p}_2}(0,0)\, M_{\vec{p}_1} \bar{M}_{\vec{p}_2} + \cdots . \tag{22}$$

Perturbatively, the first term of the expansion $\Gamma^{(2)}_{s;\vec{p}\vec{q}}(0,0)$ is proportional to $\delta_{\vec{p}\vec{q}}$. However, it is not the case of the next term. Indeed, a leading order contribution to the second term could be, at the first order in perturbative expansion for $\Gamma^{(4)}_{s;\vec{p}\vec{q};\vec{p}_1,\vec{p}_2}(0,0)$:



$$\propto \sum_{\vec{k}\in\mathbb{Z}^{d-1}} M_{\vec{k},p_{1i}} \bar{M}_{\vec{k},p_{2i}} \prod_{j\neq i} \delta_{p_{1j}p_{2j}} , \tag{23}$$

where the fat black edges correspond to Kronecker delta contractions. As a result, except for very special mean field configurations ensuring that

$$\sum_{\vec{k}\in\mathbb{Z}^{d-1}} M_{\vec{k},p_{1i}}\bar{M}_{\vec{k},p_{2i}} \propto \delta_{p_{1i}p_{2i}}\,,$$

$\Gamma^{(2)}_{s;\vec{p}\,\vec{q}}$ cannot be diagonal for non vanishing means fields[4]. In the rest of this paper, we consider only the symmetric phase and the effective vertices then can be considered as the first terms correction in means field expansion like in (22).

Finally let us ended this section by introducing the notion of *boundary graph*:

Definition 5 *Let $\mathcal{G}$ a connected Feynman graph with $2N$ external edges. The boundary graph $\partial\mathcal{G}$ is obtained from $\mathcal{G}$ keeping only the external blacks and whites nodes hooked to the external edges, connected together with colored edges following the path drawn from the boundaries of the external faces in the interior of the graph $\mathcal{G}$. $\partial\mathcal{G}$ is then a tensorial invariant itself with N blacks (resp. whites) nodes. An illustration is given on Figure* (2).

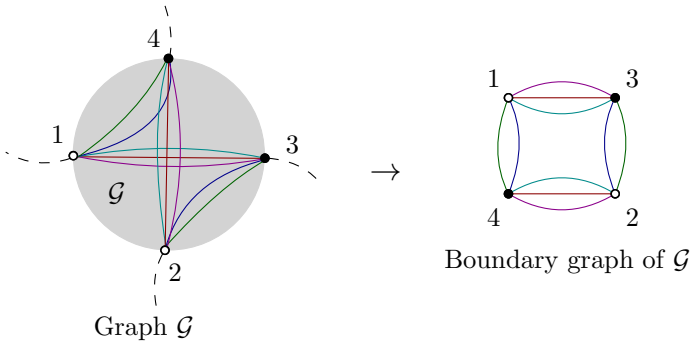


Figure 2: An opening Feynman graph with 4 external edge and its boundary graph. The strand in the interior of $\mathcal{G}$ represent the path following by the external faces.

3 Melonic and pseudo-melonic sectors

This section address the renormalization of a TGFT model, mixing standard melons and a new interacting sector called pseudo-melonic. In a first time we recall some properties of renormalizable theories and consider the purely melonic sector, which has been showed to be just-renormalizable for $d = 5$. In a second time, we define the new family that we call pseudo-melons, and show that it is power-counting renormalizable for ϕ^6 interactions.

3.1 Renormalizable sectors

Basically, a renormalizable sector is a proliferating family of divergent graphs having the same combinatorial structure and the same power counting, such that their divergences

[4]Note that the last condition holds for theory with *closure constraint*, a gauge invariance ensuring that, "on shell", $\sum_{i=1}^{d} p_i = 0$. If M and $\bar{M}$ are on shell, the product $M_{\vec{k},p_{1i}}\bar{M}_{\vec{k},p_{2i}}$ is therefore proportional to $\delta_{p_{1i}p_{2i}}$.

can be canceled from a finite set of counter-terms. For our model with kinetic laplacian term as boundary condition in the UV, the degree of divergences ω of a Feynman graph with L internal propagator edges and F internal faces is:

$$\omega = -2L + F\,. \tag{24}$$

We recall the well known classification criterion. Let us consider a given sector.

• If the degree of divergence depends only on the number of external edges, and decrease with him, the theory is said to be *superficially just-renormalizable.*

• If the degree of divergence depends on the number of external edges, and decreases both with the number of vertices and external edges, the theory is said to be *superficially super renormalizable.*

• If the degree of divergence depends on the number of external edges, and increases with the number of vertices and/or the number of external edges, the theory is said to be *superficially non-renormalizable.*

The adjective "superficially" refers to the fact that such a classification remains heuristic without a rigorous proof for finitness of renormalized amplitudes. The renormalization of TGFT models by considering only the melonic sector is given in [29]-[39] and references therein. We expect that the new sectors that we will consider in this paper requires minimal modifications on the proofs given in these references, and we will only proof the key properties allowing to extend them trivially. Moreover, we left the adjective "superficially" for the rest of this paper.

We now give a precise definition of a sector.

Definition 6 ***Families and sectors.***

• *A family $\mathcal{F}$ is a set of proliferating connected non-vacuum graphs which have the same degree of divergence and the same boundary graph. A family is then labeled with a couple $\mathcal{F} = (\omega, \gamma_n)$ with $n > 1$, γ_n being a connected invariant bubble of valence n. The leading family $\mathcal{F}_{\gamma_n,\omega_n}$ have the maximal divergence degree ω_n i.e. $\omega_n = \max_{\gamma_n} \omega$.*

• *A leading sector $\mathcal{S}$ is a set of leading families $\mathcal{S} = \{\mathcal{F}_{\gamma_n,\omega_n}\}$ such that each boundary graphs γ_n are sums of the boundaries graphs having smallest valence – up to an eventual prescription for the sum. The set of family whose boundaries graphs have the smallest valence is called root set, and their elements root families.*

• *A sub-leading sector is a sector whose families have the same boundary graphs as the families of the leading sector, but smallest degree of divergence.*

Then all the diagrams in a given familly behaves like Λ^ω with the UV cut-off Λ. Moreover, we recall the definition of the sum of connected invariants:

Definition 7 *Let γ_n and γ_m are two bubbles with valence n and m respectively. Let $n_1 \in \gamma_n$ and $n_2 \in \gamma_m$ two black and white nodes. The sum $\gamma_n *_{n_1 n_2} \gamma_m$ is the connected bubble of valence $n+m-2$ obtained from γ_n and γ_m as:*

- *Drawing an edge between n_1 and n_2*

- *Contracting it, deleting the end nodes n_1 and n_2 and connecting together the colored edges hooked to them following their respective colors.*

Figure (3) *provides an example.*

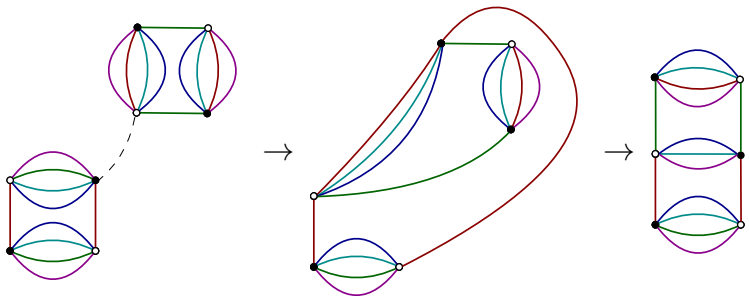


Figure 3: The sum of two connected melonics bubbles.

Among the motivations for these definition, we recall that the sum of connected tensorial invariant[5] does not change the *Gurau degree* characterizing the tensorial invariant of colored random tensor models [24]-[25]. The sectors could be then labeled with their Gurau degree.

From the definition of families and sectors, we define the notion of divergent families and sectors as follow:

Definition 8 *A family is said to be divergent if $\omega \geq 0$. Let $\mathcal{S}$ be a sector. The divergent sector $\mathcal{S}_D \subset \mathcal{S}$ is the subset $\mathcal{S}_D = \{(\omega, \gamma_n) | \, \omega \geq 0\}$ of divergent families include into $\mathcal{S}$. Note that $\mathcal{S}_D$ can be an empty set. If $\mathcal{S}_D = \emptyset$, the sector $\mathcal{S}$ is said to be safe.*

Among the families and sectors, we must make the difference between the case for which the divergent degree increase, decrease or is constant with respect to the number of vertices. Note that when the divergent degree depend on the number of vertices, the families have a short length. In contrast, when a family is made of an infinite number of graphs, the divergent degrees, for fixed n does not depends on the number of vertices. This consideration leads to the notion of *superficially renormalizable sector*:

Definition 9 *Let $S_D \subset \mathcal{S}$ the divergent sector on $\mathcal{S}$ and $\|\mathcal{S}_D\|$ the number of elements in $\mathcal{S}_D$. If $\|\mathcal{S}_D\| < \infty$ and $\forall \mathcal{F} \in \mathcal{S}_D$, $\|\mathcal{F}\| = \infty$, the sector is said to be superficially renormalizable. If $\omega = 0$, the corresponding family is said to be superficially just-renormalizable.*

[5] which is nothing that contraction of a 0-dipole, see definition (3.1).

Note that the sub-leading order sectors must have a divergent sector, requiring to be separately renormalized. The power-counting renormalizability is a first requirement to prove that a given theory is renormalizable. In particular, a renormalizable theory requires the definition of a finite set of *local counter-terms* canceling the infinities coming from the divergent families. Then, renormalization requires a *locality principle*, allowing to localize and subtract the divergences occurring in a Feynman diagram (including eventually the full diagram itself). For tensorial theories, the relevant locality principle has been given in the definition (1). Now we have to show that the *renormalized amplitudes* whose divergences have been subtracted with appropriate counter-terms, are finite at all order. Technically such a realization requires an appropriate slicing on the graphs, allowing to subtract only the dangerous parts of the divergent graphs. All these technical subtleties have been already considered in the literature for tensor field theories [30, 39], especially for melonic sector. Beyond the melonic sector, other leading order sectors have been considered in [58] call necklaces. As mentioned above, the sector that we consider in this paper in addition to the melons, the *pseudo-melonic sector* has many similarities with the melons, and a rigorous proof of its renormalizability is a small modification of the proofs given in [50]-[58] for melonic sector. We will briefly recall some of these requirements, and then we will show in a second time that (the pseudo-melonic sector) satisfy many of them. Let us mention that our presentation is highly sketched with respect to a rigorous treatment, and have to be completed with the bibliographic details for unfamiliar readers.

Then let us recall some useful definitions that we will use in the rest of this work. We start by giving the definition of k-dipoles and their contractions:

Definition 10 *Let $\mathcal{G}$ a connected Feynman graph. A k-dipole is made with two black and white nodes n and $\bar{n}$ joining together with a dotted edge and k colored edges. Contracting a k-dipole corresponds to delete the $k+1$ edges between the nodes as the nodes themselves, and reconnected together the remaining colored edges following their respective colors. An example is pictured on Figure* (4).



Figure 4: A 3-dipole (on the left) and its contraction (on the right).

Another important aspect, especially concerning the power counting theorem is the notion of *contractibility*, playing an important role in the localization and subtraction of divergences. A first important remark is that the power counting for a given graph $\mathcal{G}$ increase exactly of 2 under the contraction of spanning tree edge. Indeed, if an edge $l \in \mathcal{T}$ for $\mathcal{T} \subset \mathcal{G}$, be a spanning tree of $\mathcal{G}$, then, the graph $\mathcal{G}/l$ obtained from $\mathcal{G}$ by contracting the edge l does not change the number of internal faces. However, the number L of edges decreases to $L-1$. Contracting all the edges of the spanning tree, we then get a connected graph, said *rosette* and denoted by $\bar{\mathcal{G}}$. The divergence degrees of $\mathcal{G}$ and of one of its rosettes $\bar{\mathcal{G}}$[6] are then related by:

$$\omega(\mathcal{G}) = \omega(\bar{\mathcal{G}}) - 2(V(\mathcal{G}) - 1)\,, \tag{25}$$

[6]In general, there are more than one spanning tree in a given graph.

$V(\mathcal{G})$ being the number of bubble vertices in the initial graph $\mathcal{G}$, and $V(\mathcal{G})-1$ is the number of edges in a spanning tree of $\mathcal{G}$. A rosette is then said to be *contractible* as soon as the following definition holds:

Definition 11 *Consider the family $\mathcal{F}$, $\mathcal{G}\in\mathcal{F}$ and $\bar{\mathcal{G}}$ the corresponding rosette. $\bar{\mathcal{G}}$ is said to be contractibles if there exist $k>0$ such that all the dotted edges in $\bar{\mathcal{G}}$ can be successively contracted by k-dipole contraction.*

This definition make sense due to the fact that for a family whose rosettes are k-dipole contractible, the degree of divergence for rosettes can be easily computed leading to the following divergence degree of $\mathcal{G}$:

$$\omega(\mathcal{G})=-2L(\mathcal{G})+k(L(\mathcal{G})-V(\mathcal{G})+1). \tag{26}$$

Indeed, contracting one k dipole is equivalent to remove one dotted edge, such that the divergent degree is increased by 2. In the same time, we remove k internal faces, and therefore $\omega(\bar{\mathcal{G}})=(k-2)L(\bar{\mathcal{G}})$. Finally a relation between the number of internal edges and vertices can be easily found, expressing L in terms of a sum involving the number of vertices with a given valence [31]. Then, the renormalizability criteria may be directly investigates.

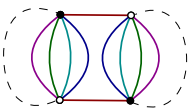
First let us consider an example of the melonic sector and let adopt the following definition useful particularly in the next section and also compatible with [24]-[25]:

Definition 12 *The melonic sector $\mathcal{S}_M$ is the sector in which, the root families have the set $\{\mathfrak{B}_i\}$ as boundary graphs. Its elements are called melonic families. Moreover, among all the families having boundaries graphs of valence n, the melonic families optimized the power counting. We call melonic bubbles and denote as $\mathbb{M}$ the set of all the tensorial invariants obtained as sums of elementary melons in the set $\{\mathfrak{B}_i\}$.*

The melonic sector has then the set $\{\mathfrak{B}_i\}$ as smallest boundaries graphs. The melonic graphs satisfy a recursive definition, and the non-vacuum diagrams can be obtained from the vacuum ones. Note that the vacuum diagrams as well as 2-point diagrams are not in the sector $\mathcal{S}_M$.

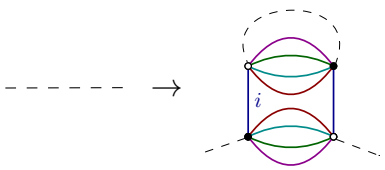
Definition 13 ***Vacuum melonic diagrams***

• *For a purely quartic model containing only the set $\{\mathfrak{B}_i\}$ as interactions, the vacuum melonic diagrams are recursively obtained from the elementary diagrams:*



(27)

by replacing any of the dotted edge as:



(28)

for arbitrary i. Figure (5) provides us an example of such quartic vacuum melons.

• *For models involving higher melonic bubbles, obtaining as sums of elementary quartic melon, the vacuum diagrams are obtained from quartic vacuum diagrams by contraction of some 0-dipole. As illustration the figure (5) provides an example of such this contraction.*

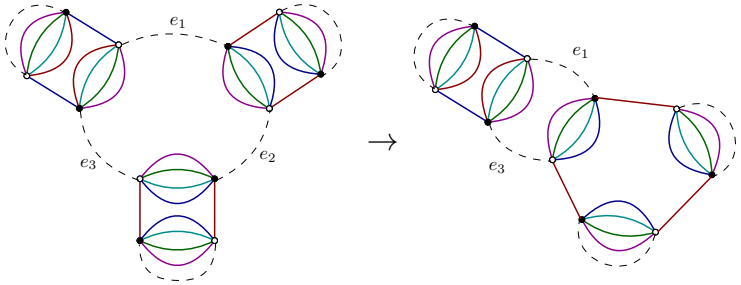


Figure 5: A quartic vacuum melonic diagrams with three vertices (on left), and a vacuum melonic diagram with one 3-valent melonic interaction obtained from the first diagram by the contraction of the edge e_2 (on right).

Note that the elementary procedure allows to replace one edge with a 2-point tadpole does not change the degree of divergence: To be more precise we add two dotted edges and therefore decrease the degree by 4, but this variation is exactly compensated from the creation of 4 internal faces. It is easy to cheek that $\omega = 5$ for the quartic vacuum diagrams, and this quantity increase exactly by $2(n-2)$ when we add a n valent melonic interaction with $n > 2$. We denote by $\mathcal{S}_{M_V}$ the set of vacuum quartic melonic diagrams. The 1PI 2-points melonic diagrams may be obtained from vacuum melons from the deletion of one dotted edge. Obviously, deleting a dotted edge along a face of length higher to 1, we obtain a 1PI graph. Then, to build a 2-point 1PI graph, we have only the choice to delete an tadpole edge. The deletion suppress 5 internal faces, and one internal edge. The degree of divergence for melonic 2-point graphs is then equal to 2. We then defined $\mathcal{S}_{M_2}$ as the set of quartic melonic 2-point graphs. The 1PI 4-points graphs will be then obtained from the deletion of another tadpole dotted edge, and it is easy to cheek that the optimal way is to delete an edge in the boundary of one external faces. A 4-point graph have then two external vertices, $2(d-1)$ external faces of length 2, whose boundaries are pairs of external edges hooked to the same external vertex, and 2 external faces running through the interior of the diagram. Figure (6) provides an example with two quartic vertices.

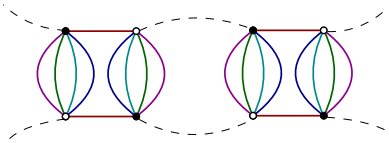


Figure 6: A 4-point melonic diagram with two vertices. We have 2×4 external faces per external vertex, and two external red faces running through the internal dotted edges.

For 1PI melonic diagrams with more external edges, we get [31]-[36]:

Proposition 1 *Let $\mathcal{G}$ be a 1PI $2N$-points diagram with more than one vertex. It has N external vertices, $d-1$ external faces per external vertex, and N external faces of the same color running through the interior of the diagram.*

Among the interesting properties of melonic diagrams, their rosettes are $d-1$-dipole contractible, so that formula (26) becomes:

$$\omega(\mathcal{G}) = -2L(\mathcal{G}) + (d-1)(L(\mathcal{G}) - V(\mathcal{G}) + 1)\,. \tag{29}$$

Counting the number of edges in a Feynman graph with N external edges, and V_k vertices of valence $2k$, we get $2L = \sum_k 2kV_k - N$ and setting $d = 5$:

$$\sum_k 2(k-2)V_k(\mathcal{G}) + 4 - N(\mathcal{G})\,, \tag{30}$$

so that the melonic interactions are just-renormalizable for the quartic set $\{\mathfrak{B}_i\}$. Then, the dangerous sector $\mathcal{S}_{D,M}$ for melonic graph only contain the leading families with boundaries graphs $\gamma_2 \in \{\mathfrak{B}_i\}$. This family is build of graphs with arbitrary size, meaning that each leading family is an infinite set. $\mathcal{S}_{D,M}$ is then a just-renormalizable divergent sector from definition (9). To this set, we have to add the infinite set $\mathcal{S}_{M_2}$ of 2-points melonic graphs, which have power counting $\omega = 2$. To illustrate how the renormalization work, let us consider the four point graph pictured on Figure (6). Let $\mathcal{A}_{\vec{p}_1,\vec{p}_2,\vec{p}_3,\vec{p}_4}$ the amplitude of the corresponding diagram. Assuming that the red edges correspond to the component 1 in the momentum space, we get:

$$\mathcal{A}(\vec{p}_1,\vec{p}_2,\vec{p}_3,\vec{p}_4) = -4\lambda^2\, A(p_{11}^2, p_{21}^2)\, \mathrm{Sym}\mathcal{V}^{(4,1)\,1}_{\vec{p}_1,\vec{p}_2,\vec{p}_3,\vec{p}_4}\,, \tag{31}$$

where:

$$A(p_{11}^2, p_{21}^2) := \sum_{\vec{q}\in\mathbb{Z}^{d-1}} \frac{1}{\vec{q}^{\,2} + p_{11}^2 + m^2}\, \frac{1}{\vec{q}^{\,2} + p_{21}^2 + m^2}\,, \tag{32}$$

and

$$\mathrm{Sym}\mathcal{V}^{(4,1)\,1}_{\vec{p}_1,\vec{p}_2,\vec{p}_3,\vec{p}_4} = \mathcal{V}^{(4,1)\,1}_{\vec{p}_1,\vec{p}_2,\vec{p}_3,\vec{p}_4} + \mathcal{V}^{(4,1)\,1}_{\vec{p}_3,\vec{p}_2,\vec{p}_1,\vec{p}_4}\,. \tag{33}$$

From power counting, $A(p_{11}^2, p_{21}^2)$ diverges logarithmically with the UV cut-off. However, any derivative with respect to the external momenta p_{11} and p_{21} is convergent. Then, only the first term in the Taylor expansion of $A(p_{11}^2, p_{21}^2)$ is divergent and requires to be subtracted:

$$\mathcal{A}(\vec{p}_1,\vec{p}_2,\vec{p}_3,\vec{p}_4) = -4\lambda^2\, A(0,0)\, \mathrm{Sym}\mathcal{V}^{(4,1)\,1}_{\vec{p}_1,\vec{p}_2,\vec{p}_3,\vec{p}_4} + \text{finite}\,. \tag{34}$$

Note that $2\mathrm{Sym}\mathcal{V}^{(4,1)\,1}_{\vec{p}_1,\vec{p}_2,\vec{p}_3,\vec{p}_4}$ is nothing but the combinatorial factor coming from the contraction of four external fields with an elementary 2-valent vertex $\mathfrak{B}_1$. The divergent term can be then exactly canceled adding in the original action the following one-loop counter-term:

$$\delta_1 S = 2\lambda^2\, A(0,0) \sum_{\{\vec{p}_i\}} \mathcal{V}^{(4,1)\,1}_{\vec{p}_1,\vec{p}_2,\vec{p}_3,\vec{p}_4} T_{\vec{p}_1} \bar{T}_{\vec{p}_2} T_{\vec{p}_3} \bar{T}_{\vec{p}_4}\,. \tag{35}$$

The counter-term is then factorized as an elementary bubble. For 2-points graphs, the the first derivative of the divergent function have to be kept, leading to a wave function

counter-term. This is in this sens that connected tensorial invariant can be viewed as locals. For melonic sector, this property may be generalized for all orders: Any divergent diagram may be factorized as an elementary melonic bubble times a divergent contribution (see [31]-[36]).

In standard field theory, interactions can be classified following their dimensions. However, in TGFT, there are no background space-time, and roughly speaking the action (2) is dimensionless. An appropriate notion of *canonical dimension* appears from renormalization group flow considerations. Renormalizable interaction in particular has zero dimension, a property corresponding to the marginal behavior of its renormalization group flow in the vicinity of the Gaussian fixed point. Such a property is recovered for tensor field theories, where just-renormalizable interactions have a marginal behavior. We can then define the *flow dimension* as follow:

Definition 14 *Let $\mathcal{S}_D$ a renormalizable leading sector and $\mathcal{F} \in \mathcal{S}_D$ a divergent family with $\omega = 0$. The flow dimension of the corresponding boundary graph γ_n is then fixed to zero.*

In words, the renormalizable interactions scales logarithmically with the UV cut-off, which is another way to say that their weight on the power counting is zero – as in equation (30) for quartic melonic diagrams. The flow dimension of renormalizable couplings being fixed for all considered renormalizable sectors, we can associate a dimension for all couplings as their optimal scaling. Moreover, this scaling may be directly read on the power counting as well, if it exist. This is explicitly the case on equation (30). Without explicit power counting, the flow dimension is obviously closely related to the degree of divergence. Moreover, ω is a sum and difference of integers, the number of dotted edges and faces, respectively weighted with 2 and 1. Added an edge decrease of 2 the degree of divergence, while added a face increase it by one. It is then coherent to associate a *canonical dimension* 2 for each edges of a theory with Laplacian type propagator, and a dimension 1 for each faces. From these considerations, we associate a canonical dimension 2 for mass and Laplacian. One more time, the dimension of these two operators being fixed, the canonical dimensions for other tensorial operators may be deduced. Moreover, canonical and flow dimension seems to be closely related, and to make contact between them, we have to show that renormalizable interactions have zero canonical dimension. In the literature [59], the *dimension estimate* $\tilde{d}_b$ of a bubble b provides an upper-bound for canonical dimension d_b:

Definition 15 *Let b be a connected tensorial bubble, and $\mathbb{G}_2(b)$ the set of one-vertex 2-point graphs obtained from b. The estimate canonical dimension $\tilde{d}_b$ of the bubble b is then defined as:*

$$\tilde{d}_b = 2 - \max_{\mathcal{G} \in \mathbb{G}_2(b)} \omega(\mathcal{G})\,, \qquad \tilde{d}_b \geq d_b\,. \tag{36}$$

Note that $\tilde{d}_b = 2$ if $\mathbb{G}_2(b) = \emptyset$, meaning that estimate canonical dimension for 2-point bubbles is then fixed to 2, with respect to our preliminary discussion. This statement may be cheeked as follows. Let us consider a 1PI $2n$-point leading graph $\mathcal{G}_n$ in a renormalizable

sector, build of bubbles γ_n with zero flow dimension. A leading order $2n$-point graph $\mathcal{G}_n$ may be obtained from a leading 2-points graphs $\mathcal{G}_2$ from deleting $n-1$ internal edges. Let $\omega(\mathcal{G}_2)$ the divergent degree of the 2-point graph. Consistency with renormalizability then requires that the leading quantum corrections for considered renormalizable sectors behave like Λ^2, then we come to

$$\omega(\mathcal{G}_2) = 2\,. \tag{37}$$

Deleting a k-dipole leads to remove one edge and at most d internal faces. However, the number of deleted faces can be reduced if we choose to delete an edge on the boundary of a maximal number of external faces. We restrict our attention on the cases of k-dipole contractible families. Then, deleting $n-1$ edges correspond to deletes $k(n-1)$ faces, and :

$$\omega(\mathcal{G}_2) - (k-2)(n-1) = 2 - (k-2)(n-1) = 0 \;\rightarrow\; k = 2 + \frac{2}{n-1}\,. \tag{38}$$

Note that this equation make sens only for $n=2$ and $n=3$. For $n>3$, the equation $2-(k-2)(n-1)=0$ have no integer solutions. Then, we expect that the only k-dipole just-renormalizable models are given when $n=2, k=4$ or $n=3, k=3$. The first condition corresponds to the quartic melonic sector. The second condition will be described later in the next subsection.

The canonical dimension of the differents boundaries bubbles for a given sectors have to be closed. From the bubbles with valence n in a k-dipole contractible family, $n-1$ valent bubbles may be obtained from optimal contraction of a k-dipole on a just renormalizable interaction γ_n. Creating such a dipole increases the number of 0-edges of 1, and then create k internal faces. The scaling is then given by:

$$\omega(\gamma_{n-1}) = \omega(\gamma_n) + (k-2) = \frac{2}{n-1}\,, \tag{39}$$

implying that $\omega(\gamma_1) = 2$ from construction. $\omega(\gamma_{n-1})$ is nothing but the optimal scaling, that is, what we call flow dimension. Moreover, it is easy to cheek that $\omega(\gamma_2) = 2-2/(n-1)$, then:

$$\omega(\gamma_{n-1}) = 2 - \omega(\gamma_2)\,, \tag{40}$$

meaning that the flow dimension for couplings in a renormalizable sector coincide with the estimated canonical dimension. The canonical dimension will be investigate in full details for the two considered renormalizable sectors of this paper at the end of the next section.

3.2 Pseudo-melonic sector

In this subsection we consider a new leading order sector that we call *pseudo melonic*. The power counting theorem and the classification of the graphs that contribute to this sector is given. Let start by the following definition:

Definition 16 *The pseudo-melonic sector $\mathcal{S}_{PM}$ is the family set of graphs whose root families boundaries are in the set $\{\mathfrak{B}_{ij}\}$. We call pseudo-melonic bubbles and denotes as*

$\mathbb{PM}$ *the set of all pseudo-melonic tensorial invariants obtained as sum of the elementary pseudo-melons in* $\{\mathfrak{B}_{ij}\}$.

An elementary investigation suggest that $d-2$ dipoles will play the same role for pseudo-melonic graphs as $d-1$ dipoles for the melonic ones. We then give the following lemma which provides the effect of a $d-2$ dipole contraction:

Lemma 1 *The set* $\mathbb{PM} \cup \{\gamma_1\}$ *is stable under* $d-2$ *dipole contraction.*

Proof. We prove this lemma recursively. Let $\gamma_n \in \mathbb{PM}$ for $n \geq 2$. First of all, for $n=2$, $\gamma_2 \in \{\mathfrak{B}_{ij}\}$ and the contraction of any $d-2$ dipole leads to the elementary graph γ_1 with valence one. We then consider the case $n>2$. From its definition, γ_n is a connected sum of 2-valent bubbles. Then, γ_n can be considered as a tree made with $n-1$ elementary pseudo-melons. Assuming that the property hold for $n=n_0$, any n_0+1 valent bubbles can be obtained from $\gamma_{n_0-1} \in \mathbb{PM}$ as sum of an elementary pseudo melon γ_2. Let $\gamma_{n_0} = \gamma_{n_0-1} * \gamma_2$. We have to distinguishes three cases. First of all, the $(d-2)$-dipole is on the added γ_2. Contracting this dipole leads to a γ_1. But γ_1 is the identity element of the $*$–algebra on $\mathbb{PM}$, then: $\gamma_{n_0-1} * \gamma_1 = \gamma_{n_0-1}$. The second case is when a $(d-2)$-dipole is contracted on the component γ_{n_0-1} itself.Moreover from induction hypothesis, the contraction leads to a connected $\gamma_{n_0-2} \in \mathbb{PM}$ of valence n_0-2, summed with γ_2, and $\gamma_{n_0-2} * \gamma_2 \in \mathbb{PM}$. The third and last possibility is to contract a $(d-2)$-dipole corresponding to a dotted edge between γ_{n_0-1} and γ_2. The only possibility is that γ_{n_0-1} and γ_2 share $(d-2)$ internal faces of length 2 as on figure (7) below. But it is easy to cheek that the contraction of the two dotted edges bounded the faces yield again the pseudo melonic bubble $\gamma_{n_0-1} \in \mathbb{PM}$.

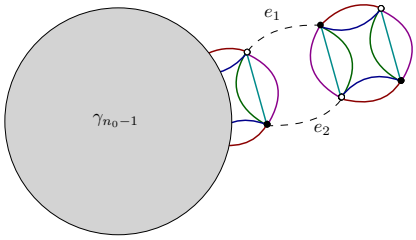


Figure 7: Illustration of the third configuration: The two pseudo-melonic connected tensorial invariants γ_{n_0-1} and γ_2 share three internal faces of length 2. Contracting e_1, we get a 3-dipole, whose contraction leads to γ_{n_0-1} itself.

□

Definition 17 *A connected Feynman graph* $\mathcal{G}$ *is said pseudo-melonic if it contain only pseudo melonic tensorial bubbles. Now contracting the* $V(\mathcal{G})-1$ *dotted edges of a spanning tree leads to a pseudo-melonic rosette with* $L(\mathcal{G})-V(\mathcal{G})+1$ *dotted edges.*

Definition 18 *For any pseudo melonic graph* $\mathcal{G}$*, we define* $\rho(\mathcal{G})$ *as:*

$$\rho(\mathcal{G}) = (d-2)(L(\mathcal{G})-V(\mathcal{G})+1) - F(\mathcal{G})\,. \tag{41}$$

Lemma 2 *For any pseudo-melonic graph,* $\rho(\mathcal{G})$ *is invariant under* $(d-2)$*-dipole contraction and also as well under a tree edge contraction.*

Proof. Let us consider an edge e in a spanning tree. Contracting it does not change the number of face as well as the combination $L - V$, due to the fact that contracting a tree edge decreases both L and V of one unit. Then, ρ is invariant under a tree edge contraction.

Let us consider a $(d-2)$-dipole. Contracting it delete exactly $d-2$ internal faces. Moreover V is invariant and L decreases of one unit. Finally, the variation of the first term exactly compensate the variation of F.

□

Proposition 2 *Let $\mathcal{G}$ a pseudo-melonic non-vacuum graph containing only 2 valent vertices. Then:*

$$\rho(\mathcal{G}) \in \mathbb{N}\,, \tag{42}$$

and

$$\rho(\mathcal{G}) = 0\,, \tag{43}$$

if and only if $\mathcal{G}/\mathcal{T}$ is $(d-2)$-dipole contractible for any spanning tree $\mathcal{T} \subset \mathcal{G}$.

Proof. We proceed by induction on the number of elementary pseudo-melonic bubbles. For $V = 1$, the proposition can be easily checked. For $V > 1$, we assume the proposition true for $V = V_0$ and consider an arbitrary pseudo-melonic graph $\mathcal{G}$ having $V = V_0 + 1$ vertices. Choosing an external vertex $b \in \mathcal{G}$, we have to distinguishes three cases (see Figure (8)a):

- Only one external edges is hooked to the vertex b. It is then connected with one, two or three connected components.
- Two external edges are hooked to the vertex b. Then one or two connected components can be hooked to him.
- Three external edges are hooked to b, and only one connected component is hooked to him.

Note that the last case with four external edge hooked to b is then excluded from the recursive hypothesis $V > 1$. Let us consider the generic case pictured having $\mathfrak{c}$ connected components $\mathcal{G}_i$. From recursive hypothesis, these two connected components satisfy $\rho(\mathcal{G}_i) \in \mathbb{N}\,, i = 1, \cdots, c$. Let $\mathcal{G}' := \cup_{i=1}^{c} \mathcal{G}_i$ the graph with c connected components obtained from $\mathcal{G}$ deleting the external vertex b. We have $F(\mathcal{G}_i) \leq (d-2)(L(\mathcal{G}_i) - V(\mathcal{G}_i) + 1)$, $\forall i$, and:

$$F(\mathcal{G}') \leq (d-2)(L(\mathcal{G}') - V(\mathcal{G}') + 1) + (d-2)(\mathfrak{c} - 1). \tag{44}$$

Moreover, $V(\mathcal{G}) = V(\mathcal{G}') + 1$ and $L(\mathcal{G}) = L(\mathcal{G}') + \ell$, where ℓ is the number of dotted edges hooked the vertex b to $\mathcal{G}'$. Obviously $\ell \geq \mathfrak{c}$, and:

$$F(\mathcal{G}') \leq (d-2)(L(\mathcal{G}') - V(\mathcal{G}') + 1) + (d-2)(\mathfrak{c} - \ell)\,. \tag{45}$$

Moreover, it is easy to cheek that, from all the possibilities listing above we have: $F(\mathcal{G}) \leq F(\mathcal{G}') + (d-2)(\ell - \mathfrak{c})$ and then $\rho(\mathcal{G}) \geq 0$.

From lemma (2), if $\mathcal{G}/\mathcal{T}$ is a $(d-2)$-dipole contractible rosette, $\rho(\mathcal{G}/\mathcal{T}) = \rho(\mathcal{G}) = 0$. Reciprocally, assuming that $\rho(\mathcal{G}) = 0$, then $\rho(\mathcal{G}/\mathcal{T}) = 0$ for any spanning tree $\mathcal{T} \subset \mathcal{G}$. Moreover, from recursion hypothesis, one has:

$$\rho(\mathcal{G}_i) = 0 \quad \forall i \;\Rightarrow\; F(\mathcal{G}_i) = (d-2)(L(\mathcal{G}_i) - V(\mathcal{G}_i) + 1) \quad \forall i\,, \tag{46}$$

and for each i, and any spanning tree $\mathcal{T}_i \subset \mathcal{G}_i$, $\mathcal{G}_i/\mathcal{T}_i$ is $(d-2)$-dipole contractible. Any spanning tree $\mathcal{T} \subset \mathcal{G}$ can be decomposed as follow: $\mathcal{T} = \cup_{i=1}^{\mathfrak{c}} \mathcal{T}_i \cup \{l_1, \cdots, l_{\mathfrak{c}}\}$, where $\{l_1, \cdots, l_{\mathfrak{c}}\} \subset \{l_1, \cdots, l_\ell\}$ is a subset of k$\mathfrak{c}$ edges hooked to b.

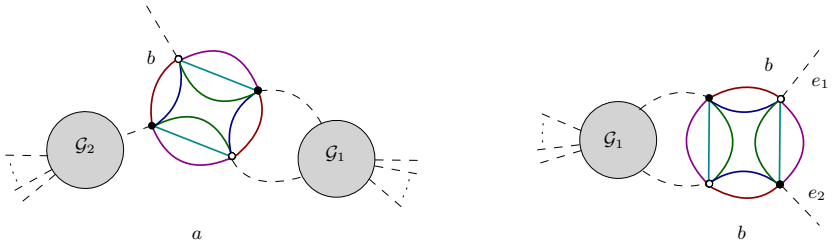


Figure 8: a) an illustration for the first item: One external edge is hooked to b, and two connected components are hooked to him, namely $\mathcal{G}_1$ and $\mathcal{G}_2$, pictured as grey disks. b) The only configuration creating $d-2$ internal faces. Note that at least one of the two edges e_1 and e_2 have to be external.

□

Contracting the edges of the trees $\mathcal{T}_i$, we get contractible rosettes which can be contracted themselves. It remains at most $\ell - \mathfrak{c}$ loops, carrying at most $d-2$ faces. Optimally, we then have to $F(\mathcal{G}) = F(\mathcal{G}') + (d-2)(\ell - \mathfrak{c})$, but it is easy to cheek that there is only such one configuration, for $\ell - \mathfrak{c} = 1$, pictured on Figure (8)b. After contraction of the remaining tree edge, we get a $(d-2)$-dipole contractible graph, completing the proof.

□

Corollary 1 *For any non-vacuum pseudo-melonic diagram $\mathcal{G}$, $\rho(\mathcal{G}) \in \mathbb{N}$. Moreover, $\rho(\mathcal{G}) = 0$ if and only if $\mathcal{G}/\mathcal{T}$ is $(d-2)$-dipole contractible, $\mathcal{T}$ being a spanning tree of $\mathcal{G}$ containing all the 0-dipole edges of the decomposition of all the pseudo-melonic bubbles into sums of elementary quartic pseudo-melonic bubbles.*

Proof. Any pseudo-melonic diagram can be obtained from a purely quartic pseudo-melonic diagram from the contraction of 0-dipole edges. However, 0-dipole contractions do not change the $\rho(\mathcal{G})$.

□

As a direct consequence, we deduce that a necklace bubble can not have more than three colored edges between a pair of black and white nodes. Otherwise, it will be possible to obtain a 4-dipole, which violate the bound $\rho \geq 0$. Indeed,

Corollary 2 *Let a non-vacuum pseudo-melonic graph $\mathcal{G}$ having $V_k(\mathcal{G})$ pseudo melonic bubbles of valence $2k$, $L(\mathcal{G})$ internal edges and $N(\mathcal{G})$ external edges. From the relation $2L(\mathcal{G}) = \sum_k 2k\, V_k(\mathcal{G}) - N(\mathcal{G})$, we then have:*

$$\omega(\mathcal{G}) = \frac{1}{2}\sum_k (2k-6)V_k(\mathcal{G}) + \left(3 - \frac{1}{2}N(\mathcal{G})\right) - \rho(\mathcal{G})\,. \tag{47}$$

Then, proposition (2) and corollary (1) motivate the following definition:

Definition 19 *For a fixed configuration $(\{V,k\},N)$, the leading order graphs satisfies $\rho = 0$. We call pseudo-melons these leading families which bound the power counting and build the pseudo-melonic sector $\mathcal{S}_{PM}$.*

From (47), it is clear that the corresponding divergent sector will be of finite size if and only if $V_k(\mathcal{G}) = 0$ for $k > 3$. In other words:

Proposition 3 *The pseudo-melonic sector is just-renormalizable up to 3-valent pseudo-melonic interactions. Moreover, power counting graphs with $N > 6$ admits the following bound:*

$$\omega \leq -\frac{N}{8}\,, \qquad N > 6\,. \tag{48}$$

For a purely 3-valent model, the power counting reduces to $\omega = 3 - N/2$, and vanish for the 3-valent leading family. We then fix to zero the canonical dimension of 3-valent pseudo-melonic bubbles. The complete set of renormalizable 3-valent interactions are given on Figure (9).

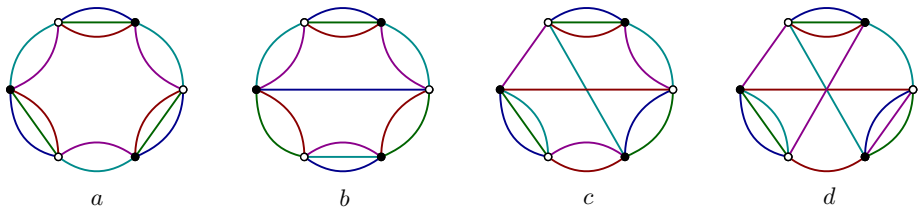


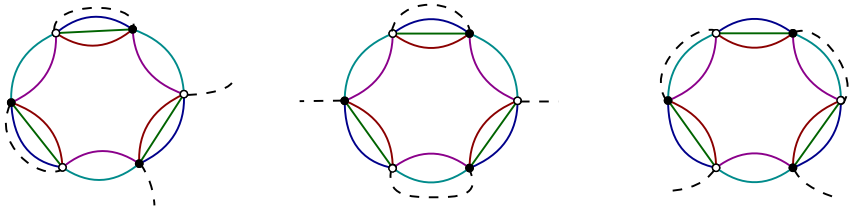
Figure 9: The complete set of just-renormalizable interactions, having zero canonical dimension.

A direct inspection show that all the divergences have not took into account in the leading divergent set of pseudo-melons. Indeed, for $\rho = 0$, 2, 4 and 6-points functions have respectively $\omega = 2$, $\omega = 1$ and $\omega = 0$. The remaining functions being power-counting convergent. However, for $\rho = 1$, the 2 and 4 point functions remains divergent, respectively as $\omega = 1$ and $\omega = 0$; and for $\rho = 2$, the 2 point function remains logarithmically divergent

$\omega = 0$. We have then two sub-leading order sectors, characterized by $\rho = 1$ and $\rho = 2$. Figure (10) provides some examples. Moreover, for $\rho > 2$, the divergent degree admits the bounds:

$$\omega \leq -\frac{N}{2}\,, \tag{49}$$

ensuring power-counting convergence. The complete renormalization of the theory then requires to renormalize sector by sector with appropriate counter-terms. In the rest of this paper, we will only focus on the leading order sectors, mixing melons and pseudo melons, which dominate the renormalization group flow in the deep UV limit.



$\rho = 0,\ \omega = 2$ $\rho = 1,\ \omega = 1$ $\rho = 2,\ \omega = 0$

Figure 10: One-vertex 2-point functions examples for leading and sub-leading orders.

From definition (15), we then deduce the estimate canonical dimension for each of the pseudo-renormalizable interactions, that is, with valence smallest or equal to 3. We then get $\tilde{d}_b = 0$ for each of the bubbles pictured on Figure (9), in agreement with their expected marginal behavior. Moreover, the dimension of the quartic bubbles in the set $\{\mathfrak{B}_{ij}\}$ is equal to 1, corresponding to an essential coupling. To close this section, we will discuss this point with some details. Let us consider the quartic melonic sector. From definition, the coupling $\lambda_{4,1}$ must have a zero flow dimension, because all leading 4-point quantum corrections have zero divergent degree and then behave logarithmically[7]. Fixing $d_{4,1} = 0$, it is easy to see that the optimal quantum corrections for 2-points functions and then for mass scales as Λ^2. The flow dimension for mass and laplacian then is fixed to 2, and then corresponds to the canonical dimension coming from power-counting itself. Moving on to the pseudo-melonic sector, the flow dimension for all the couplings corresponding to the bubbles pictured on Figure (9) have zero flow dimension. Moreover, optimal quantum corrections for 2-points function made only with these bubbles scales as Λ^2 as well from power counting (47). Finally, optimal quantum corrections for 4-points functions scales as Λ, in accordance with a canonical dimension 1. In general, from power counting and for a general tensorial invariant of valence n:

$$d_{\gamma_n} = \begin{cases} 4 - 2n & \text{In melonic sector} \\ 3 - n & \text{In pseudo-melonic sector} \end{cases} \tag{50}$$

4 EVE for a mixing tensorial theory space

This section aims at building the effective vertices for a renormaliable sector beyond the standard melonic Feynman graphs. We deduce the effective vertices for a model including melonic and pseudo-melonic renormalizable interactions as initial conditions in the

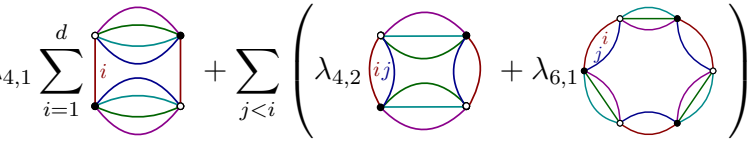
[7]In other words, added a new vertex has no additional cost, which is explicit in equation (30).

UV. For the rest of this paper, we consider 5-dimensions TGFT with this two leading contributions, and we restrict our attention on the UV sector $\Lambda \gg k \gg 1$.

4.1 Mixing melons and pseudo-melons

In this section we investigates the leading sector for a theory mixing melonic and pseudo-melonic renormalizable sectors. The theory from which we start in the deep UV is the following:

$$S_{\text{int}}(T,\bar{T}) = \lambda_{4,1} \sum_{i=1}^{d} \quad + \sum_{j<i} \left(\lambda_{4,2} \quad + \lambda_{6,1} \right) \tag{51}$$



Note that we have chosen one among the three type of interactions pictured on Figure (9). We call this sector *non-branching pseudo-melonic*. Non-branching graphs where been studied in [58]. The boundaries graphs for these restricted sectors γ_n are such that:

$$\gamma_n = \underbrace{\mathfrak{B}_{ij} * \mathfrak{B}_{ij} * \cdots * \mathfrak{B}_{ij}}_{n-1 \text{ times}} = *_{k=1}^{n-1} \mathfrak{B}_{ij} =: \mathfrak{B}_{ij}^{(n)} . \tag{52}$$

Figure (11) provides the structure of general pseudo-melonic interactions. The non-branching pseudo-melonic sector then splits into $d(d-1)$ sectors labeled with a couple (i,j), $i > j$, such that each family of valence n has boundary $\mathfrak{B}_{ij}^{(n)}$. The interest of this restriction is that the pseudo-melonic sector is stable in the deep-UV: There are no leading order quantum correction which generate effective vertex outside of the non-branching sector from the initial conditions (51). In other words, the renormalization group flow is stable on the non-branching sector.

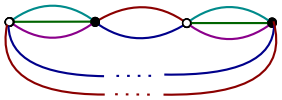


Figure 11: Structure of general pseudo-melonic interactions.

As a first step we will investigate the general structure for the leading order (LO) graphs. Let $\mathcal{G}$ is a Feynman graph obtained from the classical action (51). Moreover, let Q is the map from $\mathcal{G}$ to its *quartic representation* $\mathrm{Q}(\mathcal{G})$ i.e. the graph obtained from $\mathcal{G}$ by replacing all the 3-valent vertices with their connected sum of quartic interactions.

Definition 20 *We denote by $\mathbb{G}$ the complete set of connected Feynman graphs obtained from action* (51)*. We call quartic sector the connected Feynman graphs with only* 2*-valent vertices. We denote by $\mathrm{Q}(\mathbb{G})$ the corresponding subset.*

Obviously, for any LO graph $\mathcal{G}$, $\mathrm{Q}(\mathbb{G})$ is a LO graph in the quartic sector. Reciprocally, LO graphs in the full sector can be obtained from contraction of some 0-dipoles on a given LO quartic graph. We then investigate the quartic sector in the first step.

4.1.1 The quartic sector

The quartic sector is most conveniently studied in the Hubbard–Stratonovich (HS) representation. For tensorial theories, HS representation has been largely discussed in the literature [29]-[43]. The procedure can be summarized as follows. In the HS representation, each vertex corresponds to a cycle of edges of color 0 of the original representation. The *arcs*[8] are the edges of color 0 in the original representation. For our model, there are two type of edges in the HS representation. Monocolored edges labeled with i $(i = 1, \cdots, d)$ corresponding to melonic vertices, and bicolored edges of colors ij, $(i > j)$, corresponding to pseudo-melonic interactions, opening simultaneously both strands of color i and j between two HS vertices. Finally, external edges in the original representation are matched as *cilia* on the vertices in the HS representation, in such a way that a such vertex has at least one bear at least one cilium. The exact way to construct the correspondence can be found in [26],[64]. Then, a graph in the HS representation is made with three type of bicolored lines joining some vertices with at least one cilium, in such a way that the number of cilium in the HS representation is the half of the number of external edges in the original representation. We call *maps* the graphs in the HS representation and denotes their set as $\mathbb{M}$. Note that the correspondence between the two representations is exact, in the sens that we can construct a bijective mapping $\mathrm{F} : \mathbb{G} \to \mathbb{M}$ such that for any quartic Feynman graph $\mathcal{G}$ in the original representation we may associate an unique graph $\mathrm{F}(\mathcal{G})$ in the HS representation and reciprocally. The construction of the mapping F is pictured in Figure (12) for some example, and detailed in [65].

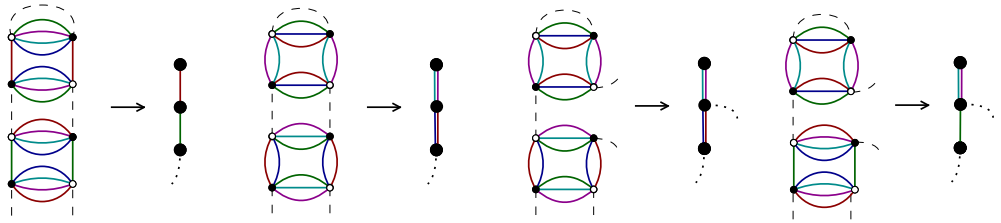


Figure 12: HS correspondence between some quartic Feynman graphs.

We will investigate the structure of the LO quartic graphs in the HS representation. We have the first result:

Proposition 4 *Leading order quartic vacuum Feynman graphs are trees in the HS representation, with power counting* $\omega = 5$.

Proof. We proceed recursively on the number of colored and bicolored edges. Let n be the number of colored edges, m the number of bicolored edges and $\mathcal{N} = n+m$ the total number of edges. For $\mathcal{N} = 1$, there is two leading configurations, corresponding to $(n = 1, m = 0)$ and $(n = 0, m = 1)$:

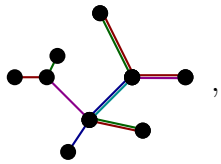


$(n = 1, m = 0)$ $\qquad$ $(n = 0, m = 1)$. (53)

[8] or *corners* in mathematical literatures.

For the first one, we have two dotted edges and 9 internal faces, then $\omega = -2 \times 2 + 9 = 5$. For the second case, we have two dotted edges and 8 internal faces. Moreover, a quartic pseudo-melonic interaction has canonical dimension 1, the complete scaling is then the same. Let $\mathcal{M}_{\mathcal{N}}$ is a map of order $\mathcal{N} > 1$. Assuming that $\mathcal{M}_{\mathcal{N}}$ is a tree,

$$\mathcal{M}_{\mathcal{N}} = \quad , \tag{54}$$



there are only four moves, to pass from $\mathcal{M}_{\mathcal{N}}$ to $\mathcal{M}_{\mathcal{N}+1}$, listing both for colored and bicolored edges on Figure (13).

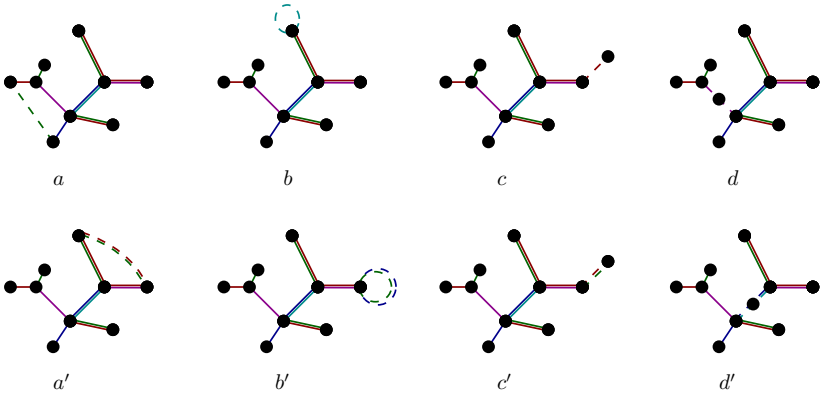


Figure 13: Elementary moves on the tree $\mathcal{M}_{\mathcal{N}}$. For a, b, c and d, we add a single–colored edge, while for a', b', c', d' we add a bicolored edge.

Investigating separately each case, we get:

1. We add a colored edge between two vertices, creating a loop a) or we add a tadpole colored edge on a single vertex b). From these moves, we create two internal propagator edges of color 0, and at most one internal faces. The variation of the power counting is then $\delta\omega = -2\delta L + \delta F \leq -3$.

2. We add a bicolored edge between two vertices, creating a loop a') or we add a tadpole bicolored edge on a single vertex b'). From these moves, we create two internal propagator edges of color 0, and at most two internal faces. Taking into account the canonical dimension of the quartic pseudo-melonic vertices, the variation of power counting is then: $\delta\omega = -2\delta L + \delta F + 1 \leq -1$.

3. We add a new monocolored leaf c) or a monocolored bridge d). From these moves, we create two internal propagator edges of color 0 and 4 internal faces. The variation of power counting is then : $\delta\omega = -2\delta L + \delta F = 0$.

4. We add a new bicolored leaf c') or a biocolored bridge d'). From these moves, we create two internal propagator edges of color 0 and 3 internal faces. The variation of power counting is then : $\delta\omega = -2\delta L + \delta F + 1 = 0$.

As a result, only the moves c, d, c' and d' do not decrease the power counting. Moreover, all these configurations preserve the tree structure, ensuring that $\mathcal{M}_{\mathcal{N}+1}$ is LO only if it is a tree itself.

□

Non-vacuum 1PI 2-point graphs are then obtained from vacuum graphs from cutting an internal dotted edge. Obviously, cutting a dotted edge on the boundary of an internal face with length upper than 1 create a 1PR graph. Then we have to cut a dotted edge with ends points hooked on the same vertex, corresponding to the leafs on the HS representation. Opening an internal dotted edge deletes 5 internal faces, the variation of power counting is then $\delta\omega = -2\delta L + \delta F = 2 - 5 = -3$, meaning that leading two points functions scales with $\omega = 2$.

1PI 4-point graphs are then obtained from deleting another tadpole. However, we have to distinguish between 4-point diagrams with melonic and pseudo-melonic boundaries.

- For melonic boundary, we have to distinguish two cases. The first one when at least one of the two boundary vertices is a melonic vertex, the second one when the two boundary vertex are pseudo-melonic. Let us start with the first case, and assume that the first deleted dotted edge is a tadpole over a melonic vertex. The second move can delete another tadpole, and will be optimal if the deleted dotted edge is on the boundary of one of the 5 opened faces from the first move. The second move then discard only 4 faces, implying $\delta\omega = 2-4 = -2$, and the LO 1PI 4-point graphs are such that $\omega = 0$. When the second deleted tadpole is pseudo-melonic we have 4 external faces of length zero on the melonic vertex and 3 on the pseudo-melonic one. We have then two external faces of the same color with length ≥ 1 passing through the two boundary vertices, and finally an external face of length ≥ 0 starting and ending on the pseudo-melonic boundary vertex. These two cases are pictured on Figure (14) a and b. The last case is when the two deleted dotted edges are pseudo-melonic tadpoles. In this case, the second move is optimal if the second deleted dotted edge is on the boundary of one of the opened external faces from the first move. There are then 3 faces of length zero per external pseudo-melonic vertices, two external faces (no necessarily of the same colors) with length ≥ 0 starting and ending on the same vertex and two external faces of the same color connecting together the boundary vertices. This configuration is pictured on Figure (14)c.
- For pseudo-melonic boundaries, the two opening tadpoles have to be pseudo-melonic, meaning that the four external dotted edges are hooked on two pseudo-melonic vertices. The optimal cutting deletes a single dotted tadpole edge in the boundary of two external faces. Then, this move delete only 3 internal faces, such that the total variation for power counting is: $\delta\omega = 2 - 3 = -1$, meaning that the LO 1PI 4-point graphs with pseudo-melonic boundaries with a power counting $\omega = 1$, in accordance to their proper canonical dimension. This configuration is pictured on Figure(14)d.

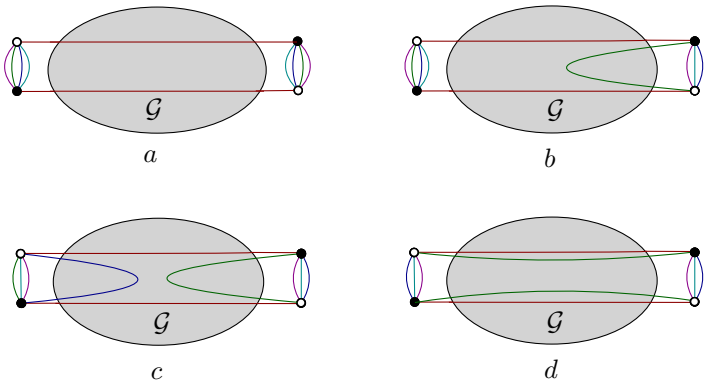


Figure 14: The four possibles boundaries. The three first ones (a) and (b) and (c) have a quartic melonic boundary while the last one (d) has a quartic pseudo-melonic boundary. The target of the external faces running through the interiors of the diagrams are pictured as internal colored edges between boundary vertices.

Non-vacuum LO diagrams with $N > 4$ may be obtained in the same way. However, the structure of the effective vertices becomes difficult to build explicitly. For this reason we will use the *Ward identities* for effective vertices with valence higher than 2.

4.1.2 Full non-branching sector

We now move on the full non-branching sector, including 3-valent non-branching interaction bubbles. As recalled in the previous section, the LO graphs may be obtained from the contraction of some 0-dipoles, corresponding to the connected sum of two quartic pseudo-melons. In the HS representation, the 0-dipoles are the arcs on vertices having more than one colored or bicolored edges. Moreover, in the non-branching sector, the contracted 0-dipoles have to be the arcs between two bicolored edges with the same couple of colors. See Figure (15)a. The contraction of the arc (e) between the two bicolored edges generates a new type of bicolored edges that we call *breaking edges*, whose breaking point correspond to the point of contact with the vertex in the HS representation. See Figure (15)b.

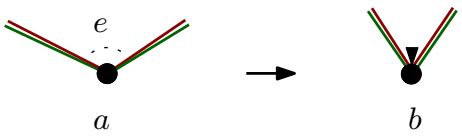


Figure 15: Contraction of a 0-dipole forming an arc (e) between two identical bicolored edges (a) and the resulting diagram (b). The 3-valent resulting from the interactions corresponds to a pair of bicolored edges with the same color hooked to the same point on the vertex. They form *breaking edges*, making a contact on a vertex with *the breaking point*, marked with a black arrow.

As a result, from proposition (4), we deduce the following:

Proposition 5 *Leading order vacuum Feynman graphs are trees in the HS representation, whose edges may be simple colored or bi colored edges as well as breaking bicolored edges.*

The power counting remains the same as for purely quartic sector: $\omega = 5$, meaning that $\rho(\mathcal{G}) = -2$ for LO vacuum graphs.

The last condition on the invariance of the power counting may be easily cheeked.

4.2 Structure equations for effective vertices

In this section we investigate the structure of the LO effective vertices with 2, 4, 6 and 8 points. We will use the method discussed on [59], by using the structure of the LO graphs established in the previous section. The aim is to get a closed set around just-renormalizable interactions, using them to parametrize the entirety of the renormalization group flow in the sector including melons and pseudo-melons. As we will see in the next section, the momentum dependence for 4-point effective vertices play a crucial role for the computation of the anomalous dimension, providing a contribution, which not included in standard crude troncations. Moreover, 6 and 8-point effective vertices are require in order to close the infinite hierarchical system coming from Wetterich equation (19). From this equation, it is clear that the flow for $\Gamma^{(n)}$ involves $\Gamma^{(n=2)}$. Then, in the melonic sector, the system will be closed if we compute the 6-point effective vertices having 3-valent melon graph as boundary graph. In the same way, to close the non-branching pseudo-melonic sector around marginal interactions requires 8-point functions with non-branching pseudo-melonic graph as boundary graph.

4.2.1 Two and four point effective vertices

Let us start with the 2-point function. We denote as Σ the leading order self energy, so that the LO effective propagators G can be decomposed as:

$$G = \big(-\Delta + m^2 + r_s - \Sigma\big)^{-1} = C_s + C_s\Sigma C_s + C_s\Sigma C_s\Sigma C_s + \cdots . \tag{55}$$

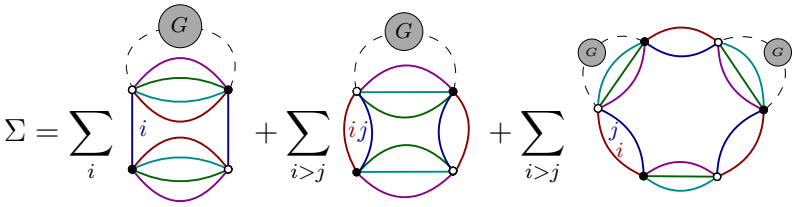
where C_s is the bare propagator given in (20). We get the following closed equation:

Proposition 6 *The leading order self energy Σ satisfy the following closed equation:*

$$\begin{aligned}\Sigma(\vec{p}) = -2\lambda_{4,1}\sum_{i=1}^{d}\sum_{\vec{q}\in\mathbb{Z}^d}\delta_{p_iq_i}\,G(\vec{q}) - 2\lambda_{4,2}\sum_{j<i}^{d}\sum_{\vec{q}\in\mathbb{Z}^d}\delta_{p_iq_i}\delta_{p_jq_j}\,G(\vec{q})\\ - 6\lambda_{6,1}\sum_{j<i}^{d}\sum_{\vec{q},\vec{q}'\in\mathbb{Z}^d}\delta_{p_iq_i}\delta_{p_jq_j}\delta_{p_iq_i'}\delta_{p_jq_j'}\,G(\vec{q})\,G(\vec{q}')\,.\end{aligned} \tag{56}$$

Proof. From the previous section, we know that LO 1PI 2-point graphs may be obtained from the cutting of an internal tadpole edge. They corresponds to leafs on the HS representation, and the final vertex on the leaf can be hooked to a single colored edge, to a bicolored edge or to a breaking bicolored edges. As a result, the opening tadpole may be localized on a quartic melonic vertex, either on a quartic pseudo melonic or on a 3-valent pseudo-melonic vertex. Opening a melonic tadpole on a LO graph, means that there are

two half dotted edges hooked to this vertex, and connecting it to the rest of the diagram. But it is easy to cheek that the remaining part of the diagram hooked to this vertex is nothing but the LO 2-point function G. The same result hold when a pseudo-melonic tadpole is deleted. Finally, when the deleted tadpole is on a 3-valent vertex, it is easy to cheek that the only 3-dipole contractible configuration corresponds to the contraction of this vertex with two effective 2-point functions in order to form two effective 3-dipoles. Graphically, all these configurations corresponds to the equation:

$\Sigma =$  (57)

By expressing these diagrams as an equation and taking into account all the symmetry factors, we obtain the closed equation (56).

□

The structure of 1PI 4-point function may be obtained from the same strategy in terms of elementary essential or marginal couplings, as well as effective 2-point functions. All the configurations for boundary vertices are pictured on Figure (14). Note that, for the quartic pseudo-melonic boundaries, we have to add the ones coming from 3-valent pseudo melonic vertices. The interior of the diagram can be determined for each configurations with the two following statements:

1. The structure of the graph is a tree in the HS representation.
2. The connectivity of the external faces between the boundary vertices have to be ensured following their respective nature.

For the rest of this paper we focus our attention on the renormalization group flow for local interactions, corresponding to purely tensorial invariants. We focus on the zero-momenta effective vertices. Even with this simplification, the computation of the zero-momenta 4-point function remains difficult, especially when the boundary graph is a quartic melon, due to the large number of configurations. Then, to simplify the proofs, we split the computation into some partial results, corresponding the elementary "building block" configurations.

First, let us consider a LO 4-point graph having quartic melonic boundary, such that the external edges are fully connected to melonic vertices. Such a configuration corresponds to Figure (14)a. Let us call "red" the color of the external faces running through the interior of the diagram between the ends vertices. In the HS representation, such a graph corresponds to a 2-ciliated tree and the two cilia being joined together with a red path made of a succession of colored or bicolored edges whose one of them be red. Figure (16) provides an example of this configuration. We call this path the *skeleton*, and the length

of the skeleton the number of edges building with him. Moreover, we call *purely melonic* the LO 2-ciliated trees whose skeleton edges have a single color.

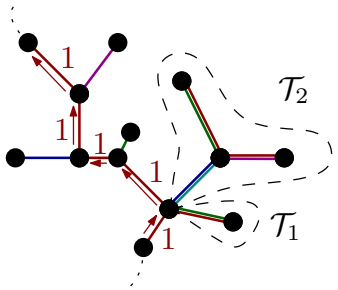


Figure 16: A tree with two cilia contributing to the LO 4-point function with melonic boundary. The red arrows follow the path of the skeleton corresponding to the color 1, joining together the boundary vertices.

Let $\Gamma^{(4)}_a(\vec{p}_1,\vec{p}_2,\vec{p}_3,\vec{p}_4)$ be the LO 4-point function obtained as a sum of Feynman graphs having melonic boundary, with non-zero external momenta. The skeleton being labeled with a single color, taking into account the structure of the ends vertices, $\Gamma^{(4)}_a(\vec{p}_1,\vec{p}_2,\vec{p}_3,\vec{p}_4)$ have to be decomposed as:

$$\Gamma^{(4)}_a(\vec{p}_1,\vec{p}_2,\vec{p}_3,\vec{p}_4) =: \sum_{i=1}^{d} \Gamma^{(4),i}_a(\vec{p}_1,\vec{p}_2,\vec{p}_3,\vec{p}_4)\,, \tag{58}$$

where:

$$\Gamma^{(4),i}_a(\vec{p}_1,\vec{p}_2,\vec{p}_3,\vec{p}_4) =: \Pi^{(2)}_a(p_{1i},p_{3i})\,\mathrm{Sym}\mathcal{V}^{(4,1)\,i}_{\vec{p}_1,\vec{p}_2,\vec{p}_3,\vec{p}_4}\,, \tag{59}$$

in accordance with the perturbative expansion (34). In the rest of this paper, we will refers to $\Pi^{(2)}_a(p_{1i},p_{3i})$ as *effective skeleton function*, and we denote by $\Pi^{(2)}_a \equiv \Pi^{(2)}_a(0,0)$ its zero momenta value. Note that the upper index 2 indicates the number of cilia on the graphs contributing to it. From their structure, obviously, $\Pi^{(2)}_a$ split into purely melonic contributions, whose skeletons are chain of melons, and mixing contributions, whose skeletons includes bicolored edges insertions. We will denote them respectively as $\Pi^{(2)}_{a,0}$ and $\Pi^{(2)}_{a,1}$, such that:

$$\Pi^{(2)}_a = \Pi^{(2)}_{a,0} + \Pi^{(2)}_{a,1}\,. \tag{60}$$

The decomposition (58) can be generalized for all the contributions pictured on Figure (14). From connectivity of the boundary graphs, it is clear that the configurations (a), (b) and (c) contribute to the effective vertex function having melonic boundary, while the last one (d) contribute to the effective vertex function having pseudo-melonic boudnary. From the configurations (a), (b) and (c), the corresponding trees in HS representation have skeleton labeled with a single color, while the skeleton of the configuration (d) have bicolored skeleton, labeled by a pair of different colors. We then have the decomposition:

$$\Gamma^{(4)}_{\mathrm{melo}}(\vec{p}_1,\vec{p}_2,\vec{p}_3,\vec{p}_4) =: \sum_{i=1}^{d} \Gamma^{(4),i}_{\mathrm{melo}}(\vec{p}_1,\vec{p}_2,\vec{p}_3,\vec{p}_4)\,, \tag{61}$$

$$\Gamma^{(4)}_{\text{pseudo–melo}}(\vec{p}_1,\vec{p}_2,\vec{p}_3,\vec{p}_4) =: \sum_{j<i}^{d} \Gamma^{(4),ij}_{\text{pseudo–melo}}(\vec{p}_1,\vec{p}_2,\vec{p}_3,\vec{p}_4)\,, \tag{62}$$

where:

$$\Gamma^{(4),i}_{\text{melo}}(\vec{p}_1,\vec{p}_2,\vec{p}_3,\vec{p}_4) = \Pi^{(2)}_1(p_{1i},p_{3i})\,\text{Sym}\mathcal{V}^{(4,1)\,i}_{\vec{p}_1,\vec{p}_2,\vec{p}_3,\vec{p}_4}\,, \tag{63}$$

with

$$\Pi^{(2)}_1(p_{1i},p_{3i}) := \Pi^{(2)}_a(p_{1i},p_{3i}) + \Pi^{(2)}_b(p_{1i},p_{3i}) + \Pi^{(2)}_c(p_{1i},p_{3i})\,, \tag{64}$$

and:

$$\Gamma^{(4),ij}_{\text{pseudo–melo}}(\vec{p}_1,\vec{p}_2,\vec{p}_3,\vec{p}_4) = \Pi^{(2)}_{2,ij}(p_{1i},p_{1j};p_{3i},p_{3j})\text{Sym}\mathcal{V}^{(4,2)\,ij}_{\vec{p}_1,\vec{p}_2,\vec{p}_3,\vec{p}_4} \tag{65}$$

with

$$\Pi^{(2)}_{2,ij}(p_{1i},p_{1j};p_{3i},p_{3j}) := \Pi^{(2)}_{d,ij}(p_{1i},p_{1j};p_{3i},p_{3j})\,, \tag{66}$$

$\Pi^{(2)}_{d,ij}$ being the skeleton function corresponding to the configuration (d) on Figure (14). The following result holds:

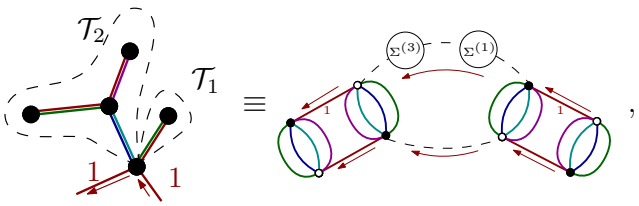
Lemma 3 *The zero-momenta effective skeleton function for purely melonic graphs,* $\Pi^{(2)}_{a,0}$ *writes as:*

$$\Pi^{(2)}_{a,0} = \frac{2\lambda_{4,1}}{1+2\lambda_{4,1}\mathcal{A}_{4;2}} \tag{67}$$

where :

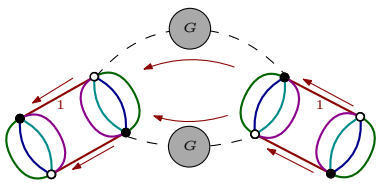
$$\mathcal{A}_{m;n} := \sum_{\vec{p}\in\mathbb{Z}^m} G^n(\vec{p})\,. \tag{68}$$

Proof. Let us consider a LO-tree having purely melonic red skeleton. To each vertices in the way of this red path are hooked some connected components $\mathcal{T}_1,\mathcal{T}_2,\cdots$. They are 1PI 2-point graphs from construction, and it is easy to cheek that all of them provides a contribution to the effective self energy Σ:



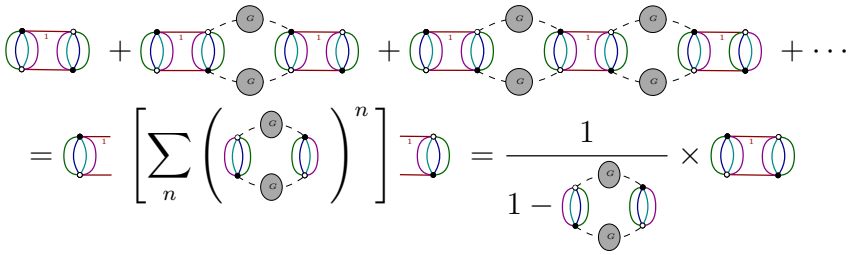
, (69)

where $\Sigma^{(n)}$ denote a contribution of order n for the self energy. Then, the two skeleton edges hooked to a vertex in the HS representation split him into two corners, to which some connected trees can be hooked. Summing over all possible trees we then reconstruct the effective 2-point function (55) to each corners between skeleton edges:



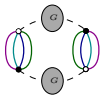
. (70)

The same structure may be repeated along the length of the skeleton. Then, summing over lengths, we get the first contribution to the 1PI 4-point function with melonic vertices on its boundaries:



(71)

This is formally the structure of the 4-point vertex. The effective loop of length two can be easily computed, and we get, once again in accordance with (34):



$$= -2\lambda_{4,1}\mathcal{A}_{4,2}\,. \tag{72}$$

Note that the factor 2 in front of this expression comes to the symmetry of the melonic vertices insertion. Figure (17) below provide us an illustration.

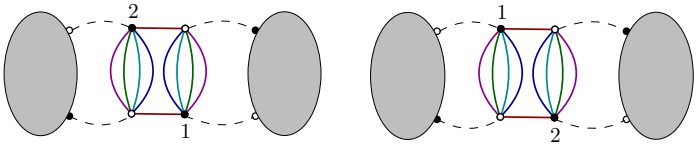
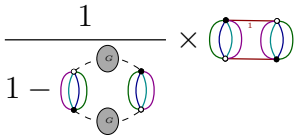


Figure 17: The two configurations for a melonic insertion. The black node labeled by 1 can be contracted on the right or on the left.

The translation of the final diagram (71) into equation is then straightforward, and we get:



$$= \frac{1}{1+2\lambda_{4,1}\mathcal{A}_{4,2}} \times 4\lambda_{4,1} = 2\Pi^{(2)}_{a,0}\,, \tag{73}$$

the last equality, coming from definition (59) completing the proof.

□

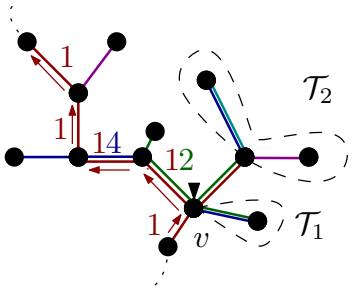
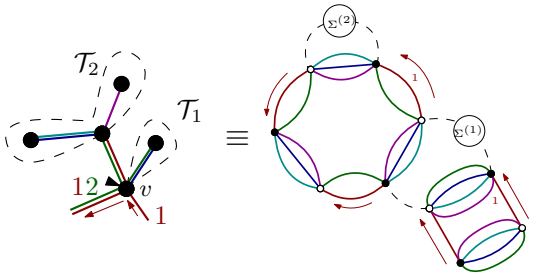


Figure 18: A skeleton with two pseudo-melonic insertion. The red arrows follow the path of the skeleton corresponding to the color 1, joining together the boundary melonic vertices.

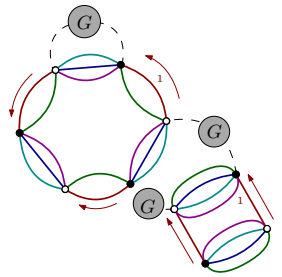
In addition to purely melonic configurations, we have to take into account bicolored edges insertions along the skeleton. Moreover from Figure (14)a, it is clear that all these bicolored insertions have to contain the color red in the pair. An example is pictured on Figure(18). Note that this constraint on the existence of a common color for the edges along the skeleton as well as the linear topology of the skeleton will be a precious help for enumeration of the different configurations.

Took into account bicolored insertions introduce another difficulty. Quartic pseudo melons are not the only source of bicolored edges. We have to take into account a new type of edge, coming from breaking edges. To understand how they occurs in the way of the skeleton, let us consider the example pictured on Figure (18). We have one breaking edge, with colors red and green (1 and 2), and following the same argument leading to equation (69) the contribution of the vertex labeled with v writes explicitly as:



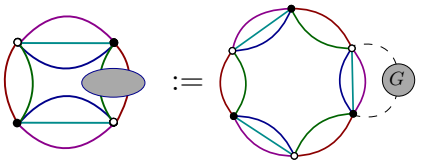
(74)

As a result, summing over all trees having the same skeleton, we get, as for equation (70):



(75)

We then observe that we have to distinguish two types of quartic pseudo-melons for the counting. The purely quartic pseudo-melonic interactions, that we call *type 1*, and the effective quartic pseudo-melonic interactions, arising from the contraction of a 6-point pseudo melon with an effective 2-point function, that we call *type 2* quartic pseudo-melon. We denote them by:



(76)

Type 2 vertices behaves like Type-1 ones. They have the same canonical dimension and the same boundary graph, the only difference comes from their respective weight. Nevertheless, in order to investigate the combinatorial structure of the skeleton, we have to sum over all repetitions of the same (type 1 or type 2) vertex, as for the melonic chain in equation (71). To this end, we introduce the zero momenta purely pseudo melonic effective skeleton

functions $\Pi^{(2)}_{d,1i}$, with $i \neq 1$, so that $\Pi^{(2)}_{d,1i}$ is a chain of pseudo melons of type 1 or 2 with intermediate colors $1i$. Obviously, such a configurations corresponds to the structure pictured on Figure (14)d, this is why we labeled these effective function with a lower index d. Figure (19) provides an example of tree with two cilia and a purely bicolored skeleton.

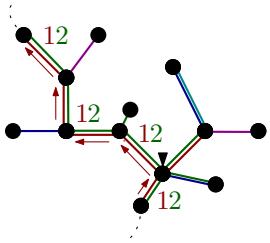


Figure 19: A typical contribution for $\Gamma^{(4)}_d$

Therefore we have an analogious lemma to lemma (3):

Lemma 4 *The zero momenta purely pseudo-melonic function $\Pi_{d,1i}$ has the following expression:*

$$\Pi^{(2)}_{d,12} := \frac{\pi_{d,1} + \pi_{d,2} + \pi_{d,1}\pi_{d,2}}{1 - \pi_{d,1}\pi_{d,2}}\,, \tag{77}$$

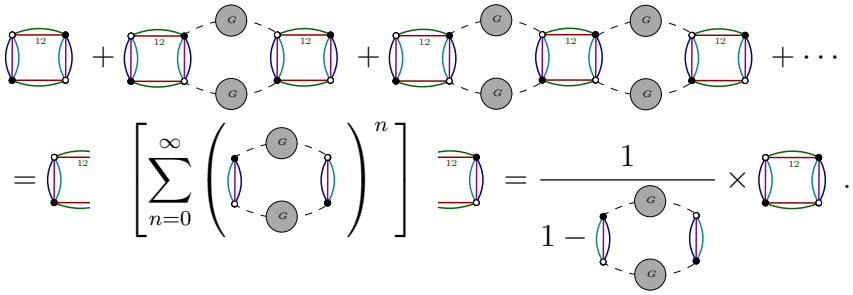
where the partial effective purely pseudo-melonic skeleton functions $\pi_{d,1}$ and $\pi_{d,2}$ are defined as:

$$\pi_{d,1} = \frac{2\lambda_{4,2}}{1 + 2\lambda_{4,2}\mathcal{A}_{3,2}} \qquad \pi_{d,2} = \frac{6\lambda_{6,1}\mathrm{b}}{1 + 6\lambda_{6,1}\mathrm{b}\,\mathcal{A}_{3,2}}\,, \tag{78}$$

with

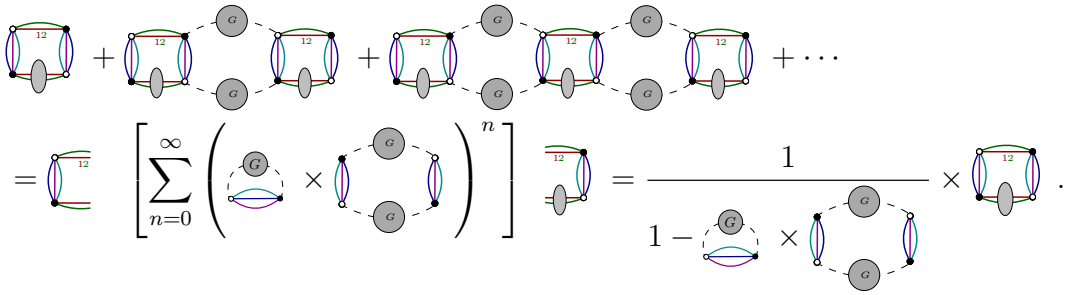
$$\mathrm{b} := \sum_{\vec{q}\in\mathbb{Z}^3} G(\vec{q})\,. \tag{79}$$

Proof. The graphs structure is very reminiscent to the pure melonic case. The essential difference comes from the fact that we have to distinguish two elementary building block configurations, respectively made of chains of type-1 and type–2 pseudo melons. For the first case, when elementary quartic type–1 pseudo-melons form a chain with zero momenta running thought the boundaries of the external faces, we have the formal sum :



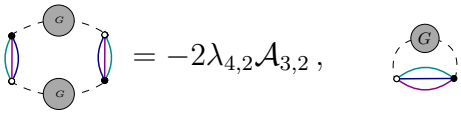
(80)

The second case is when type-2 pseudo-melonic interactions, coming from 3-valent vertices build a chain:



(81)

The two kernels in brackets must be computed explicitly. Introducing the function b it is easy to cheek:



(82)

so that the formal equations (80) and (81) leads to the two partial effective skeleton functions $\pi_{d,1}$ and $\pi_{d,2}$. Note the factor 2 occurring in the denominator of the formula has the same origin as the factor 2 occurring in expression (71): It comes from the symmetry exchange for the pseudo-melonic vertices. Moreover, the factor 3 in front of b comes from the rotational symmetry of the 3-valent vertices : there are 3 different ways to build a effective 4-dipole on a 3-valent vertex to obtain a type-2 quartic pseudo melon.

To obtain the complete 4-point kernel $\Pi_{d,1i}$, we then have to sum over all possible partitions of type-1 and type-2 domains. We have to distinguish three cases:

- The boundary vertices are both of type–1,
- The boudnary vertices are both of type–2,
- One boundary vertex is of type–1, the second of type–2.

For the two first ones cases, we have the sequences:

$$\pi_{d,1} + \pi_{d,1}\pi_{d,2}\pi_{d,1} + \pi_{d,1}\pi_{d,2}\pi_{d,1}\pi_{d,2}\pi_{d,1} + \cdots = \pi_{d,1}\sum_{n=0}^{\infty}(\pi_{d,2}\pi_{d,1})^n\,, \tag{83}$$

for type–1 boundary vertices, and

$$\pi_{d,2} + \pi_{d,2}\pi_{d,1}\pi_{d,2} + \pi_{d,2}\pi_{d,1}\pi_{d,2}\pi_{d,1}\pi_{d,2} + \cdots = \pi_{d,2}\sum_{n=0}^{\infty}(\pi_{d,2}\pi_{d,1})^n\,, \tag{84}$$

for type–2 boundaries. For the heteroclite boundaries however, fixing the ends vertices we get:

$$\pi_{d,1}\pi_{d,2} + \pi_{d,1}\pi_{d,2}\pi_{d,1}\pi_{d,2} + \cdots = \sum_{n=1}^{\infty}(\pi_{d,1}\pi_{d,2})^n\,. \tag{85}$$

All the sums can be easily computed as geometric progressions. Computing them, we finally get the effective skeleton function $\Pi_{d,12}$.

□

As we will see, a large part of contributions to the effective function $\Pi^{(2)}_{a,1}$ require the knowledge of the momentum-dependence of the effective pseudo-melonic function $\Pi^{(2)}_{d,12}(p_1,p_2;p'_1,p'_2)$. More precisely, because we are only interested for zero momenta 4-point functions, we consider the restriction $p_1 = p'_1 = 0$, $p_2 = p'_2 = p$:

$$\tilde{\Pi}^{(2)}_{d,12}(p) := \Pi^{(2)}_{d,12}(0,p;0,p)\,, \tag{86}$$

which can be easily deduced from the previous proof:

Corollary 3

$$\tilde{\Pi}^{(2)}_{d,12}(p) = \frac{\pi_{d,1}(p) + \pi_{d,2}(p) + \pi_{d,1}(p)\pi_{d,2}(p)}{1 - \pi_{d,1}(p)\pi_{d,2}(p)}\,, \tag{87}$$

where the momentum-dependents effective vertex functions $\pi_{d,1}(p)$ and $\pi_{d,2}(p)$ are defined as:

$$\pi_{d,1}(p) = \frac{2\lambda_{4,2}}{1 + 2\lambda_{4,2}\mathcal{A}_{3,2}(p)} \quad \pi_{d,2} = \frac{6\lambda_{6,1}\mathrm{b}(p)}{1 + 6\lambda_{6,1}\mathrm{b}(p)\,\mathcal{A}_{3,2}(p)}\,, \tag{88}$$

and:

$$\mathcal{A}_{3,2}(p) = \sum_{\vec{q}\in\mathbb{Z}^4} \delta_{q_2,p}\, G^2(\vec{q})\,, \qquad \mathrm{b} := \sum_{\vec{q}\in\mathbb{Z}^4} \delta_{q_2,p}\, G(\vec{q})\,. \tag{89}$$

From these elementary "pure" building blocs functions, we can easily deduce all the allowed configurations for each configurations on Figure (14)a, b and c, and the complete skeleton functions may be summarized with the following statement:

Proposition 7 *The complete zero momenta skeleton functions $\Pi^{(2)}_1$ and $\Pi^{(2)}_{2,12}$ are given in terms of the essential and marginal couplings $\lambda_{4,1}$, $\lambda_{4,2}$, $\lambda_{6,1}$ and effective 2-point function $G(\vec{p})$ as:*

$$\Pi^{(2)}_1 = \Pi^{(2)}_{a,0} + \frac{\Pi_{a,0}\,\mathcal{B}\,\Pi_{a,0}}{1 - \Pi_{a,0}\,\mathcal{B}} + (1+\bar{\mathcal{B}})\frac{\Pi_{a,0}\,\bar{\mathcal{B}}}{1 - \Pi_{a,0}\mathcal{B}} + \mathcal{D}\,, \tag{90}$$

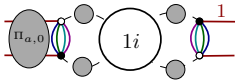
$$\Pi^{(2)}_{2,12} = \frac{\pi_{d,1} + \pi_{d,2} + \pi_{d,1}\pi_{d,2}}{1 - \pi_{d,1}\pi_{d,2}}\,, \tag{91}$$

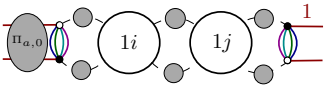
where $\mathcal{B}$, $\bar{\mathcal{B}}$ and $\mathcal{D}$ are respectively given by formulas (114), (118), (120).

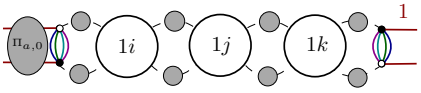
Proof. The components $\Pi^{(2)}_{d,12}$ and $\Pi^{(2)}_{a,0}$ have been computed and are given equations (67) and (77). To complete the proof , we then have to compute the components $\Pi^{(2)}_{a,1}$, $\Pi^{(2)}_b$ and $\Pi^{(2)}_c$. To this end, we will proceed step by step, computing each component separately.

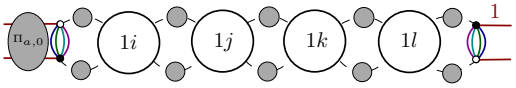
• *Computation of* $\Pi^{(2)}_{a,1}$.
The skeletons of trees contributing to $\Pi^{(2)}_{a,1}$ have melonic boundaries and common color on their edges, with at least one bicolored edge. The most general configuration corresponds to a succession of colored and bicolored edges; and to take into account all possible configurations, we introduce a new elementary building block replacing the purely melonic

pattern (70). This elementary building block is itself a sum of blocs, made of a succession of pure pseudo-melonic blocs between melonic boundaries. The first ones of these elementary building blocs are then:

$\mathcal{A}_{1i} :=$  , (92)

$\mathcal{A}_{1ij} :=$  , (93)

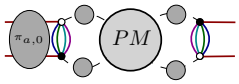
$\mathcal{A}_{1ijk} :=$  , (94)

$\mathcal{A}_{1ijkl} :=$  . (95)

$\cdots$

where the grey bubble represent the insertion of an effective purely melonic pattern $\Pi^{(2)}_{a,0}$, and the white bubbles represent the insertion of a pure bicolored pattern $\Pi^{(2)}_{d,1i}$ i.e. the color 1 (red on the figures) being common on melonic and pseudo-melonic insertions. The indices i, j, k and l are such that consecutive indices are different. There are then $d-1=4$ different ways to choose the first index i, and $d-2=3$ ways for all successive indices j, k, l, ...

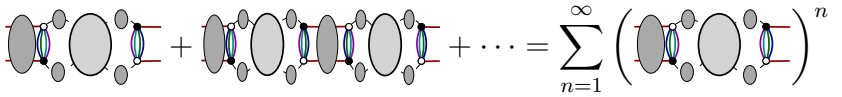
The value of each diagram being independent to the choice of the selected values for these indices, the complete elementary pattern including pseudo-melonic contributions may be written as:

 $\equiv \Pi_{a,0}\mathcal{B}\,,$ (96)

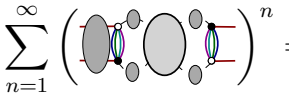
with:

$$\Pi_{a,0}\mathcal{B} := 4(\mathcal{A}_{12} + 3\mathcal{A}_{123} + 3^2\mathcal{A}_{1232} + 3^3\mathcal{A}_{12323} + \cdots)\,. \tag{97}$$

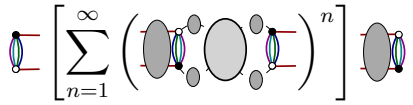
where the big grey bubble that we called "PM" denotes the sum of contributions coming from chains of pseudo-melonic interactions. As for the elementary purely melonics patterns (70), the same scheme can be repeated up to infinity, as in (71):

 , (98)

and the formal sum can be explicitly computed as a geometric progression, leading to:

 $= \dfrac{\Pi_{a,0}\,\mathcal{B}}{1-\Pi_{a,0}\,\mathcal{B}}\,.$ (99)

Finally the complete effective vertex function $\Gamma^{(4),1}_{a,1}$ having skeleton function $\Pi^{(2)}_{a,1}$ and completing (71) is decomposed as:

$\Gamma^{(4),1}_{a,1} =$  . (100)

Explicitly:

$$\Gamma^{(4),1}_{a,1}(\vec{0},\vec{0},\vec{0},\vec{0}) = 2 \times \left[\frac{\Pi_{a,0}\,\mathcal{B}\Pi_{a,0}}{1-\Pi_{a,0}\,\mathcal{B}}\right] . \tag{101}$$

Note that all the effective functions commute. We preserved their order to keep the structure of the diagrams. Moreover, note that the skeleton with length one has been included on the purely melonic contribution $\Pi^{(2)}_{a,0}$.

• *Computation of* $\Pi^{(2)}_b$ *and* $\Pi^{(2)}_c$.
The next contributions coming from Figure (14)b and c, and whose effective skeleton functions are respectively denoted as $\Pi^{(2)}_b$ and $\Pi^{(2)}_c$ can be computed in the same way. On Figure (20) we give a picture of typical trees contributing to each of these two functions.

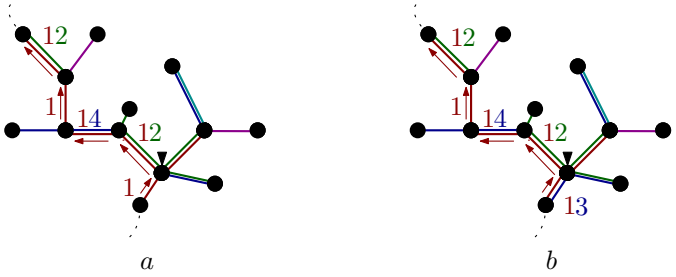


Figure 20: Typical contributions to $\Gamma^{(4)}_b$ (a) and $\Gamma^{(4)}_c$ (b).

Let us start with the computation of $\Pi^{(2)}_b$, whose building trees have a melon and a pseudo melon on their boundaries as on Figure (20)a. Obviously, the first edge have to be monocolored, and the ending edge have to be bicolored. The effective skeleton function then have to begin with an effective melon and end with an effective pseudo-melonic function, connecting together with an history involving all possible configurations of edges having a common color. The elementary pattern then connect together the effective boundaries. For the next term, the same pattern repeats, and we get the structure:

$$\sum_{i\neq 1} \quad + \sum_{i,j\neq 1} \quad + \cdots , \tag{102}$$

where the effective white pseudo-melonic vertex denoted as "PM" is nothing but that we called "PM" with a grey bubble, whose we have extracted a boundary pseudo-melonic vertex. Completing the series in (102), we then get:

$$\left[\sum_{n=0}\left(\sum_{i\neq 1}\right)^n\right]\sum_{i\neq 1} \quad . \tag{103}$$

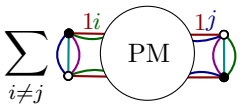
Obviously, the elementary building block in the bracket is nothing that we called $\Pi_{a,0}\mathcal{B}$ in equation (97). Moreover, the diagram on the right is nothing but this elementary building block amputated from its right external loop. We denote it as $\Pi_{a,0}\bar{\mathcal{B}}$:

$$\Pi_{a,0}\bar{\mathcal{B}} := \sum_{i\neq 1} \quad , \tag{104}$$

and we get:

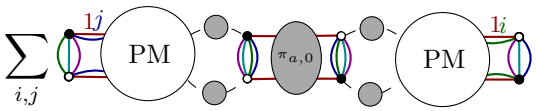
$$\Pi_b^{(2)} := \frac{\Pi_{a,0}\bar{\mathcal{B}}}{1-\Pi_{a,0}\mathcal{B}}\,. \tag{105}$$

Finally, for the computation of $\Pi_c^{(2)}$, we have to distinguish the pairs of colors of the boundary pseudo-melonic vertices. We will denote them as $(1i)$ and $(1j)$, we have to treat separately the case $i=j$ and the case $i\neq j$. For the case $i\neq j$, the elementary pattern must be the following, connecting together two effective pseudo-melonic functions of type $(1i)$ and $(1j)$:



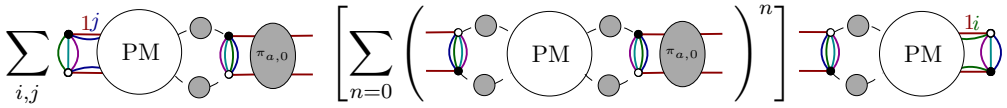
$$=: 2\mathcal{D}\,, \tag{106}$$

The white bubble being a sum over skeleton with pseudo-melonic interactions only. The factor 2 coming from $\mathrm{Sym}\mathcal{V}^{(4,1)\,i}_{\vec{0},\vec{0},\vec{0},\vec{0}}, = 2$ for zero external momenta.
This elementary pattern have to be completed with melonic insertions between the two effective boundaries, leading to the contribution:



. (107)

Note that, because of the melonic insertions, the external faces of colors i and j do not cross one in the other, and the constraint $i\neq j$ can be removed. The same structure can be repeated up to infinity and leading to the sum:



. (108)

then, the kernel $\Pi_c^{(2)}$ is written as:

$$\Pi_c = \mathcal{D} + \bar{\mathcal{B}}\,\Pi_b^{(2)}\,. \tag{109}$$

• *Computation of $\mathcal{B}$, $\bar{\mathcal{B}}$ and $\mathcal{D}$.*

To complete the proof we have to compute the kernels $\mathcal{B}$, $\bar{\mathcal{B}}$ and $\mathcal{D}$. Let us start with $\mathcal{B}$ defined in (97). The successive contributions in this equations i.e. $\mathcal{A}_{12}$, $\mathcal{A}_{123}$, ... can be easily expressed clearly. First of all, we get:

$$\mathcal{A}_{12} = \Pi_{a,0}^{(2)} \sum_p \mathcal{A}_{3,2}(p)\Pi_{2,12}^{(2)}(p)\mathcal{A}_{3,2}(p)\,. \tag{110}$$

Now, let $\mathcal{A}_{123}$ be a quantity obtained from gluing $\Pi_{d,12}$ and $\Pi_{d,13}$. In addition to the "short" faces of length two, coming from gluing of the two effective vertices, there are two long faces of effective length four, for colors 2 and 3, such that:

$$\mathcal{A}_{123} = \Pi_{a,0}^{(2)} \sum_{p,p'} \mathcal{A}_{3,2}(p)\Pi_{2,12}^{(2)}(p)\mathcal{C}(p,p')\Pi_{2,13}^{(2)}(p')\mathcal{A}_{3,2}(p')\,,$$

where we defined:

$$\mathcal{C}(p,p') := \sum_{\vec{q}\,\vec{q}'\in\mathbb{Z}^{d-1}} G^2(\vec{q})\delta_{q_2p}\delta_{q_3p'}\,. \tag{111}$$

Note that we have distinguished the indices on $\Pi^{(2)}_{2,12}(p)$ and $\Pi^{(2)}_{2,13}(p)$ for convenience; the structure of $\mathcal{C}$ took into account the strand structure of the diagram. Then, we may use the indice of $\Pi^{(2)}_{2,12}(p)$ only. Then, in the same way, for $\mathcal{A}_{1232}$, we get:

$$\mathcal{A}_{1232} = \Pi^{(2)}_{a,0} \sum_{p,p',p''} \mathcal{A}_{3,2}(p)\Pi^{(2)}_{2,12}(p)\mathcal{C}(p,p')\Pi^{(2)}_{2,12}(p')\mathcal{C}(p',p'')\Pi^{(2)}_{2,12}(p'')\mathcal{A}_{3,2}(p'')\,. \tag{112}$$

In order to write conveniently the general term, we introduce the compact matrix notation:

$$\mathcal{A}_{1232} = \Pi^{(2)}_{a,0} \sum_{p,p'} \mathcal{A}_{3,2}(p) \left[\Pi^{(2)}_{2,12}\,\mathcal{C}\,\Pi^{(2)}_{2,12}\,\mathcal{C}\,\Pi^{(2)}_{2,12}\right](p,p')\mathcal{A}_{3,2}(p'')\,. \tag{113}$$

The equation (97) becomes therefore :

$$\mathcal{B} = 4\Pi^{(2)}_{a,0} \sum_{p,p'} \mathcal{A}_{3,2}(p)\mathcal{K}(p,p')\mathcal{A}_{3,2}(p')\,, \tag{114}$$

with

$$\mathcal{K} := \Pi^{(2)}_{2,12}\left(1 + 3\mathcal{C}\,\Pi^{(2)}_{2,12} + (3\mathcal{C}\,\Pi^{(2)}_{2,12})^2 + \cdots\right) = \Pi^{(2)}_{2,12}(1 - 3\mathcal{C}\,\Pi^{(2)}_{2,12})^{-1}\,. \tag{115}$$

In the same way, we defined the function $\bar{\mathcal{B}}$ as $\mathcal{B}$ amputated to the right external loop as:

$$\bar{\mathcal{B}} := 4(\bar{\mathcal{A}}_{12} + 3\bar{\mathcal{A}}_{123} + 3^2\bar{\mathcal{A}}_{1232} + 3^3\bar{\mathcal{A}}_{12323} + \cdots)\,. \tag{116}$$

with:

$$\bar{\mathcal{A}}_{12} = \Pi^{(2)}_{a,0}\,\mathcal{A}_{3,2}\Pi^{(2)}_{2,12}\,, \tag{117}$$

$$\bar{\mathcal{A}}_{123} = \Pi^{(2)}_{a,0} \sum_{p} \mathcal{A}_{3,2}(p)\Pi^{(2)}_{2,12}(p)\mathcal{C}(p,0)\Pi_{d,13}\,,$$

such that, in a compact matrix form:

$$\bar{\mathcal{B}} = 4\Pi^{(2)}_{a,0} \sum_{p,p'} \mathcal{A}_{3,2}(p)\mathcal{K}(p,0)\,. \tag{118}$$

Finally, the last function that we have to compute is $\mathcal{D}$, build of chains of pseudo-melons of type-1 or type-2, such that the boundaries are of type $(1i)$ and $(1j)$ with $i \neq j$. It can be easily deduced from decomposition (97), keeping only the contributions having such a boundary. We get:

$$\mathcal{D} = 4 \times 3 \left[\Pi^{(2)}_{2,12}\mathcal{C}\,\Pi^{(2)}_{2,12}\,\left(1 + 2\,(\mathcal{C}\,\Pi^{(2)}_{2,12}) + (2\,\mathcal{C}\,\Pi^{(2)}_{2,12})^2 + \cdots\right)\right](0,0)\,, \tag{119}$$

which can be computed as formula (115):

$$\mathcal{D} = 12 \left[\Pi^{(2)}_{2,12}\mathcal{C}\,\Pi^{(2)}_{2,12}\,\left(1 - 2\,(\mathcal{C}\,\Pi^{(2)}_{2,12})\right)^{-1}\right](0,0)\,. \tag{120}$$

□

The *renormalization conditions* impose the values of zero-momenta couplings. They define the asymptotic couplings in the IR, that is given for $s \to -\infty$, so that:

$$\Pi^{(2)}_{1}(s \to -\infty) = 2\lambda^{r}_{4,1}\,, \tag{121}$$

$$\Pi^{(2)}_{2,12}(s \to -\infty) = 2\lambda^{r}_{4,2}\,, \tag{122}$$

the upper index r for "renormalized" referring to the finitness of the corresponding quantities in the continuum limit $\Lambda \to \infty$. Note that this is not obvious, because some quantities like b and $\mathcal{A}_{mn}$ are divergent. The finitess of the limit is guarantee from renormalizability of the theory. In practice, counter-terms may be defined in order to ensure the finitness of the effective skeleton function for arbitrary s, from deep UV. In this intermediate regime, these functions define *effective couplings* at scale s:

Definition 21 *The effective essential and marginal couplings at scale s, $\lambda_{4,1}(s)$ and $\lambda_{4,2}(s)$, respectively associated to the quartic melonic and quartic pseudo-melonic interactions are defined as*

$$\Pi^{(2)}_{1}(s) = 2\lambda_{4,1}(s)\,, \tag{123}$$

and:

$$\Pi^{(2)}_{2,12}(s) = 2\lambda_{4,2}(s)\,. \tag{124}$$

Note that in this equations, we introduce the explicit dependence on s for effective vertex functions. This dependence come from their definition, and have been left without all confusion in the hope to simplify the notations.

4.2.2 Six and eight point effective vertices

The equations for LO 4-point function is obtained above. We have to compute the same equations for 6 and 8-point effective vertices in this section. We will investigate successively the effective 6 and 8-points vertices having melonic, pseudo-melonic or intertwining boundary graphs. Indeed, we will see that, in addition to the melonic and pseudo-melonic boundaries, we get mixing boundaries, having intermediate canonical dimensions between melons and pseudo-melons as mentioned in our introduction. These mixing boundaries corresponds to connected sums of elementary quartic melons and/or pseudo-melons, with colors respecting the LO tadpole deletions leading to 6 and 8 points function from LO 4-point functions. We will detail all of them for each cases. However before starting this investigation, let make a remark about the existence of mixing configurations. An elementary example, corresponding to the connected sum of a quartic melon and a quartic pseudo-melon is given on Figure(22) b, and it is easy to see that it comes from the contraction of a 0-dipole between two vertices, as pictured on Figure (21).

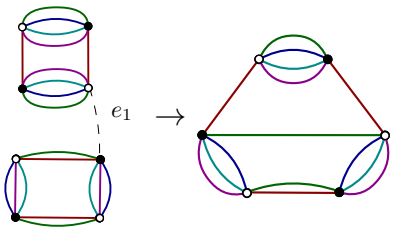
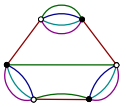


Figure 21: Contraction of a zero dipole e_1 between a melonic vertex and a pseudo-melonic vertex. The contraction leads to the intertwining diagram on right.

Then, even if the initial theory space is a direct sum $\mathcal{S}_M \oplus \mathcal{S}_{PM}$, the theory space does not remains along this subspace under the renormalization group flow. A new type of graphs arise in the theory space, mixing melons and pseudo-melons, and having intermediate power counting between them. Schematically:

$$\text{“}\frac{d}{ds}\left(\mathcal{S}_M \oplus \mathcal{S}_{PM}\right) = \mathcal{S}_M \oplus \mathcal{S}_{PM} \oplus \left\{ \quad + \cdots \right\}\text{”} \tag{125}$$



As for 4-point functions, the LO 6-point function are obtained from deletion of melonic or pseudo-melonic tadpole along the boundary of an external face from a LO 4-point graphs. Then, the allowed boundaries for LO graphs may be all deduced from the four leading order configurations pictured on Figure (14), and it is easy to see from the deletion procedure that there are only four allowed boundaries for LO graphs, see Figure (22).

The first graph of Figure (22) denoted by (a) is an element of the non-branching melonic family, obtained as connected sum of two identical quartic melons[9]. The second one (b) is a branching melon graph, obtained from Figure (14)b opening a melonic tadpole on the boundary of the green external face, whose ends points are hooked on the pseudo-melonic opened boundary vertex. The last diagram (d) corresponds to the non-branching pseudo-melonics, obtained as connected sum of two identical quartic pseudo-melons. Finally, the boundary graph of type (c) corresponds to the intertwining graphs, obtained from Figure (14)d.

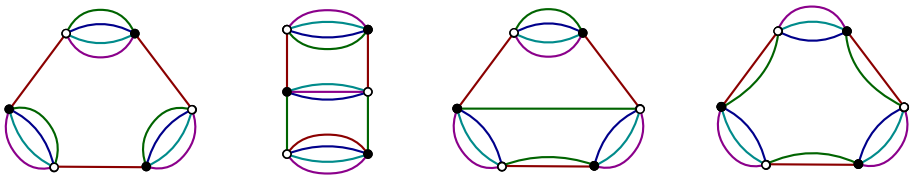


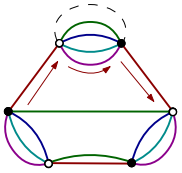
Figure 22: The four possible LO boundary graphs for melonic, pseudo-melonic and intertwining graphs. A non-branching 3-valent melon (a), a 3-valent branching melon (b), a non-branching pseudo-melon (d) and an intertwiner diagram (c). The canonical dimensions are also indicated.

However, from deletion of three melonic and/or pseudo-melonic tadpole, it is easy to cheek that the connectivity of the external faces allows three configurations and all of these are pictured on Figure (22). The first one (a) corresponds to a non-branching melon. The last one (c) corresponds to a non-branching pseudo-melon. The intermediate one (b) however, corresponds to the connected sum of a quartic melon and a quartic pseudo-melon, and intertwine between the two sectors. It is clear from the canonical dimensions, indicated

[9]As for pseudo-melons, non-branching melons are obtain as connected sums of the same elementary quartic melon. These graphs are described in [56],[59].

on Figure (22). Note that we have to take into account the intermediate diagram for the computation of the the flow equations, due to the fact that the leading contraction building from a 4-dipole has a quartic pseudo-melon as boundary graph.

The intertwining configurations are relevant for our analysis. Indeed, we will use two kind of equations in the next section: The flow equation (19) in order to compute the evolution of the essential and marginal couplings; and the Ward identities, to compute the first derivative with respect to the external momenta of the effective vertex functions, involved in the computation of the anomalous dimension. In any cases, all our computations involves a single effective loop, and our restriction in the deep UV sector requires to consider only the LO contractions i.e. having the maximal degree of divergences, as relevant contributions for the flow of the couplings and the value of the anomalous dimension. Then, even is its canonical dimension is smaller than the one of the pseudo-melon on Figure (22) d, the graph on Figure (22) c will contribute to the flow of the quartic pseudo-melonic coupling, and have to be retain as a relevant contribution on the Ward identity. Indeed, it compensates its lack of canonical dimension with a melonic "pole", allowing to create a 4-dipole. For instance, the following graph



, (126)

has power counting $\omega = -2+4-1 = 1$, and it is easy to cheek that its boundary graph is a quartic pseudo-melon. The same behavior will be arise for 8-point functions, for which we will only retains those LO 6-points non-branching pseudo-melon after one-loop contraction.

Let us start with non-branching melonic 6-point effective vertices. As for 4-point functions, the 6-point effective vertex have to be a sum indexed with the color of its external face, being as well the color of the skeleton in the corresponding tree in HS representation.

$$\Gamma^{(6)}_{s\,,\mathrm{a},\ \mathrm{melo}}(\{\vec{p}_j\}) = \sum_{i=1}^{d} \Gamma^{(6)\,i}_{s\,,\mathrm{a},\ \mathrm{melo}}(\{\vec{p}_j\})\,, \tag{127}$$

the index a referring to the Figure (22) a. For the 4-point functions, we seen that the LO graphs are trees organized around a skeleton having the topology of a line. For the 6-point functions, the skeleton will be a *tripod*, with three *arms* hooked to a common vertex. More precisely, investigating the structure of 3-cilialted trees with skeleton of color 1, we get two type of tripods, distinguished both on Figure (23). In the first one case (a), the three arms of color 1 hooked to the three opened tadpoles and are fully hooked on the same vertex v with non-breaking edges. In the second case (b), the three arms are hooked to the same vertex v from a common breaking edge. As for 4-point functions, we can fix the size of the tripod skeleton and sum over trees having such a skeleton, relaxing in a second time the length of the different arms. Precisely as for the 4-point functions, we define the zero-momenta melonic *effective tripod function* $\Pi^{(3)}_{1,a}$ as:

$$\Gamma^{(6)\,i}_{s\,,\mathrm{a,melo}}(\vec{0},\vec{0},\vec{0},\vec{0},\vec{0},\vec{0}) =: 3!\,\Pi^{(3)}_{1,a}\,, \tag{128}$$

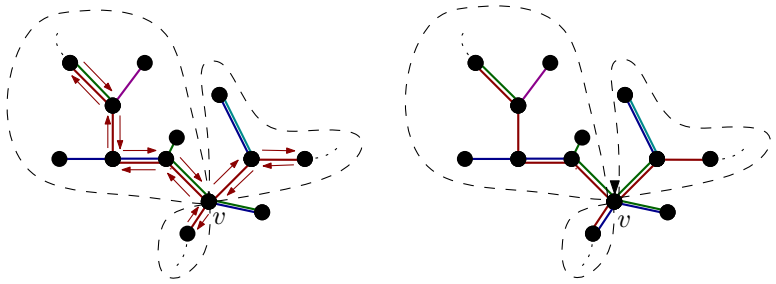


Figure 23: Typical tree configurations contributing to the LO 6-point functions with melonic boundaries. In (a), the three arms of the red skeleton are hooked on the same vertex v from non-breaking edges. In (b), they are hooked to v with a common breaking edge.

Similarly, effective vertex having boundaries of type (b) and (c) on Figure (22) may be denoted by $\Gamma^{(6)\,ij}_{s\,,\mathrm{b,melo}}$ and $\Gamma^{(6)\,ij}_{s\,,\mathrm{c,inter}}$ and both these contributions depend on a pair of indices. We define the corresponding effective skeleton functions as:

$$\Gamma^{(6)\,ij}_{s\,,\mathrm{b,melo}}(\vec{0},\vec{0},\vec{0},\vec{0},\vec{0},\vec{0}) =: 3!\,\Pi^{(3)}_{1,b}\,, \tag{129}$$

$$\Gamma^{(6)\,ij}_{s\,,\mathrm{c,inter}}(\vec{0},\vec{0},\vec{0},\vec{0},\vec{0},\vec{0}) =: 3!\,\Pi^{(3)}_{1,c}\,. \tag{130}$$

and we have the following statement:

Proposition 8 *The effective zero-momenta tripod functions $\Pi^{(3)}_{1,a}$, $\Pi^{(3)}_{1,b}$ and $\Pi^{(3)}_{1,b}$ are expressed in term of the essential and marginal couplings as*[10]*:*

$$\Pi^{(3)}_{1,a} = 8\left\{\left(\lambda^3_{4,1}(s)\mathcal{A}_{4,3} + 12\lambda^2_{4,1}(s)\lambda_{4,2}(s)\mathcal{A}_{3,3} + 36\lambda^2_{4,2}(s)\lambda_{4,1}(s)\mathcal{A}_{2,3} + 24\lambda^3_{4,2}(s)\mathcal{A}_{1,3}\right) - 12\lambda^3_{4,1}(s)\sum_{p\in\mathbb{Z}}\lambda_{6,1}(p,s)(\mathcal{A}_{3,2}(p))^3 + 12\lambda_{6,1}(s)\lambda^2_{4,1}(s)(\mathcal{A}_{3,2})^2\right\}, \tag{131}$$

$$\Pi^{(3)}_{1,b} = 3!\times 8\left\{2\lambda^2_{4,1}(s)\lambda_{4,2}(s)\mathcal{A}_{3,3} + 3\lambda_{6,1}(s)\lambda^2_{4,1}(s)(\mathcal{A}_{3,2})^2\right\}, \tag{132}$$

$$\Pi^{(3)}_{1,c} = 3!\times\left\{8\lambda_{4,1}(s)\lambda^2_{4,2}(s)\mathcal{A}_{3,3} + 24\lambda^3_{4,2}(s)\mathcal{A}_{2,3} - 6\lambda_{4,1}(s)\lambda_{6,1}(s)\mathcal{A}_{3,2})\right\}. \tag{133}$$

where $\lambda_{4,1}(s)$, $\lambda_{4,2}(s)$ and $\lambda_{6,1}(s)$ are effective couplings at scale s and $\lambda_{6,1}(p,s)$ is the p dependent effective coupling a the momentum p given by:

$$\begin{aligned}\lambda_{6,1}(p,s) &= \left(\frac{\lambda_{6,1}(s) - \frac{4}{3}\lambda^3_{4,2}(s)\mathcal{A}_{3,3}}{1 - 3!\lambda_{4,2}(s)\mathcal{A}_{3,2} + 12\lambda^2_{4,2}(s)\mathcal{A}^2_{3,2} - 8\lambda^3_{4,2}(s)\mathcal{A}^3_{3,2}}\right)\Big(1 - 3!\lambda_{4,2}(s)\mathcal{A}_{3,2}(p)\\ &+ 12\lambda^2_{4,2}(s)\mathcal{A}^2_{3,2}(p) - 8\lambda^3_{4,2}(s)\mathcal{A}^3_{3,2}(p)\Big) + \frac{4}{3}\lambda^3_{4,2}(s)\mathcal{A}_{3,3}(p)\end{aligned} \tag{134}$$

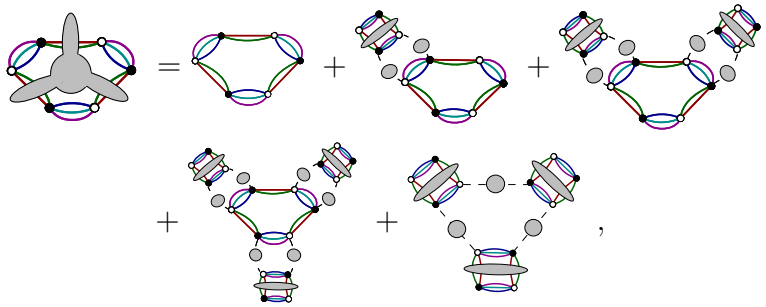
[10]note that, as for 4-point functions, the upper index 3 refers to the number of cilia.

In order prove this statement, we have to consider the intermediate result about effective non-branching pseudo-melonic functions:

Lemma 5 *The bare coupling $\lambda_{6,1}$ may be expressed in term of the effective essential and marginal effective pseudo-melonic couplings at scale s as:*

$$\lambda_{6,1} = \frac{\lambda_{6,1}(s) - \frac{4}{3}\lambda_{4,2}^3(s)\mathcal{A}_{3,3}}{1 - 3!\lambda_{4,2}(s)\mathcal{A}_{3,2} + 12\lambda_{4,2}^2(s)\mathcal{A}_{3,2}^2 - 8\lambda_{4,2}^3(s)\mathcal{A}_{3,2}^3}\,. \tag{135}$$

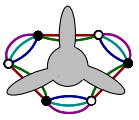
Proof. As for the trees having melonic boundary, the LO trees contributing to the effective tripod function $\Pi^{(3)}_{2,ij}$ split into two families: the trees whose three arms are hooked to a common vertex, and the trees whose arms are hooked to a common breaking edge corresponding to the boundary graph of the global tree. Listing all the possible LO configurations, we get :



(136)

where the first term with grey bubble represent the effective 6-point vertex having pseudo-melonic boundary with fixed bicolored edges (red and green on the figure):

$$\Gamma^{(6)\,ij}_{s\,,\text{pseudo-melo}}(\vec{0},\vec{0},\vec{0},\vec{0},\vec{0},\vec{0}) \equiv \tag{137}$$



the function $\Gamma^{(6)\,ij}_{s\,,\text{melo}}$ being defined such that the effective vertex function for pseudo-melonic boundaries is written as $\Gamma^{(6)}_{s\,,\text{pseudo-melo}} = \sum_{j<i}\Gamma^{(6)\,ij}_{s\,,\text{pseudo-melo}}$. The function $\Gamma^{(6)\,ij}_{s\,,\text{pseudo-melo}}$ may be then computed directly from renormalization conditions for 4-point functions (122). Taking into account the symmetry factors, we get:

$$\begin{aligned}\Gamma^{(6)\,ij}_{s\,,\text{pseudo-melo}} = (3!)^2\lambda_{6,1}\left[1 - 3!\lambda_{4,2}(s)\mathcal{A}_{3,2} + 2\times 3!\lambda_{4,2}^2(s)\mathcal{A}_{3,2}^2 - 2^3\lambda_{4,2}^3(s)\mathcal{A}_{3,2}^3\right]\\ + 3!2^3\lambda_{4,2}^3(s)\mathcal{A}_{3,3}\,.\end{aligned} \tag{138}$$

Note that the symmetry factors as well as relative signs may be easily understood and computed considering the first terms of the perturbative expansion, and identifying them with the corresponding terms in this expansion. Moreover, note that we reintroduced the variable s to make difference between effective and bare couplings. Defining the effective tripod skeleton function $\Pi^{(3)}_{2,ij}$ as:

$$\Gamma^{(6)\,ij}_{s\,,\text{pseudo-melo}} = (3!)^2\Pi^{(3)}_{2,ij}. \tag{139}$$

With the renormalization conditions, we provide new definition, which completes the previous definition (21):

Definition 22 *The effective marginal coupling $\lambda_{6,1}(s)$ at scale s is defined as:*

$$\Pi^{(3)}_{2,ij} = \lambda_{6,1}(s)\,, \qquad \Pi^{(3)}_{2,ij}(s \to -\infty) = \lambda^r_{6,1}\,, \tag{140}$$

we get the equality:

$$\lambda_{6,1}(s) = \lambda_{6,1}\left[1 - 3!\lambda_{4,2}(s)\mathcal{A}_{3,2} + 2\times 3!\lambda^2_{4,2}(s)\mathcal{A}^2_{3,2} - 2^3\lambda^3_{4,2}(s)\mathcal{A}^3_{3,2}\right] + \frac{4}{3}\lambda^3_{4,2}(s)\mathcal{A}_{3,3}\,. \tag{141}$$

which ends the proof.

□

However, using the lemma (5), we are able to provide the proof of proposition (8).

Proof of proposition (8).
We will proceed as for the proof of the previous lemma, listing all the allowed configurations compatible with the corresponding boundary diagram, pictured on Figure (22)a. As explained before, we have to distinguish the case when the three arms are hooked to the same vertex, and the case when the three arms are hoked to a common breaking edge, having a common color with the three arms hooked to him. These two configurations are pictured on Figure (23). However, the classification have to be refined from lemma (5). Indeed, among the configurations of type (23)a, some of them are made with a tripod kernel having a pseudo-melonic boundary graph, and allows to build an effective breaking edge to which are hooked three arms. This kernels are nothing that the fourth contribution in the equation (136). Added it to the other ones having a common breaking edge for the three arms, we build an effective 6-point vertex having pseudo-melonic boundary, with melonic arms hooked to him, corresponding to effective melonic 4-point functions. It is easy to cheek that all allowed configurations are those pictured on Figure (24), the configurations (e) and (f) having a kernel corresponding to an effective pseudo-melonic function. Taking into account the respective canonical dimensions for each effective insertions, it is easy to see that all these configurations have the same power-counting, $\omega = -2$, in accordance with the expected canonical dimension for 3 valent melonic bubbles given equation (50) . From renormalization conditions (121), (122) and (140); and taking into account relative signs and symmetry factors considering the first terms of the perturbative expansion, we get:

$$\Gamma^{(6)\,i}_{s\,,\mathrm{a},\,\mathrm{melo}} = 3!\times 8\left\{\left(\lambda^3_{4,1}(s)\mathcal{A}_{4,3} + 12\lambda^2_{4,1}(s)\lambda_{4,2}(s)\mathcal{A}_{3,3} + 36\lambda^2_{4,2}(s)\lambda_{4,1}(s)\mathcal{A}_{2,3}\right.\right.$$
$$\left.\left. + 24\lambda^3_{4,2}(s)\mathcal{A}_{1,3}\right) - 12\lambda^3_{4,1}(s)\sum_{p\in\mathbb{Z}}\lambda_{6,1}(p,s)(\mathcal{A}_{3,2}(p))^3 + 12\lambda_{6,1}(s)\lambda^2_{4,1}(s)(\mathcal{A}_{3,2})^2\right\}. \tag{142}$$

We then deduce the expression of $\Pi^{(3)}_{1,a}$ for definition (128).

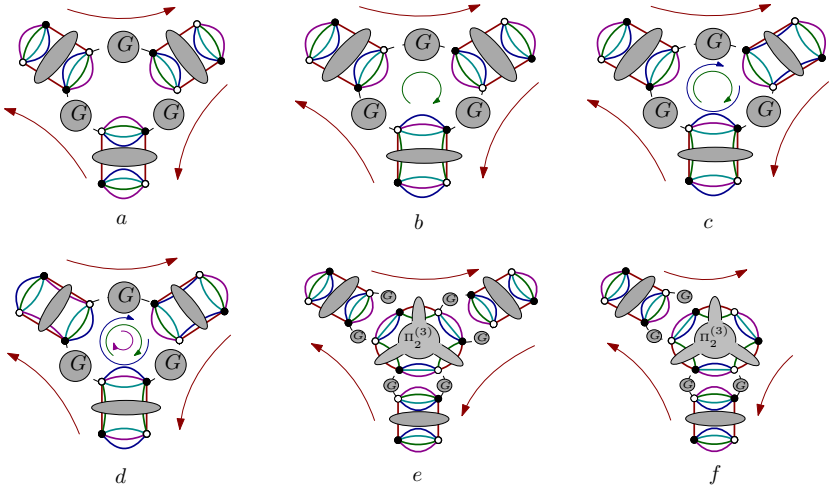


Figure 24: All the possible configurations having a non-branching melon as boundary graph. The grey bubbles denotes effectives vertices whose boundaries graphs are explaned. The trajectories of the external faces running in the interior of the diagrams are pictured with colored arrows.

In the same way, the configurations contributing to effective 6-point vertex functions having branching melonic and intertwining boundaries can be easily obtained from a list of all allowed configurations. As for the previous case, some of these contributions can be resumed as effective pseudo-melonic effective vertices, such that the relevant LO contributions for each case are pictured on Figure (25) and Figure (26) below.

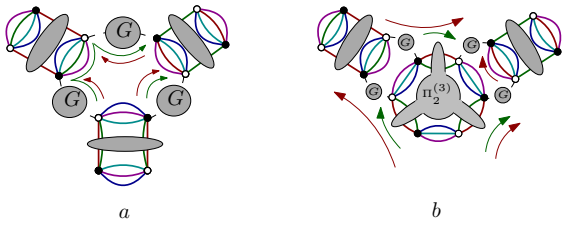


Figure 25: Two configurations contributing to the 6-point effective vertices having branching melonic boundaries.

Expressing this relationship in detail, we get for zero external momenta effective functions:

$$\Gamma^{(6)\,ij}_{s\,,\mathrm{b,melo}} = (3!)^2 \times 8 \left\{ 2\lambda^2_{4,1}(s)\lambda_{4,2}(s)\mathcal{A}_{3,3} + 3\lambda_{6,1}(s)\lambda^2_{4,1}(s)(\mathcal{A}_{3,2})^2 \right\} , \tag{143}$$

for branching melonic boundaries, and :

$$\Gamma^{(6)\,ij}_{s\,,\mathrm{c,inter}} = (3!)^2 \times \left\{ 8\lambda_{4,1}(s)\lambda^2_{4,2}(s)\mathcal{A}_{3,3} + 24\lambda^3_{4,2}(s)\mathcal{A}_{2,3} - 6\lambda_{4,1}(s)\lambda_{6,1}(s)\mathcal{A}_{3,2}) \right\} , \tag{144}$$

for intertwining boundaries.

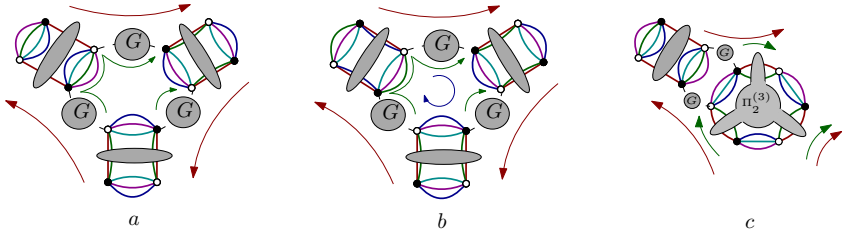


Figure 26: Three configurations contributing to the intertwining 6-point effective vertices.

□

Let us now focus on the leading order 8-point functions. They can be obtained as for 4 and 6 point function from deleting a new tadpole in the boundary of an opened face running through the interior of the diagrams. Once again all the 8-point function can be classified from their power-counting and their boundary graphs. Moreover, in the flow equations, the melonic interactions becomes closed from 6-point functions. Then, the 8-point functions are relevant only to close the pseudo-melonic interactions. As a result, only the leading order functions having a boundary graph whose one-loop contraction leads to a pseudo-melonic boundary will contribute in our flow equations. Figure (28) provides us an example.

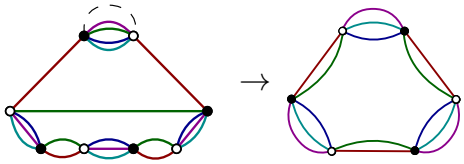
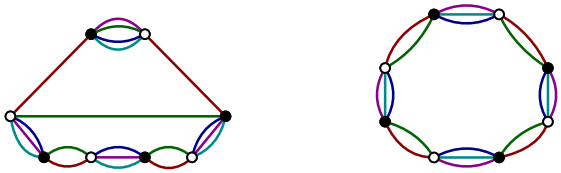


Figure 27: One-loop contraction on the melonic "pole" in a 8-point boundary graph. The corresponding 8-point function has divergent degree bounded as $\omega = -2$. The created 4-dipole then increases it of 2; so that the global scaling becomes $\omega + 2 = 0$.

From these considerations, it is easy to cheek that there are only two relevant boundaries for leading order 8 points graphs, pictured on Figure (28) below.



$d = -2$ $\qquad$ $d = -1$

a $\qquad$ b

Figure 28: Allowed boundaries for relevant 8-point functions with their respective canonical dimensions. As for 6-point boundaries, type (a) intertwine between melons and pseudo-melons and have a single melonic "pole", whereas type (b) is a purely non-branching 8-point graph.

In both cases, the corresponding 8-point functions are labeled with a pair of indices:

$$\Gamma^{(8)}_{s\,,\text{pseudo-melo}} = \sum_{j<i} \Gamma^{(8)\,,ij}_{s\,,\text{pseudo-melo}}\,, \qquad \Gamma^{(8)}_{s\,,\text{inter}} = \sum_{j<i} \Gamma^{(8)\,,ij}_{s\,,\text{inter}}\,, \tag{145}$$

and we define their respective zero momenta skeleton functions as:

$$\Gamma^{(8)\,,ij}_{s\,,\text{inter}} =: 4!\Pi^{(4)}_1\,, \quad \Gamma^{(8)\,,ij}_{s\,,\text{pseudo-melo}} =: 4!\Pi^{(4)}_2\,. \tag{146}$$

As for 6-point functions, there are essentially two different configurations for the four arms of the skeleton:

1. The four arms hooked to external deleted pseudo-melonic tadpole can be hooked to the same vertex.

2. The four arms can be hooked to form effective tripods, hooked together with a common bicolored path.

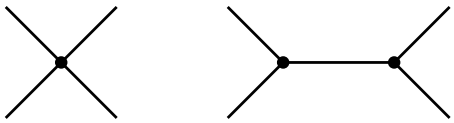


Figure 29: Two allowed topology for configurations of the four arms of the leading order 8-point functions. In the case (1), the four arms are hooked to the same vertex. In the case (2), the arms form effective tripods, hooked together with a bicolored path.

Figure (30) provides some examples of trees corresponding to these two configurations for the pseudo-melonic boundary. The first one (a) correspond to the configuration (1): The four arms of the bicolored skeleton are hooked to the same vertex. The second (b) and third (c) both correspond to the configuration (2): The four arms are organized as two 3-valent tripods and are hooked together with a common bicolored path.

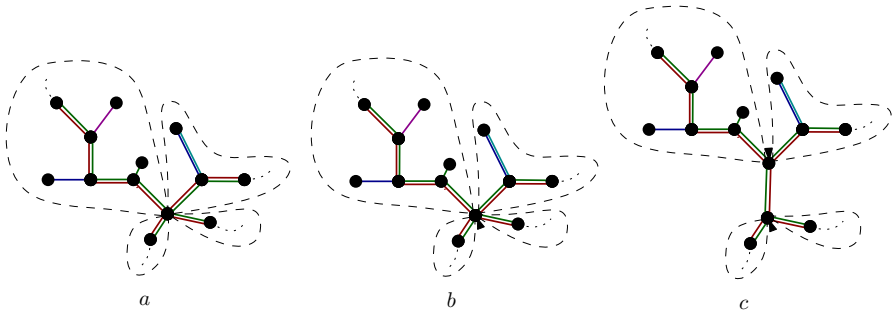


Figure 30: Three configurations for the arms of the four skeletons. In (a), the four arms are hooked to the same vertex. In (b) two arms are hooked to the same breaking edge. In (c) the two remaining edges are hooked to another common breaking edge.

We have the following statement:

Proposition 9 *The zero-momenta skeleton functions* $\Pi_1^{(4)}$ *and* $\Pi_2^{(4)}$ *are given in terms of essential and marginal effective couplings at scale* s, $\lambda_{4,1}(s)$, $\lambda_{4,2}(s)$ *and* $\lambda_{6,1}(s)$ *as:*

$$\begin{aligned}\Pi_1^{(4)} =& -\frac{4!2^4}{3!}\lambda_{4,2}^3\lambda_{4,1}\mathcal{A}_{3,4} - \frac{(4!)^2}{3!}\Pi_{1,c}^{(3)}\lambda_{4,2}^2(s)\mathcal{A}_{3,3} + \lambda_{6,1}(s)\lambda_{4,2}(s)\lambda_{4,1}(s)\mathcal{A}_{3,3} \\ &+ \frac{4!}{2}\Pi_{1,c}^{(3)}\frac{\lambda_{6,1}(s) - \frac{4}{3}\lambda_{4,2}^3(s)\mathcal{A}_{3,3}}{1 - 3!\lambda_{4,2}(s)\mathcal{A}_{3,2} + 12\lambda_{4,2}^2(s)\mathcal{A}_{3,2}^2 - 8\lambda_{4,2}^3(s)\mathcal{A}_{3,2}^3} \\ &\times\left(1 - 4\lambda_{4,2}(s)\mathcal{A}_{3,2} + 4\lambda_{4,2}^2(s)\mathcal{A}_{3,2}^2\right), \end{aligned} \tag{147}$$

$$\Pi_2^{(4)} = -\frac{9\times 4!}{2}\lambda_{6,1}(s)\frac{\lambda_{6,1}(s) - \frac{4}{3}\lambda_{4,2}^3(s)\mathcal{A}_{3,3}}{1 - 3!\lambda_{4,2}(s)\mathcal{A}_{3,2} + 12\lambda_{4,2}^2(s)\mathcal{A}_{3,2}^2 - 8\lambda_{4,2}^3(s)\mathcal{A}_{3,2}^3}$$
$$\times \left(1 - 4\lambda_{4,2}(s)\mathcal{A}_{3,2} + 4\lambda_{4,2}^2(s)\mathcal{A}_{3,2}^2\right) - 2^4\lambda_{4,2}^4(s)\mathcal{A}_{3,4} + \frac{4!}{2}\lambda_{6,1}(s)\lambda_{4,2}^2\mathcal{A}_{3,3}\,. \qquad (148)$$

Proof.
Like for 4 and 6 point functions, we have to list all leading order configurations and, for each of them, compute their respective boundaries graphs and their divergent degrees. From this analysis, and taking into account effective summations like for 6-points graphs, we easily cheek that there are only five configurations whose complete set is given on Figure (31), having pseudo-melonic boundary graph.

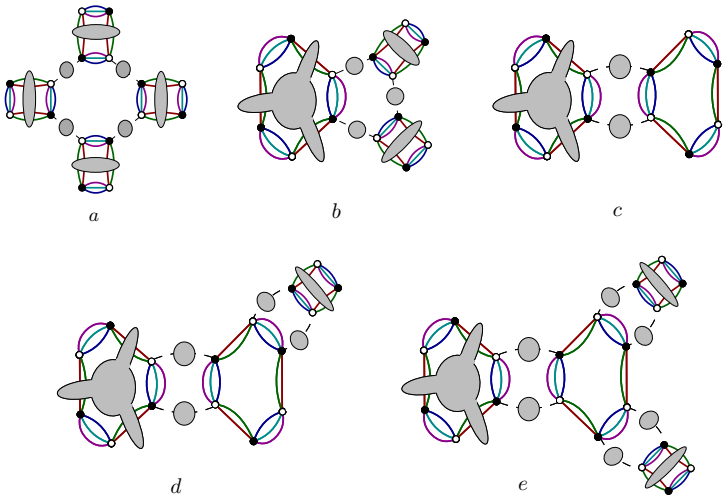


Figure 31: The three leading order configurations for 8-point functions having non-branching pseudo melonic boundaries.

The two first ones configurations (a) and (b) can be easily computed from renormalization conditions (121), (122) and (140), and symmetry factors as well as the relative signs may be fixed from comparison with lowest orders of the perturbative expansion. The three remaining configurations (c), (d) and (e) require to be careful checked on the counting procedure. We get explicitly, using lemma (5):

$$\Gamma^{8,ij}_{s\,,\text{pseudo-melo}} = -\frac{9\times (4!)^2}{2}\lambda_{6,1}(s)\frac{\lambda_{6,1}(s) - \frac{4}{3}\lambda_{4,2}^3(s)\mathcal{A}_{3,3}}{1 - 3!\lambda_{4,2}(s)\mathcal{A}_{3,2} + 12\lambda_{4,2}^2(s)\mathcal{A}_{3,2}^2 - 8\lambda_{4,2}^3(s)\mathcal{A}_{3,2}^3}$$
$$\left(1 - 4\lambda_{4,2}(s)\mathcal{A}_{3,2} + 4\lambda_{4,2}^2(s)\mathcal{A}_{3,2}^2\right) - 4!2^4\lambda_{4,2}^4(s)\mathcal{A}_{3,4} + \frac{(4!)^2}{2}\lambda_{6,1}(s)\lambda_{4,2}^2\mathcal{A}_{3,3}\,. \qquad (149)$$

Then the expression of $\Pi_2^{(4)}$ can be derived easily.

Moving on to the configurations having intertwining boundaries, it is easy to cheek that the only ones allowed such a boundaries are pictured on Figure (32) below; and the

corresponding zero momenta 8-point function writes as:

$$\Gamma^{(8)\,ij}_{s\,,\text{inter}} = -\frac{(4!)^2 2^4}{3!}\lambda^3_{4,2}\lambda_{4,1}\mathcal{A}_{3,4} - \frac{3(4!)^2 2^3}{3!}\Pi^{(3)}_{1,c}\lambda^2_{4,2}(s)\mathcal{A}_{3,3} + 4!\lambda_{6,1}(s)\lambda_{4,2}(s)\lambda_{4,1}(s)\mathcal{A}_{3,3}$$
$$+ \frac{(4!)^2}{2}\Pi^{(3)}_{1,c}\frac{\lambda_{6,1}(s) - \frac{4}{3}\lambda^3_{4,2}(s)\mathcal{A}_{3,3}}{1 - 3!\lambda_{4,2}(s)\mathcal{A}_{3,2} + 12\lambda^2_{4,2}(s)\mathcal{A}^2_{3,2} - 8\lambda^3_{4,2}(s)\mathcal{A}^3_{3,2}}$$
$$\times\left(1 - 4\lambda_{4,2}(s)\mathcal{A}_{3,2} + 4\lambda^2_{4,2}(s)\mathcal{A}^2_{3,2}\right), \tag{150}$$

Where the 1/3! in front of the effective skeleton function $\Pi^{(3)}_{1,c}$ comes from its definition (133) – it suppress the counting of the external contractions on blacks (or whites) nodes.

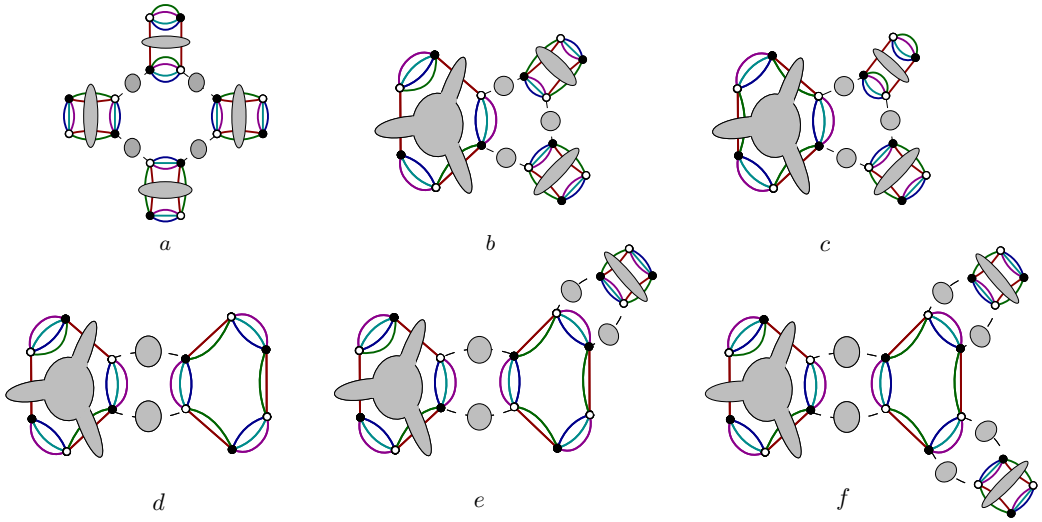


Figure 32: The four leading order configurations for 8-point functions having intertwining boundaries.

□

5 Flow equations and their fixed points

The leading effective vertex being obtained, let us now focus on the building of the leading order renormalization group flow corresponding to the initial conditions (51), from effective interactions generated from essential and marginal couplings at scale s. Once again, we limit our investigation on the UV regime $\Lambda \gg e^s \gg 1$.

5.1 Flow for local couplings

From definition (3), local interactions corresponds to pure connected tensorial invariants. Therefore, we have define the effective couplings at scale s as the zero-momenta n-point functions corresponding to a given boundary graph. Then, we can compute the successive functional derivatives of the Wetterich equation (19), and identify in both sides the terms corresponding, at leading order to the same boundary graph when the external momenta

are setting to zero.

The effective couplings at scale s have been defined from equations (123), (124) and (140). To complete the definitions (21) and (22), we have to define the *dynamical mass* $m^2(s)$; which is a relevant coupling with canonical dimension equal to 2:

Definition 23 *The effective mass at scale s is defined as:*

$$m^2(s) := \Gamma_s^{(2)}(\vec{p} = \vec{0}\,)\,. \tag{151}$$

We have the following proposition:

Proposition 10 *In the deep UV sector ($\Lambda \gg e^s \gg 1$) and in the symmetric phase, the exact flow equation for essential and marginal coupling in the sector mixing melons and non-branching pseudo-melons are given by:*

$$\dot{m}^2 = -10\,\lambda_{4,1}\mathcal{I}_{4,2} - 40\lambda_{4,2}\mathcal{I}_{3,2}\,, \tag{152}$$

$$\dot{\lambda}_{4,1} = -\left(2\Pi_{1,a}^{(3)} + \frac{2}{3}\Pi_{1,b}^{(3)}\right)\mathcal{I}_{4,2} + 4\lambda_{4,1}^2\mathcal{I}_{4,3} + 16\lambda_{4,1}\lambda_{4,2}\mathcal{I}_{3,3}\,, \tag{153}$$

$$\dot{\lambda}_{4,2} = -\left(3\lambda_{6,1} + \frac{1}{6}\Pi_{1,c}^{(3)}\right)\mathcal{I}_{3,2} + 4\lambda_{4,2}^2\mathcal{I}_{3,3}\,, \tag{154}$$

$$\dot{\lambda}_{6,1} = -\left(\frac{1}{6}\Pi_2^{(4)} + \frac{1}{4!}\Pi_1^{(4)}\right)\mathcal{I}_{3,2} + 12\lambda_{4,2}\lambda_{6,1}\mathcal{I}_{3,3} - 8\lambda_{4,2}^3\mathcal{I}_{3,4}\,. \tag{155}$$

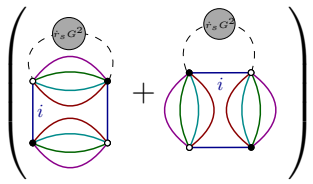
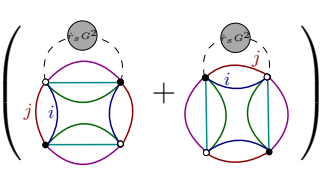
Where the dot means derivative with respect to s, and:

$$\mathcal{I}_{m,n} := \sum_{\vec{p}\in\mathbb{Z}^m} \dot{r}_s(\vec{p})\, G^n(\vec{p})\,. \tag{156}$$

Proof. Deriving the exact flow equation (19) with respect to M and $\bar{M}$, we deduce an equation describing the flow of the 2-point function $\Gamma_s^{(2)}$ in terms of $\Gamma_s^{(4)}$ only, in the symmetric phase:

$$\dot{\Gamma}_s^{(2)}(\vec{p}) = -\sum_{\vec{q}} \Gamma_s^{(4)}(\vec{p},\vec{q};\vec{p},\vec{q})\,\frac{\dot{r}_s(\vec{q})}{[\Gamma_s^{(2)}(\vec{q}) + r_s(\vec{q})]^2}\,, \tag{157}$$

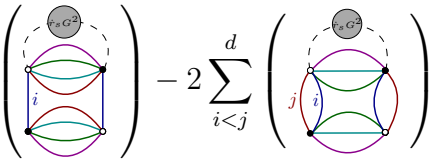
where $\partial_s A =: \dot{A}$. First, $\Gamma^{(4)}_{s,\vec{p}\vec{q};\vec{p},\vec{q}}$ split into melonic and pseudo-melonic contributions. We just considered only the boundary graphs of the effective functions to simplify the notations and then the previous equation is written graphically as:

$$\dot{\Gamma}_s^{(2)}(\vec{p}) = -\sum_{i=1}^{d}$$  $$-\sum_{i<j}^{d}$$  . (158)

In the deep UV limit, the second and fourth contributions may be discarded. Indeed, with respect to the first one, the second diagram lack 3 faces, and its proper power counting

is $\omega = -1$. In the same way, the fourth diagram scale as $\omega = 1$, while the first and third diagrams scale as $\omega = 2$. The relevant contributions are then:

$$\dot{\Gamma}_s^{(2)}(\vec{p}) = -2\sum_{i=1}^{d} \left(\right) - 2\sum_{i<j}^{d} \left(\right) . \tag{159}$$



The dynamic mass $m^2(s)$ has been defined in definition (23). Then, setting $\vec{p} = \vec{0}$ in the previous equation, we get:

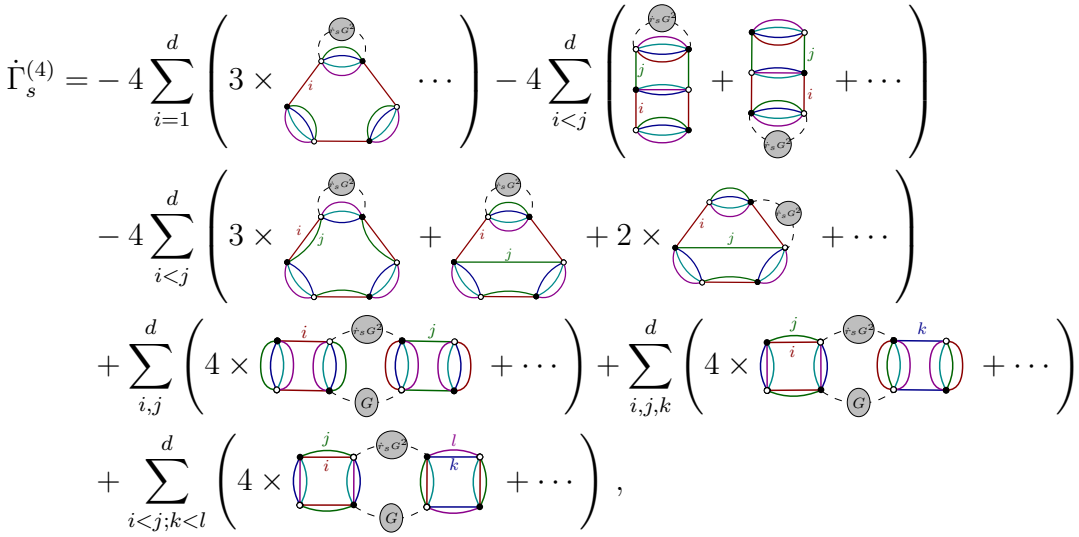
$$\dot{m}^2 = -2d\,\lambda_{4,1} \sum_{\vec{p}\in\mathbb{Z}^{d-1}} \dot{r}_s(\vec{p})\, G^2(\vec{p}) - 2d(d-1)\lambda_{4,2} \sum_{\vec{p}\in\mathbb{Z}^{d-2}} \dot{r}_s(\vec{p})\, G^2(\vec{p})\,. \tag{160}$$

In the same way, for the 4-point functions we have to derive once again one time with respect to M and $\bar{M}$; and keep only the even N-point functions, having the same number of derivatives with respect to the two means fields. We get:

$$\begin{aligned}\dot{\Gamma}_s^{(4)} = -\sum_{\vec{p}} \dot{r}_s(\vec{p}) G_s^2(\vec{p}) \Big[\Gamma_s^{(6)}(\vec{p},\vec{0},\vec{0},\vec{p},\vec{0},\vec{0}\,) - 2\sum_{\vec{p}'} \Gamma_s^{(4)}(\vec{p},\vec{0},\vec{p}',\vec{0}\,) G_s(\vec{p}') \Gamma_s^{(4)}(\vec{p}',\vec{0},\vec{p},\vec{0}\,)\Big] \\ + 2\sum_{\vec{p}} \dot{r}_s(\vec{p}) G_s^3(\vec{p}) [\Gamma_s^{(4)}(\vec{p},\vec{0},\vec{p},\vec{0}\,)]^2\,. \end{aligned} \tag{161}$$

Graphically, we get the contributions (we left the external momenta to simplify the notations):

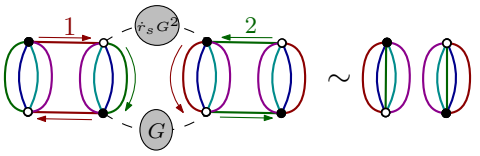
$$\begin{aligned}\dot{\Gamma}_s^{(4)} =& -4\sum_{i=1}^{d} \left(3\times \right) - 4\sum_{i<j}^{d} \left(+ \right) \\ & -4\sum_{i<j}^{d} \left(3\times + + 2\times \right) \\ & + \sum_{i,j}^{d} \left(4\times \right) + \sum_{i,j,k}^{d} \left(4\times \right) \\ & + \sum_{i<j;k<l}^{d} \left(4\times \right) , \end{aligned} \tag{162}$$



where once again we only drawn the boundary graphs of effective functions. The factors involved in this relation count the number of contractions leading to the corresponding diagram, including permutations of the external points. This is the origin of the factor $4 = (2!)^2$ in front of the 6-point contractions. Moreover, the same factor 4 in the front of the 4-point contributions comes from the derivation itself : A first factor 2 comes from the derivative of G^2 in (157); and a second factor 2 comes from a discarded term in the

first derivation, involving 3-point functions. The absence of the factor coming from permutation of external points arise because of the definition of the corresponding skeleton functions.

However, among these contractions, some of them contribute to the melonic sector, and some other contribute to the pseudo-melonic one; and we have to classify them with respect to their boundary graphs. For instance, in the first line, the two first diagrams have melonic boundnaries, while the two first diagrams in the second line have pseudo-melonic boundary. The diagrams in the third and fourth lines require to be careful analysed because their boudnary graphs depend on the selected indices i, j, k, l. For instance, for $i = j$, the first diagram in the third line has pseudo-melonic boundary, while it has disconnected boundary for $i \neq j$:



(163)

Such this diagram will not be taken into account, for melonic and pseudo-melonic flows. Moreover, it is completely discarded in the UV limit, its proper power counting begin $\omega = -2$; while the one of the case $i = j$ is $\omega = 0$, as expected for a relevant contribution to the flow of the marginal coupling $\lambda_{4,1}$[11]. In the same way, the second contribution in the third line is melonic for $k = j$ or $k = i$, and completely disconnected for $i \neq j \neq k$. Therefore, taking into account only the relevant contributions for each sectors we get:

$$\dot{\Gamma}^{(4)}_{s\,,\text{melo}} = -4\sum_{i=1}^{d}\left(3\times\right) - 4\sum_{i<j}^{d}\left(\quad+\quad\right)$$
$$+\sum_{i}^{d}\left(4\times\right)+\sum_{i}^{d}\left(4\times\right), \tag{164}$$

$$\dot{\Gamma}^{(4)}_{s\,,\text{pseudo-melo}} = -4\sum_{i<j}^{d}\left(3\times\quad+\quad\right)+\sum_{i<j}^{d}\left(4\times\right).$$

Finally, using renormalization conditions (123), (124) and (140) to identify the relevant couplings on both sides as $\Gamma^{(4)}_{s\,,\text{melo}} = 4\lambda_{4,1}$ and $\Gamma^{(4)}_{s\,,\text{pseudo-melo}} = 4\lambda_{4,2}$, we get:

$$\dot{\lambda}_{4,1} = -\left(2\Pi^{(3)}_{1,a} + \frac{2}{3}\Pi^{(3)}_{1,b}\right)\sum_{\vec{p}\in\mathbb{Z}^{d-1}} \dot{r}_s(\vec{p})\, G^2(\vec{p}) + 4\lambda^2_{4,1}\sum_{\vec{p}\in\mathbb{Z}^{d-1}} \dot{r}_s(\vec{p})\, G^3(\vec{p})$$
$$+ 16\lambda_{4,1}\lambda_{4,2}\sum_{\vec{p}\in\mathbb{Z}^{d-2}} \dot{r}_s(\vec{p})\, G^3(\vec{p}) \tag{165}$$

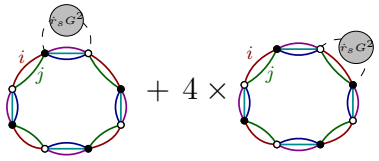
[11] Disconnected contributions can be took into account; and mixing sectors involving their contributions have be investigated in [55], from a truncation approach.

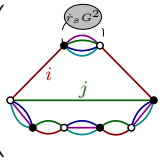
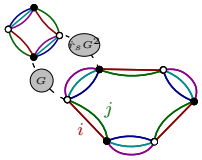
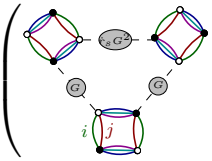
and :

$$\dot{\lambda}_{4,2} = -\left(3\lambda_{6,1} + \frac{1}{6}\Pi^{(3)}_{1,c}\right) \sum_{\vec{p}\in\mathbb{Z}^{d-2}} \dot{r}_s(\vec{p})\, G^2(\vec{p}) + 4\lambda^2_{4,2} \sum_{\vec{p}\in\mathbb{Z}^{d-2}} \dot{r}_s(\vec{p})\, G^3(\vec{p})\,, \tag{166}$$

Finally, following the same strategy, we get for the 6-point function:

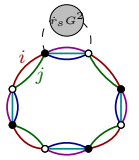
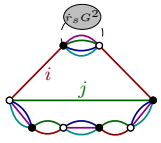
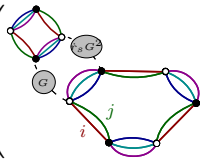
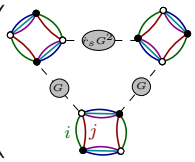
$$\begin{aligned}
\dot{\Gamma}^{(6)}_s = &-\sum_{\vec{p}} \dot{r}_s(\vec{p}) \Big[\Gamma^{(8)}_s(\vec{p},\vec{0},\vec{0},\vec{0},\vec{p},\vec{0},\vec{0},\vec{0}) G^2(\vec{p}) - 18\Gamma^{(4)}_s(\vec{p},\vec{0},\vec{p},\vec{0})\Gamma^{(6)}_s(\vec{p},\vec{0},\vec{0},\vec{p},\vec{0},\vec{0}) G^3(\vec{p}) \\
&+ 36(\Gamma^{(4)}_s(\vec{p},\vec{0},\vec{p},\vec{0}))^3 G^4(\vec{p})\Big] \\
= &-(3!)^2 \sum_{i<j}^{d} \Bigg(4 \times \quad + 4 \times \quad + \cdots \Bigg) - (3!)^2 \sum_{i<j}^{d} \Bigg(\quad + \cdots \Bigg) \\
&+ 18 \times 4 \times \sum_{j<i}^{d} \Bigg(3 \times \quad \cdots \Bigg) - 36 \sum_{i<j}^{d} \Bigg(\quad + \cdots \Bigg)\,,
\end{aligned}$$



where the additional factor 4 in front of the first term in line four comes from the counting of the permutation of the external points hooked to the 6-point effective vertex. Then, from the renormalization condition (140), we have $\Gamma^{(6)}_{s\,,\text{pseudo-melo}} = (3!)^2\lambda_{6,1}$, and keeping only the relevant contributions in the UV having pseudo-melonic boundnaries, we get finally:

$$\dot{\lambda}_{6,1} = -\Bigg(4 \times \quad + \quad \Bigg) + 216 \times \Bigg(\quad \Bigg) - 36 \times \Bigg(\quad \Bigg)\,. \tag{167}$$

equivalently we get

$$\begin{aligned}
\dot{\lambda}_{6,1} = &-\left(\frac{1}{6}\Pi^{(4)}_2 + \frac{1}{4!}\Pi^{(4)}_1\right) \sum_{\vec{p}\in\mathbb{Z}^{d-2}} \dot{r}_s(\vec{p})\, G^2(\vec{p}) + 12\lambda_{4,2}\lambda_{6,1} \sum_{\vec{p}\in\mathbb{Z}^{d-2}} \dot{r}_s(\vec{p})\, G^3(\vec{p}) \\
&- 8\lambda^3_{4,2} \sum_{\vec{p}\in\mathbb{Z}^{d-2}} \dot{r}_s(\vec{p})\, G^4(\vec{p})\,,
\end{aligned} \tag{168}$$

which ends the proof.

□

5.2 Anomalous dimension

Until now we have no explicitly introduced counter-terms. However, fields and couplings in the original action (51) have to be completed with some counter-terms so that the quantum corrections are finites. For all couplings, including mass, these counter-terms have to be understood included in the definition of the bare couplings themselves; the renormalization conditions in the deep IR fixing the renormalization prescription. However, we need for our discussion to appear explicitly the wave-function counter-terms, that we call $Z_{-\infty}$ following the notations used in [59] – the subscript $-\infty$ referring to the deep IR limit $s \to -\infty$, in which the asymptotic renormalization prescription are fixed. The bare kinetic kernel $C^{-1}(\vec{p})$ is then replaced by:

$$C^{-1}(\vec{p}) = (Z_{-\infty}\vec{p}^2 + m^2)\Theta_a^{-1}(\Lambda^2 - \vec{p}^2)\,, \tag{169}$$

where $\Theta_a^{-1}(\Lambda^2 - \vec{p}^2)$ is a smooth invertible distribution depending on a real parameter a, such that $\lim_{a\to 0}\Theta_a(x) = \Theta(x)$. As example we write:

$$\Theta_a(x) := \frac{1}{a\sqrt{\pi}}\int_{-\infty}^{x} e^{-y^2/a^2}dy\,. \tag{170}$$

Moreover, because $\Lambda > e^s$ the regulator is unaffected from the modification $r_s \to r_s/\Theta_a$ in the limit $a \to 0$; so that the regularized propagator C_s can be written as

$$C_s^{-1} = (Z_{-\infty}\vec{p}^2 + m^2 + r_s(\vec{p}))\Theta_a^{-1}(\Lambda^2 - \vec{p}^2)\,. \tag{171}$$

Our renormalization prescriptions, defining the asymptotic mass m_r^2 in the same time, is such that (see [59]):

$$\Gamma_{s\to-\infty}(\vec{p}) = m_r^2 + \vec{p}^2 + \mathcal{O}(\vec{p}^2)\,. \tag{172}$$

Note that this definition match only if the trajectory does not cross a non-Gaussian fixed point. A more general definition, including this case, fix the renormalization conditions to a finite scale s_0 so that $e^{s_0} \ll e^s$. For arbitrary s, we conventionally define the wave-function renormalization and the anomalous dimension such that :

Definition 24 ***Anomalous dimension.*** *The wave function renormalization $Z(s)$ and the anomalous dimension $\eta(s)$ – both depending on s are defined as:*

$$Z(s) := \frac{\partial}{\partial p_1^2}\Gamma_s^{(2)}(\vec{p})\Big|_{\vec{p}=\vec{0}}, \quad \eta(s) := \frac{\dot{Z}}{Z}\,. \tag{173}$$

The flow equations deduced in the previous section are "exact" i.e. up to the limit of our approximation scheme. However, the anomalous dimension, formally given from equation (173) remains unknown. To exploit our flow equations, we then have to complete our approximation scheme. We have expressed all the LO effective vertices in terms of essential and marginal couplings, as well as effective 2-point functions $\Gamma_s^{(2)}$. Formally, these functions are fixed from closed equation (56); however, solving exactly this equation remains an open challenge in tensor field theories [62]-[63]. Following the method explained in [59], in order to extract available equations for renormalization group flow, especially in view of a numerical analysis, we have to fix the form of $\Gamma_s^{(2)}$; and we adopt the following definition:

Definition 25 *In the symmetric phase, and in the range of momenta contributing significantly in the domain defined by the distribution $\dot{r}_s$; the effective 2-point function $\Gamma_s^{(2)}$ is assumed to be truncated around the two first terms in derivative expansion*

$$\Gamma_s^{(2)}(\vec{p}) := Z(s)\vec{p}^{\,2} + m^2(s)\,, \tag{174}$$

so that $Z(s)$ match with the definition (173)*.*

Note that this definition is compatible with usual truncations in the symmetric phase, that is with derivative and mean field expansion considered in the literature [84]-[85]. Moreover, in non-symmetric phase, a dependence of $Z(s)$ on the means fields M and $\bar{M}$ is expected. Finally, the domain of the momentas defined by the distribution $\dot{r}_s$ is important. It corresponds to the relevant integration domain involved in the flow equations (19); and may be viewed in a sense as an approximation "slice by slice" along the flow line. However, it can not be used globally in the full range of momenta, especially in the deep UV, for $\vec{p}^{\,2} \sim \Lambda^2$, without dangerous contradictions with Ward-identity, as we will briefly discuss at the end of this section.

In addition to this definition, we recall the usual definition for *renormalized and dimensionless* couplings:

Definition 26 *In the deep UV, the dimensionless and renormalized couplings, $\bar{m}^2$, $\bar{\lambda}_{4,1}$, $\bar{\lambda}_{4,2}$ and $\bar{\lambda}_{6,1}$ are defined as:*

$$m^2 = Ze^{2s}\bar{m}^2\,, \quad \lambda_{4,1} = Z^2\bar{\lambda}_{4,1}\,, \quad \lambda_{4,2} = Z^2e^s\bar{\lambda}_{4,2}\,, \quad \lambda_{6,1} = Z^3\bar{\lambda}_{6,1}\,. \tag{175}$$

Moreover, we denote respective by β_m, $\beta_{4,1}$, $\beta_{4,2}$ and $\beta_{6,1}$ their derivative with respect to s.

Now, let us give the set of WT-identities, which will help to extract the anomalous dimension η.

Proposition 11 ***(UV-regularized Ward-Takahashi identity)***
Let $Z_s(J,\bar{J})$ is the one-parameter generating functional for the theory with microscopic action (51)*:*

$$Z_s(J,\bar{J}) := \int d\mu_{C_s}[T,\bar{T}]e^{-S_{int}(T,\bar{T})+\bar{J}T+\bar{T}J}\,, \quad d\mu_{C_s}[T,\bar{T}] := dTd\bar{T}\,e^{-\bar{T}C_s^{-1}T}\,. \tag{176}$$

The free energy $W_s(J,\bar{J}) := \ln Z(J,\bar{J})$ satisfy the functional differential equation:

$$\sum_{\vec{p}_\perp,\vec{p}'_\perp}\prod_{j\neq 1}\delta_{p_jp'_j}\left\{\left(C_s^{-1}(\vec{p}) - C_s^{-1}(\vec{p}')\right)\left[\frac{\partial^2 W_s}{\partial\bar{J}_{\vec{p}'}\,\partial J_{\vec{p}}} + \bar{M}_{\vec{p}}M_{\vec{p}'}\right] - \bar{J}_{\vec{p}}\,M_{\vec{p}'} + J_{\vec{p}'}\bar{M}_{\vec{p}}\right\} = 0\,, \tag{177}$$

where the means fields M and $\bar{M}$ have been defined in (17)*, and $\vec{p}_\perp := (0,p_2,\cdots,p_d) \in \mathbb{Z}^{d-1}$.*

Proof (Sketched). The Ward–Takahashi identity was extensively discussed in the literature [59]. We provide only the sketch of this proof, to take into account the little modifications coming from the sharp UV-regulation; and the new boundary graphs coming from pseudmelonic sector. The given proofs follows the steps detailed in [59].

Let us consider the unitary transformations $\mathbf{U} \in \mathcal{U}^{\times d}$ acting independently over each components of the tensors T and $\bar{T}$. $\mathbf{U}$ is a d-dimensional vector $\mathbf{U} = (U_1, U_2, \cdots, U_d)$ whose components U_i are unitary matrices acting on the indices of color i. The action of $\mathbf{U}$ on the two tensors is defined as (we sum over repeated indices):

$$\mathbf{U}[T]_{p_1,p_2,\cdots,p_d} := [U_1]_{p_1 q_1}[U_2]_{p_2 q_2}\cdots[U_d]_{p_d q_d} T_{q_1,q_2,\cdots,q_d} \tag{178}$$

$$\mathbf{U}[\bar{T}]_{p_1,p_2,\cdots,p_d} := [U_1^*]_{p_1 q_1}[U_2^*]_{p_2 q_2}\cdots[U_d^*]_{p_d q_d} \bar{T}_{q_1,q_2,\cdots,q_d}\,, \tag{179}$$

where the star exponent $*$ means the complex conjugation. Obviously, $\sum_{\vec{p}} \bar{T}_{\vec{p}} T_{\vec{p}}$ and any higher valence tensorial interactions are invariant under any such transformations. Then:

$$\mathbf{U}[S_{\rm int}] = S_{\rm int}\,. \tag{180}$$

In contrast, it is not the case for the kinetic and source terms, due to the non-trivial propagator and sources J and $\bar{J}$, which breaks the unitary invariance. However, the functional integral defining the generating functional $Z_s(J,\bar{J})$ have to be insensitive on the bad transformation of the kinetic term because of the formal translation invariance of the Lebesgue integration measure. Then, it has to be invariant under any unitary transformation; and as a direct consequence, the 2-point function $\langle \bar{T}_{\vec{p}} T_{\vec{q}} \rangle$ and any higher functions transforms like a representation of $\mathbf{U} \otimes \mathbf{U}^*$.

We can translate this conclusion as follows: In the vicinity of the unity we can write $U = \mathbb{I} + i\epsilon$, where $\epsilon = \epsilon^\dagger$ is an hermitian matrix and $\mathbb{I}$ the identity matrix. Then, at the first order

$$\mathbf{U} = \mathbf{I} + \sum_i \vec{\epsilon}_i\,, \tag{181}$$

where $\mathbf{I} := \mathbb{I}^{\otimes d}$ and $\vec{\epsilon}_i = \mathbb{I}^{\otimes(i-1)} \otimes \epsilon_i \otimes \mathbb{I}^{d-i+1}$. In this infinitesimal prescription, the invariance of the generating functional simply means $\vec{\epsilon}_i[Z_s(J,\bar{J})] = 0$. Explaining each terms at the first order in ϵ_i, we then get:

$$\int \vec{\epsilon}_i[d\mu_{C_s}] e^{-S_{\rm int}+\bar{J}T+\bar{T}J} + \int d\mu_{C_s} \left\{ \vec{\epsilon}_i[S_{\rm int}] + \bar{J}\,\vec{\epsilon}_i[T] + \vec{\epsilon}_i[\bar{T}]J \right\} e^{-S_{\rm int}+\bar{J}T+\bar{T}J} = 0\,. \tag{182}$$

Obviously, this equation have to be true for all i. From equation (180), it follows that $\vec{\epsilon}_i[S_{\rm int}] = 0$. Moreover, from definition (179), it is easy to deduce the infinitesimal variations for singles tensor fields:

$$\vec{\epsilon}_i[T]_{\vec{p}} = \sum_{\vec{p}'} \epsilon_{i\,p_i p_i'} \prod_{j\neq i} \delta_{p_j p_j'}\, T_{\vec{p}'}\,. \tag{183}$$

Finally, from definition (176); the variation of the Gaussian measure $d\mu_{C_s}$ can be easily computed. In matrix notation:

$$\vec{\epsilon}_i[d\mu_{C_s}] = -(\vec{\epsilon}_i[\bar{T}] C_s^{-1} T + \bar{T} C_s^{-1} \vec{\epsilon}_i[T]) d\mu_{C_s}\,. \tag{184}$$

Because of the hermiticity of the matrix ϵ_i, the two terms in bracket have opposite relative signs. Then consider the equation (182), and let us used the explicit variation (183) and finally rewriting each tensor field T and $\bar{T}$ respectively as $\partial/\partial\bar{J}$ and $\partial/\partial J$, we deduce the formula (177) setting $i = 1$.

□

In practice, in the symmetric phase, the Ward identity allows to link up $\Gamma_s^{(n+2)}$ to the $\Gamma_s^{(n)}$ and their derivative. In this paper, we only keep the two first ones relations, involving only essential and marginal sectors and write the following corollary:

Corollary 4 ***First and second LO zero-momenta WT-identities*** *In the symmetric phase, the zero momenta* 4 *and* 6*-point functions satisfy:*

$$Z_{-\infty}\left(\Pi_1^{(2)}\mathcal{L}_1 + 4\Pi_2^{(2)}\mathcal{L}_2\right) = -\frac{\partial}{\partial p_1^2}\left[\Gamma_s^{(2)}(\vec{p}) - C^{-1}(\vec{p})\right]\Big|_{\vec{p}=\vec{0}}, \tag{185}$$

$$Z_{-\infty}\left(\mathcal{L}_1\left(2\Pi_{1,a}^{(3)} + \frac{2}{3}\Pi_{1,b}^{(3)}\right) - 8\lambda_{4,1}^2\,\mathcal{U}_1 - 32\lambda_{4,1}\lambda_{4,2}\mathcal{U}_2\right) = -\frac{\partial}{\partial p_1^2}\,\Pi_1^{(2)}(p_1,0)\Big|_{p_1=0}, \tag{186}$$

$$Z_{-\infty}\left(\mathcal{L}_2\left(12\lambda_{6,1} + \frac{2}{3}\Pi_{1,c}^{(3)}\right) - 8\lambda_{4,2}^2\,\mathcal{U}_2\right) = -\frac{\partial}{\partial p_1^2}\,\Pi_2^{(2)}(p_1,0)\Big|_{p_1=0}, \tag{187}$$

where:

$$Z_{-\infty}\mathcal{L}_i := \sum_{\vec{p}_\perp\in\mathbb{Z}^{d-i}} \frac{\partial C_s^{-1}(\vec{p}_\perp)}{\partial p_1^2}\,G^2(\vec{p}_\perp)\,, \quad Z_{-\infty}\mathcal{U}_i := \sum_{\vec{p}_\perp\in\mathbb{Z}^{d-i}} \frac{\partial C_s^{-1}(\vec{p}_\perp)}{\partial p_1^2}\,G^3(\vec{p}_\perp)\,, \tag{188}$$

Proof (Sketched). Assuming we are in the symmetric phase and taking the derivative of the equation (177) with respect to $M_{\vec{q}'}$ and $\bar{M}_{\vec{q}}$; and vanishing the sources $J = \bar{J} = 0$, we get:

$$\sum_{\vec{p}_\perp,\vec{p}_\perp{}'}\prod_{j\neq 1}\delta_{p_jp'_j}\Bigg[\left[C_s(\vec{p}^{\,2}) - C_s(\vec{p}'^{\,2})\right]\left[\frac{\partial^2 G_{\vec{p},\vec{p}'}}{\partial M_{\vec{q}'}\,\partial\bar{M}_{\vec{q}}} + \delta_{\vec{p}\vec{q}}\,\delta_{\vec{p}',\vec{q}'}\right] - \Gamma^{(2)}_{s\,,\vec{q}\vec{p}}\,\delta_{\vec{q}'\vec{p}'} + \Gamma^{(2)}_{s\,,\vec{q}'\vec{p}'}\delta_{\vec{p}\vec{q}}$$
$$- r_s(\vec{p}^{\,2})\delta_{\vec{q}\vec{p}}\,\delta_{\vec{q}'\vec{p}'} + r_s(\vec{p}'^{\,2})\delta_{\vec{q}'\vec{p}'}\delta_{\vec{p}\vec{q}}\Bigg] = 0\,, \tag{189}$$

where we used the fact that following (16) the inverse of the 2-point function $G = \partial^2 W_s/\partial J\partial\bar{J}$ is $\Gamma_s^{(2)} + r_s$, implying : $\partial\Gamma_s/\partial M = \bar{J} - r_s\bar{M}$. Then it is easy to check that:

$$\frac{\partial^2 G_{\vec{p},\vec{p}'}}{\partial M_{\vec{q}'}\,\partial\bar{M}_{\vec{q}}} = -G(\vec{p})\Gamma_s^{(4)}(\vec{p}_\perp,\vec{p}_\perp,\vec{0},\vec{0})G(\vec{p}')\,. \tag{190}$$

Inserting this relation in the equation (189), and taking the limit $p_1 \to p'_1 \to 0$ and $\vec{q} = \vec{q}' = \vec{0}$, we get:

$$\sum_{\vec{p}_\perp} G^2(\vec{p}_\perp)\,\Gamma_s^{(4)}(\vec{p}_\perp,\vec{p}_\perp,\vec{0},\vec{0}) = -\frac{\partial}{\partial p_1^2}\left[\Gamma_s^{(2)}(\vec{p}) - C^{-1}(\vec{p})\right]\Big|_{\vec{p}=\vec{0}} \tag{191}$$

recall that $C^{-1} := C_s^{-1} - r_s$. In fact, it is easy to see that the LO contractions of G^2 are those building a 4-dipole in the melonic contribution, and a 3-dipole in the pseudo-melonic one. In the first case, this implies that we have to keep only the contribution of $\Gamma^{(4),1}_{s\,\text{melo}}$. In the second case, we keep only the contributions of $\Gamma^{(4),1i}_{s\,\text{pseudo-melo}}$ for $i \neq 1$. Finally, due to the Sym is the decomposition of the 4-point functions, only half of them contribute at LO. The formula (185) follows.

To prove the formulas (186) and (187), we have to derive two times with respect to M, and two times with respect to $\bar{M}$. Straightforwardly we get:

$$\sum_{\vec{p}_\perp, \vec{p}'_\perp} \delta_{\vec{p}_\perp \vec{p}'_\perp} \Delta C_s(\vec{p}, \vec{p}')\, \tilde{\Gamma}^{(6)}_{s,\vec{p}_4\vec{p}_2\vec{p}';\vec{p}_3\vec{p}_1\vec{p}} G_s(\vec{p}) G_s(\vec{p}') + \sum_{\vec{p}_\perp, \vec{p}'_\perp} \delta_{\vec{p}_\perp \vec{p}'_\perp} X_{\vec{p}_1,\vec{p}_2,\vec{p}_3,\vec{p}_4;\vec{p}\vec{p}'} = 0\,, \quad (192)$$

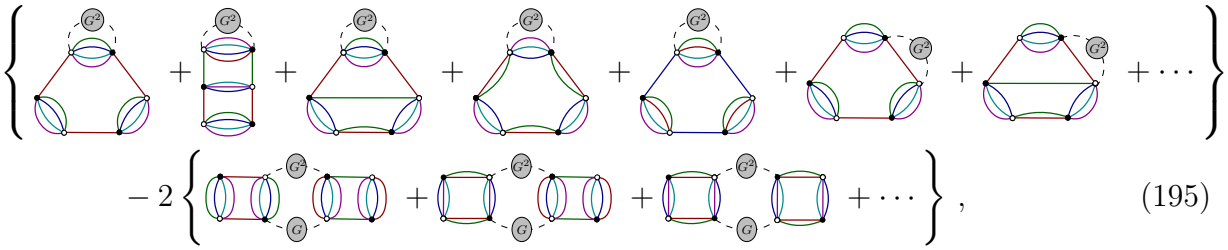
where we used the following definitions:

$$\tilde{\Gamma}^{(6)}_{s,\vec{p}_4\vec{p}_2\vec{p}';\vec{p}_3\vec{p}_1\vec{p}} := \Gamma^{(6)}_{s,\vec{p}_4\vec{p}_2\vec{p}';\vec{p}_3\vec{p}_1\vec{p}} - 2\Gamma^{(4)}_{s,\vec{p}\vec{p}_4;\vec{p}_1\vec{p}''} G_s(\vec{p}'') \Gamma^{(4)}_{s,\vec{p}''\vec{p}_2;\vec{p}_2\vec{p}'}\,, \quad (193)$$

and

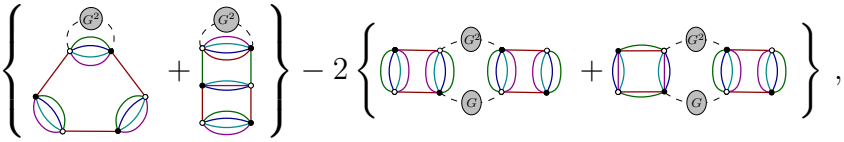
$$X_{\vec{p}_1,\vec{p}_2,\vec{p}_3,\vec{p}_4;\vec{p}\vec{p}'} := -\delta_{\vec{p}_3\vec{p}'} \Gamma^{(4)}_{s,\vec{p}_2\vec{p}_4;\vec{p}\vec{p}_1} - \delta_{\vec{p}_1\vec{p}'} \Gamma^{(4)}_{s,\vec{p}_2\vec{p}_4;\vec{p}\vec{p}_3} + \delta_{\vec{p}_4\vec{p}} \Gamma^{(4)}_{s,\vec{p}'\vec{p}_2;\vec{p}_1\vec{p}_3} + \delta_{\vec{p}_2\vec{p}} \Gamma^{(4)}_{s,\vec{p}'\vec{p}_4;\vec{p}_1\vec{p}_3} \quad (194)$$

and finally we introduced the notation $\Delta C_s(\vec{p}, \vec{p}') := C_s(\vec{p}^{\,2}) - C_s(\vec{p}'^{\,2})$. There is an important difference with the previous Ward identity. While the boundary graph of any connected 2 point graph is the elementary melon, denoted as γ_1 in the Section (3.2); the boundaries of connected 4-point graphs can be melonics or pseudo-melonics. In both sides of the equation (192), we then have to identify the contributions having the same boundary graphs; exactly like for the flow equations in the previous section, equation (162) for instance. Moreover, the intertwining sector has to be taken into account in the computation of the pseudo-melonic contribution. Once again, picturing only the boundary structure of the effective vertices, the left hand side of the equation (192) write as:

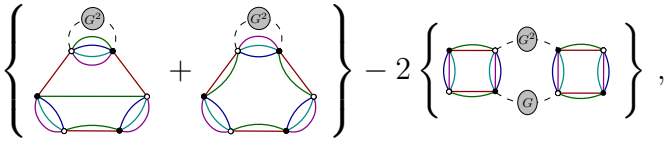


(195)

and it is not hard to select, among these contractions, the LO ones, having respectively melonic or pseudo-melonic boundaries. For instance, the first one in the upper line has quartic melonic boundary, while the second ones have pseudo-melonic boundaries. We then have to split the series of allowed contractions as:



for relevant melonic, and



(196)

for relevant pseudo-melonic. Then, setting $\vec{p}_3 = \vec{p}_4 = \vec{0}$ in a first time, $\vec{p}_1 = (p_1', \vec{0}_\perp)$, in a second time $\vec{p}_2 = (p_1, \vec{0}_\perp)$, and finally $p_1 \to p_1' \to 0$, we get the two formula (186) and (187); taking into account the renormalization conditions (123), (124) and (140).

□

To complete this proposition, we may compute the derivative in both sizes, for C^{-1} and $C_s^{-1} = C^{-1} + r_s$, using the regularized version (169) and (171) of these kinetic kernels, we get:

$$\frac{\partial C^{-1}}{\partial p_1^2}(\vec{p}) = Z_{-\infty}\Theta_a^{-1}(\Lambda^2 - \vec{p}^{\,2}) - (Z_{-\infty}\vec{p}^{\,2} + m^2)\frac{\Theta_a'}{\Theta_a^2}(\Lambda^2 - \vec{p}^{\,2})\,. \tag{197}$$

Then, taking the limit $a \to 0$, and due to the fact that $\Theta' = \delta$, we get, for the right hand side:

$$\frac{\partial C^{-1}}{\partial p_1^2}(\vec{p} = \vec{0}\,) = Z_{-\infty}\,. \tag{198}$$

In the same way:

$$\frac{\partial C_s^{-1}}{\partial p_1^2}(\vec{p}) = \left(Z_{-\infty} + \frac{\partial r_s}{\partial p_1^2}(\vec{p})\right)\Theta_a^{-1}(\Lambda^2 - \vec{p}^{\,2}) - (Z_{-\infty}\vec{p}^{\,2} + m^2)\frac{\Theta_a'}{\Theta_a^2}(\Lambda^2 - \vec{p}^{\,2})\,. \tag{199}$$

Moreover, we have to take into account the factors Θ_a^2 of Θ_a^3 coming from G^2 of G^3 in the definitions of the functions $\mathcal{L}_i$ and $\mathcal{U}_i$. Indeed:

$$G = \frac{C_s}{1 - C_s\Sigma(\vec{p})} \propto \Theta(\Lambda^2 - \vec{p}^{\,2})\,, \tag{200}$$

which leads to, in the limit $a \to 0$:

$$Z_{-\infty}\,\mathcal{L}_i := \sum_{\vec{p}_\perp \in \mathbb{Z}^{d-i}} \left(Z_{-\infty} + \frac{\partial r_s}{\partial p_1^2}(\vec{p})\right) G^2(\vec{p}_\perp) - \frac{5-i}{2}(Z_{-\infty}\Lambda^2 + m^2)G^2(\Lambda)\Omega_{d-i}\Lambda^{3-i}\,, \tag{201}$$

$$Z_{-\infty}\,\mathcal{U}_i := \sum_{\vec{p}_\perp \in \mathbb{Z}^{d-i}} \left(Z_{-\infty} + \frac{\partial r_s}{\partial p_1^2}(\vec{p})\right) G^3(\vec{p}_\perp) - \frac{5-i}{2}(Z_{-\infty}\Lambda^2 + m^2)G^3(\Lambda)\Omega_{d-i}\Lambda^{3-i}\,, \tag{202}$$

where for the "boundary terms" we used the fact that $G(\vec{p})$ only depends on $\vec{p}^{\,2}$, from which we introduced the notation: $G(\vec{p})\delta(\Lambda^2 - \vec{p}^{\,2}) =: G(\Lambda)\delta(\Lambda^2 - \vec{p}^{\,2})$. Moreover, we computed the following sum using integral approximation:

$$\sum_{\vec{p}_\perp} \delta(\Lambda^2 - \vec{p}_\perp^{\,2}) \sim \int d^{d-i}x\, \delta(\Lambda^2 - \vec{x}^{\,2}) = \frac{1}{2}(5-i)\Omega_{d-i}\Lambda^{3-i}\,. \tag{203}$$

In the continuum limit i.e. for a large Λ, the boundaries terms in equations (201) are irrelevant for $\mathcal{U}_i$ for $i = 1$ and 2; and for $\mathcal{L}_i$ for $i = 2$. For $i = 1$, the boundary term remains of order 1. The first term, proportional to $Z_{-\infty}\Lambda^2$ may be discarded with respect to the logarithm divergence of the first term. Taking into account the proper scaling of the mass, including counter-term, the second term is as well of order 1; but a difficulty arises from the fact that it does not share the factor $Z_{-\infty}$ allowing to compare it with the first term. However, our investigations are far away from the scale Λ. Then this constant term, only depending on the microscopic initial condition at this scale does not compromise our conclusions, which are essentially based on variations with respect to the IR scale $k = e^s$. Finally, other regularization scheme allows to prevent the occurrence of such a boundary terms. This is especially the case of dimensional regularization working on the dimension of the internal group manifold, $U(1)$, which becomes $U(1)^D$. The integrals may be analytically continued in D, and the divergences localized around the poles in $\epsilon = 1-D$. All the incoming conclusions may be deduced from one or the other regularization scheme, with the corresponding definition:

Definition 27 *In dimensional regularization, the continuum limit corresponds to $D \to 1$.*

The Ward identity allows to compute the derivative of the 4-point functions at zero momenta, or in other word, to keep an additional information coming from the momentum dependence of the effective vertex. Note that such a dependence do not appears in the standard crude truncations; as it can be easily cheeked from Appendix (B) where the truncation method around just-renormalizable interactions has been briefly recalled to compare with the flow equations deduced from effective vertex method. The knowledge of these derivative allows to compute the anomalous dimension from its definition (173) like any other couplings. However, the Ward identities (185), (186), and (187) are not directly practicable because of the presence of $Z_{-\infty}$ and divergent quantities like $\mathcal{L}_1$. These quantities refers to the global history of the flow, but to be usable, the local flow equation (19) requires local information. Then, we have to deals with these divergent terms to extract local information from Ward identities. To this end, let us first consider the case of the pure melonic sector, setting $\lambda_{4,2} = \lambda_{6,1} = 0$. Note that this sector is stable, in the sens that relevant pseudo-melonic contributions can not be generated from the melonic sector itself in the UV. In a second time, we will consider the mixing sector.

- **Melonic sector**

Setting $\lambda_{4,2} = \lambda_{6,1} = 0$, only the melonic sector remains in the theory, and the relevant theory space in the UV sector contains only melonic functions, having melonic graphs as boundary. The effective marginal coupling $\lambda_{4,1}(s) \equiv \lambda(s)$ remains the only relevant parameter to control the large behavior of the flow. Then, all correlations function may be expressed in term of this parameter as well as effective 2-point functions. The corresponding 6-point function may be obtained from our results of the section (4) vanishing the pseudo-melonic couplings (see [59] for more detail). As mentioned before, the interest of this discussion allows only to understand the way to deals with non-local terms in the Ward identity, a point which in not discussed in the previous work. For convenience, and because it have to be precised, we limit our study to the standard *modified Litim regulator*

[79]-[80]:

$$r_s(\vec{p}) := Z(s)(e^{2s} - \vec{p}^{\,2})\Theta(e^{2s} - \vec{p}^{\,2})\,, \tag{204}$$

In the melonic sector, and using (201) and (198), the Ward identities (185), (186) are reduce to[12] :

$$2Z_{-\infty}\lambda\,\mathcal{L} = -Z + Z_{-\infty}\,, \tag{205}$$

$$2Z_{-\infty}\Pi^{(3)}\,\mathcal{L} - 8Z_{-\infty}\lambda^2\,\mathcal{U} = -\frac{d}{dp^2}\Pi^{(2)}\,, \tag{206}$$

where to simplify the notations we left the irrelevant lower index 1 for $\mathcal{L}$ and $\mathcal{U}$, and we denote as $\Pi^{(3)}$ and $\Pi^{(2)}$ the quantities respectively called $\Pi^{(3)}_{1,a}$ and $\Pi^{(2)}_1$. Defining $\bar{Z} := Z/Z_{-\infty}$, we get from the first equation (205):

$$\bar{Z} = 1 - 2\lambda\mathcal{L}\,. \tag{207}$$

Note that this equation has been derived in [59] directly from closed equation (56). A first important relation between beta functions and anomalous dimension can be deduced from the first relation (205). This is useful as a consistency ingredient for our incoming approximation as well as a test for other approximations schemes. This is the case like the ones considered in the reference paper [59] for the computation of the effective loop integrals involved in the EVE method, and for other methods like truncation, considered in Appendix (B). From the definition (173), $\eta = \dot{\bar{Z}}/\bar{Z}$, and from definition (207):

$$\dot{\bar{Z}} = -2(\dot{\lambda}\mathcal{L} + \lambda\dot{\mathcal{L}}) = \frac{\dot{\lambda}}{\lambda}(\bar{Z} - 1) - 2\lambda(\dot{\mathcal{A}}_{4,2} + \dot{\Delta})\,. \tag{208}$$

The difference $\Delta := \mathcal{L} - \mathcal{A}_{4,2}$ involves the derivative of the regulator function: $\Delta = \frac{1}{Z_{-\infty}}\sum_{\vec{p}\in\mathbb{Z}^{d-1}} G^2(\vec{p})r'_s(\vec{p})$, the "prime" meaning derivative with respect to the variable p_1^2, setting equal to zero. For the Litim regulator:

$$r'_s(\vec{p}) = -Z(s)\Theta(e^{2s} - \vec{p}^{\,2}) \to \dot{r}_s(\vec{p}) = -[\eta(e^{2s} - \vec{p}^{\,2}) + 2e^{2s}]r'_s(\vec{p})\,. \tag{209}$$

The two distributions r'_s and $\dot{r}_s$ are proportionals. Thus, the approximation (25) used for computation of the sums $\mathcal{I}_{n,m}$ in the flow equations must be used for computation of Δ and $\dot{\Delta}$. However, as explained before the definition (25), this approximation becomes totally wrong for the computation of $\dot{\mathcal{A}}_{2,4}$, and all divergent quantities, for which the deep UV terms survive. We will discuss this point carefully. From now, let us consider the structure equations for melonic 4-point functions. They only involves $\Pi^{(2)}_{1,a} \equiv \Pi^{(2)} = 2\lambda(s)$, and it is explicitly given from lemma (3):

$$\lambda(s) = \frac{\lambda}{1 + 2\lambda\mathcal{A}_{4,2}}\,, \tag{210}$$

where, in the right hand side, coupling without explicit s dependence designates the bare coupling. Deriving it with respect to s, we get:

$$\dot{\lambda}(s) = -2\lambda^2(s)\dot{\mathcal{A}}_{4,2}\,. \tag{211}$$

[12] we discard the boundary terms for this discussion.

Finally, because of the definition of r_s, Δ is proportional to $\bar{Z}/Z^2$. Extracting this factor as $\Delta =: \frac{\bar{Z}}{Z^2}\bar{B}(s)$, and defining the renormalized coupling following definition (26) $\bar{\lambda} := \lambda/Z^2$, we obtain from equation (208):

$$\eta = \frac{\dot{\lambda}}{\lambda} - 2\bar{\lambda}(-\eta\bar{B}(s) + \dot{\bar{B}}(s))\,. \tag{212}$$

The contribution $\bar{B}(s)$ can be easily computed using integral approximation, valid for $e^s \gg 1$,

$$\bar{B}(s) = -\frac{\Omega_{d-1}}{(1+\bar{m}^2)^2} \;\to \dot{\bar{B}}(s) = 2\frac{\Omega_{d-1}}{(1+\bar{m}^2)^3}\,\beta_m\,, \tag{213}$$

where Ω_{d-1} denote the hyper-volume of the unit ball in dimension $d-1$. Inserting this result in equation (208), and using the definition of $\beta_\lambda = (\dot{\lambda} - 2\eta\lambda)/Z^2$, we get:

Corollary 5 *In the deep UV and for purely melonic sector, and with approximation* (25)*, the Ward identity rely the beta functions and anomalous dimension as:*

$$\beta_\lambda = -\eta\bar{\lambda}\left(1 - 2\bar{\lambda}\frac{\Omega_{d-1}}{(1+\bar{m}^2)^2}\right) + 4\bar{\lambda}\frac{\Omega_{d-1}}{(1+\bar{m}^2)^3}\,\beta_m\,. \tag{214}$$

This equation is an additional constraint on the flow, and among their consequences, it adds a strong constraint on the fixed points. Indeed, let us defined a fixed point $p = (\bar{m}_*^2, \bar{\lambda}_*)$ such that $\beta_\lambda(p) = \beta_m(p) = 0$, we must have:

$$\eta_* = 0\,, \quad \text{or} \quad 2\bar{\lambda}_*\frac{\Omega_{d-1}}{(1+\bar{m}_*^2)^2} = 1\,. \tag{215}$$

The fixed point found in [59], recovered in section (5.3) and Appendix (B) was such that $p \approx (-0,55, 0,003)$, $\eta \approx 0,7$ and violate the two previous conditions. This seems to be a strong argument in favor of a disappearance of the fixed point, which violate the Ward identities. However, this argument require to be careful analyzed. First of all, the Ward identity is written in the symmetric phase. Also, the constraint depend on the choice of the regulator, except for one and two loop approximation as well, in accordance to their universality. Then, such a statement requires a proper analysis on the influence of the regulator. However, the strong gap between the obtained values and the requirement of the constraint seems to indicate that this fixed point is well a spurious consequence of the lack of the Ward identity constraint. We keep this important discussion for a work in preparation. At this stage, the constraint given from corollary (5) provides us an important information for the computation of the integrals. Indeed, if we try to compute the integral $\mathcal{A}_{4,2}$ using approximation (25), introducing a cut off on the high momenta, we get:

$$\mathcal{A}_{4,2} = (\bar{B} + a\ln(\Lambda))/Z^2. \tag{216}$$

The derivative with respect to s then generate a factor $-2\eta\mathcal{A}_{4,2}$, having the same expected behavior in Λ as $\bar{Z}$. As a result, we generate a term $-2\eta\bar{\lambda}$, which exactly compensates the same term coming from $\dot{\lambda}/\lambda$. As a consequence, the leading term in $\bar{\lambda}$ writes as $\beta_\lambda^{(2)} = \eta^{(1)}\bar{\lambda}$, where $\eta^{(1)}$ denote the first order term in the expansion of η in power of

λ. From Appendix (B) or from a direct computation, we get $\eta^{(1)} = 8\Omega_{d-1}\lambda$, implying $\beta_\lambda^{(2)} = 8\Omega_{d-1}\lambda^2 \geq 0$. This result is in complete violation of universality. Indeed, a direct calculation show that the theory is asymptotically free and $\beta_\lambda^{(2)} = -\eta^{(1)}\bar{\lambda}$. In the decomposition of $\mathcal{A}_{4,2}$, the problem come from the big logarithm term $a\ln(\Lambda)/Z^2(s)$, and especially from the dependence on $Z(s)$. The bound of the integration is so far from the allowed windows of momenta ensuring validity of the approximation, and the factor in front of this big logarithm does not have to depend on s. With this hypothesis, and assuming that $1/\bar{Z} \to 0$ in the continuum limit $\Lambda \to \infty$, we recover the exact result (5). For this reason, we will use this approximation only for convergent integrals, and more generally whenever that these deep UV contributions are completely discarded. This is the case for the integral approximations used in the reference [59].

Even to close this discussion, let us return on the expression (207). From renormalization conditions, $Z(s \to -\infty) = 1$ and $\lambda(s \to -\infty) = \lambda_r$, we have:

$$Z_{-\infty}^{-1} = 1 - 2\lambda_r A_{-\infty}\,, \tag{217}$$

where $A_{-\infty} := \mathcal{L}(s \to \infty)$. From the condition $r_{s\to-\infty} = 0$, we have explicitly:

$$A_{-\infty} = \sum_{\vec{p}\in\mathbb{Z}^{d-1}} \frac{1}{\left[\Gamma_{s\to-\infty}(\vec{p})\right]^2} = \sum_{\vec{p}\in\mathbb{Z}^{d-1}} \left[\frac{1}{Z_{-\infty}\vec{p}^{\,2} + m^2 - \Sigma_{-\infty}(\vec{p})}\right]^2 . \tag{218}$$

The counter-terms subtract all the sub-divergences, except the global one[13]. Then, we expect that $Z_{-\infty}^{-1}$ diverge logarithmically in the continuum limit $\Lambda \to \infty$ ($D \to 1$), or equivalently $Z_{-\infty} \to 0$ like $1/\ln(\Lambda)$. Then $Z \approx -2Z_{-\infty}\lambda\mathcal{L}$, without contradiction with the formula (5); as we can show from a straightforward computation. Moreover, in the second Ward identity (206):

$$Z\Pi^{(3)} + 8Z_{-\infty}\lambda^3\mathcal{U} = \lambda\frac{d}{dp^2}\Pi^{(2)}\,. \tag{219}$$

As for $\mathcal{L}$, the quantity $\mathcal{U}$ splits as:

$$\mathcal{U} = \mathcal{A}_{4,3} + \frac{\bar{Z}}{Z^3}\bar{C}(s). \tag{220}$$

However, $\mathcal{A}_{4,3}$ is superficially convergent and all the sub-divergences have been canceled from renormalization. Then, in the continuum limit, we have $Z_{-\infty}\mathcal{A}_{4,3} \to 0$. Recall that $\Pi^{(3)}$ is given in section (4.2.2), proposition (8). Then, using integral approximation for the computation of the sum, and the definition (25) for the computation of the convergent integral, we get with $\Omega_4 = \pi^2/2$:

$$\Pi^{(3)} = 8\lambda^3\mathcal{A}_{4,3} = 8\lambda^3\frac{1}{2Z^3e^{2s}}\frac{\pi^2}{1+\bar{m}^2}\left(\frac{1}{(1+\bar{m}^2)^2} + \frac{1}{1+\bar{m}^2} + 1\right), \tag{221}$$

[13]We lack the final subtraction in the Zimmerman forest formula.

and :

$$\bar{C}(s) = -\frac{1}{2e^{2s}} \frac{\pi^2}{(1+\bar{m}^2)^3}\,, \tag{222}$$

so that equation (219) becomes:

$$\frac{d}{dp^2}\Pi^{(2)} = \frac{1}{2Z^2e^{2s}}\lambda^2 \frac{\pi^2}{1+\bar{m}^2}\left(\frac{1}{1+\bar{m}^2}+1\right)\,. \tag{223}$$

The right hand side of the equation (219) may be computed from the same approximation. Because of the structure equation for 4-point function, it is easy to cheek that (see [59]):

$$\frac{d}{dp^2}\Pi^{(2)} = -2\lambda^2(s)\frac{d}{dp^2}\mathcal{A}_{4,2}(p=0)\,, \tag{224}$$

where $\mathcal{A}_{4,2}(p) := \sum_{\vec{q}\in\mathbb{Z}^d} \delta_{pq_1} G^2(\vec{q})$. Once again this function can be computed using approximation (25), because the derivative with respect to p_1^2 is insensitive on the deep UV effect depending on the UV cut-off. Explicitly, we get:

$$\frac{d}{dp^2}\mathcal{A}_{4,2}(p=0) = -\frac{1}{2Z^2e^{2s}} \frac{\pi^2}{1+\bar{m}^2}\left(\frac{1}{1+\bar{m}^2}+1\right)\,, \tag{225}$$

so that equation (223) is identically verified. Then, this simple cheeking ensure at least the coherence of our approximation for the computation of convergent integral with Ward identities.

- **Mixing sector**

In the mixing sector, and following the Ward identity (185), the formula (205) is replaced by:

$$\bar{Z} = 1 - 2\lambda_{4,1}\mathcal{L}_1 - 8\lambda_{4,2}\mathcal{L}_2\,. \tag{226}$$

As for the purely melonic sector, we expect that $\bar{Z} \sim \ln(\Lambda)$ in the continuum limit. Moreover, once again, we have $\bar{Z}(s\to-\infty) = 1/Z_{-\infty}$, so that :

$$Z_{-\infty}^{-1} = 1 - 2\lambda_{4,1}^r\mathcal{A}_{4,2}(-\infty) - 8\lambda_{4,2}^r\mathcal{A}_{3,2}(-\infty)\,, \tag{227}$$

and $Z_{-\infty}\to 0$ like $1/\ln(\Lambda)$ in the continuum limit. As in the melonic sector, this allows to simplify the Ward identities. However, an additional strong simplification come from the fact that $\mathcal{A}_{3,2}(-\infty)$ is a superficially convergent integral, whose sub-divergences are canceled from renormalization. Then, we have $Z_{-\infty}^{-1} \approx -2\lambda_{4,1}^r\mathcal{A}_{4,2}(-\infty)$, meaning that $Z_{-\infty}\mathcal{A}_{3,2}\to 0$ in the continuum limit. This can be translated as an approximation for Z itself. Indeed, decomposing $\mathcal{L}_i$ as

$$\mathcal{L}_i = \mathcal{A}_{5-i,2} + \bar{Z}\bar{B}_i/Z^2, \tag{228}$$

with

$$\bar{B}_i = -\frac{\Omega_{d-i}}{(1+\bar{m}^2)^2}\,, \tag{229}$$

and imposing in the continuum limit that $Z_{-\infty}\mathcal{A}_{3,2} \to 0$, we get: $Z \approx -2Z_{-\infty}\lambda_{4,1}\mathcal{L}_1 - 8\lambda_{4,2}\bar{B}_2/Z$. Also $\mathcal{U}_i$ is decomposed as:

$$Z_{-\infty}\mathcal{U}_i = Z_{-\infty}\mathcal{A}_{5-i,3} + \frac{1}{Z}\bar{\mathcal{C}}_i\,, \quad \bar{\mathcal{C}}_i = -\frac{\Omega_{d-i}}{(1+\bar{m}^2)^3}\,. \tag{230}$$

Because $\mathcal{A}_{5-i,3}$ is a superficially convergent quantity, we expect that, up to the sub-divergences canceled from renormalization, it is insensitive on the UV cut of. Therefore, we have to impose $Z_{-\infty}\mathcal{A}_{5-i,3} \to 0$ in the continuum limit and the Ward identities (186) and (187) reduce to[14]:

$$\frac{\partial\Pi_1^{(2)}}{\partial p_1^2} = \frac{Z}{\lambda_{4,1}}\left(\Pi_{1,a}^{(3)} + \frac{1}{3}\Pi_{1,b}^{(3)}\right)\left(1 + \frac{32\lambda_{4,2}\pi}{3Z^2(1+\bar{m}^2)^2}\right) - \frac{4\lambda_{4,1}\pi}{(1+\bar{m}^2)^3}\left(\pi\lambda_{4,1} + \frac{32}{3}\lambda_{4,2}\right)\,, \tag{231}$$

$$\frac{\partial\Pi_2^{(2)}}{\partial p_1^2} = \frac{4\pi}{3Z}\frac{1}{(1+\bar{m}^2)^2}\left(12\lambda_{6,1} + \frac{2}{3}\Pi_{1,c}^{(3)}\right) - \lambda_{4,2}^2\,\frac{32}{3Z}\frac{\pi}{(1+\bar{m}^2)^3}\,. \tag{232}$$

The knowledge of these derivative is the last ingredient required for computation of the anomalous dimension. Moreover, to find non-trivial fixed point require to use *renormalized couplings* defined in definition (26). To this end, we introduce the dimensionless renormalized sums $\bar{\mathcal{I}}_{m,n}$ as:

$$\mathcal{I}_{m,n} =: Z^{1-n}e^{(m+2-2n)s}\bar{\mathcal{I}}_{m,n}\,. \tag{233}$$

Generally, we will adopt the convention that any bared quantity $\bar{x}$ is renormalized and dimensionless, in the sense that we have extracted its proper Z and e^s dependence:

$$x = Z^\alpha e^{d_x\, s}\bar{x}\,, \tag{234}$$

d_x being the *canonical dimension* of x. From these definitions, the two equations (231) and (232) admit dimensionless and renormalized versions as:

$$\bar{\Pi}_1^{(2)\prime} = \frac{1}{\bar{\lambda}_{4,1}}\left(\bar{\Pi}_{1,a}^{(3)} + \frac{1}{3}\bar{\Pi}_{1,b}^{(3)}\right)\left(1 + \frac{32\bar{\lambda}_{4,2}\pi}{3(1+\bar{m}^2)^2}\right) - \frac{4\bar{\lambda}_{4,1}\pi}{(1+\bar{m}^2)^3}\left(\pi\bar{\lambda}_{4,1} + \frac{32}{3}\bar{\lambda}_{4,2}\right)\,, \tag{235}$$

$$\bar{\Pi}_2^{(2)\prime} = \frac{4\pi}{3}\frac{1}{(1+\bar{m}^2)^2}\left(12\bar{\lambda}_{6,1} + \frac{2}{3}\bar{\Pi}_{1,c}^{(3)}\right) - \bar{\lambda}_{4,2}^2\,\frac{32}{3}\frac{\pi}{(1+\bar{m}^2)^3}\,. \tag{236}$$

Moving on the computation of the anomalous dimension, from equation (157) and definition (173), we get:

$$\dot{Z} = -\frac{d}{dp_1^2}\left[\sum_{\vec{q}}\Gamma_s^{(4)}(\vec{p},\vec{q};\vec{p},\vec{q})\,\frac{\dot{r}_s(\vec{q})}{[\Gamma_s^{(2)}(\vec{q}) + r_s(\vec{q})]^2}\right]\Bigg|_{p_1=0}\,. \tag{237}$$

Keeping only the LO terms like for the computation of β_m, we get:

$$\dot{Z} = -\Pi_1^{(2)\prime}\bar{\mathcal{I}}_{4,2} - 4\Pi_2^{(2)\prime}\bar{\mathcal{I}}_{3,2} - \Pi_1^{(2)}\bar{\mathcal{I}}'_{4,2} - 4\Pi_2^{(2)}\bar{\mathcal{I}}'_{3,2}\,. \tag{238}$$

Then, from renormalization conditions (121), using definitions (26) and (233), as well as (173); and from the flow equation (10), we deduce the following final statement:

[14] We recall that $\Omega_3 = 4\pi/3$.

Proposition 12 *In the symmetric phase and in the continuum limit, the anomalous dimension $\eta(s)$ defined in* (173) *satisfy the equation:*

$$\eta(s) = \frac{(4\bar{\lambda}_{4,1} - \Pi_1^{(2)\prime})\pi^2 + (3\bar{\lambda}_{4,2} - \Pi_2^{(2)\prime})\frac{32\pi}{3}}{(1+\bar{m}^2)^2 + (\Pi_1^{(2)\prime} - 6\bar{\lambda}_{4,1})\frac{\pi^2}{6} + (\Pi_2^{(2)\prime} - 5\bar{\lambda}_{4,2})\frac{32\pi}{15}}, \tag{239}$$

and the autonomous system for beta functions:

$$\beta_m = -(2+\eta)\bar{m}^2 - 10\,\bar{\lambda}_{4,1}\bar{\mathcal{I}}_{4,2} - 40\bar{\lambda}_{4,2}\bar{\mathcal{I}}_{3,2}\,, \tag{240}$$

$$\beta_{4,1} = -2\eta\bar{\lambda}_{4,1} - \left(2\bar{\Pi}_{1,a}^{(3)} + \frac{2}{3}\bar{\Pi}_{1,b}^{(3)}\right)\bar{\mathcal{I}}_{4,2} + 4\bar{\lambda}_{4,1}^2\bar{\mathcal{I}}_{4,3} + 16\bar{\lambda}_{4,1}\bar{\lambda}_{4,2}\bar{\mathcal{I}}_{3,3}\,, \tag{241}$$

$$\beta_{4,2} = -(1+2\eta)\bar{\lambda}_{4,2} - \left(3\bar{\lambda}_{6,1} + \frac{1}{6}\bar{\Pi}_{1,c}^{(3)}\right)\bar{\mathcal{I}}_{3,2} + 4\bar{\lambda}_{4,2}^2\bar{\mathcal{I}}_{3,3}\,, \tag{242}$$

$$\beta_{6,1} = -3\eta\bar{\lambda}_{6,1} - \left(\frac{1}{6}\bar{\Pi}_2^{(4)} + \frac{1}{4!}\bar{\Pi}_1^{(4)}\right)\bar{\mathcal{I}}_{3,2} + 12\bar{\lambda}_{4,2}\bar{\lambda}_{6,1}\bar{\mathcal{I}}_{3,3} - 8\bar{\lambda}_{4,2}^3\bar{\mathcal{I}}_{3,4}\,, \tag{243}$$

where we defined:

$$\bar{\mathcal{I}}_{m,n}(p) := \frac{1}{Z^{1-n}e^{(m+2-2n)s}}\sum_{\vec{p}\in\mathbb{Z}^{m+1}}\delta_{p,p_1}\dot{r}_s(\vec{p})\,G^n(\vec{p})\,; \qquad \bar{\mathcal{I}}'_{m,n} = \frac{\partial\bar{\mathcal{I}}_{m,n}}{\partial p_1^2}(0)\,. \tag{244}$$

All the dimensionless sums involved in this propositions may be easily computed using integral approximation. The details are given in Appendix (A), we get:

$$\bar{\mathcal{I}}_{m,n}(p) = \frac{e^{-(m+2)s}\Omega_m}{(1+\bar{m}^2)^n}\left[2e^{2s} + \eta\left(e^{2s} - \left(\frac{m}{m+2}(e^{2s}-p^2)+p^2\right)\right)\right](e^{2s}-p^2)^{m/2}\,. \tag{245}$$

Finally, from the approximation $Z \approx -2Z_{-\infty}\lambda_{4,1}\mathcal{L}_1 - 8\lambda_{4,2}\bar{B}_2/Z$ used before, and from a straightforward computation following the same steps as for the purely melonic sector, we deduce the complementary statement of corollary (5):

Corollary 6 *In the symmetric phase, and taking the continuum limit, the beta functions for ϕ^4-couplings are related to the anomalous dimension as*

$$\begin{aligned}\eta\bar{\lambda}_{4,1} = (\beta_{4,1} + 2\eta\bar{\lambda}_{4,1})\left(1 - \frac{32\pi}{3}\frac{\bar{\lambda}_{4,2}}{(1+\bar{m}^2)^2}\right) - \frac{\pi^2\bar{\lambda}_{4,1}^2}{(1+\bar{m}^2)^2}\left(\eta + \frac{2\beta_m}{1+\bar{m}^2}\right)\\ + \frac{32}{3}\frac{\pi\bar{\lambda}_{41}}{(1+\bar{m}^2)^2}\left(\beta_{4,2} + (1+2\eta)\bar{\lambda}_{4,2}\right) - \frac{32}{3}\frac{\pi\bar{\lambda}_{4,1}\bar{\lambda}_{4,2}}{(1+\bar{m}^2)^2}\left(\eta + \frac{2\beta_m}{1+\bar{m}^2}\right)\,.\end{aligned} \tag{246}$$

Once again, this relations which depends only on the choice of the regulator and on the continuum limit can be used to analyse the robustness of the fixed points obtained from flow equation (19). Like for the melonic case, we will extend the discussion about this constraint in forthcoming works.

5.3 Investigations on the phase space structure

To conclude this section, we will investigate the structure of the phase space, and the existence of non trivial fixed points. We divide these investigations into two parts. In a first time we will study the vicinity of the Gaussian fixed point, and argue in favor of an asymptotic safety scenario. In a second time, we will move on to the research of non-trivial fixed points in accordance to this scenario. Due to the complicated structure of the flow equations, we use numerical methods for this purpose. Another important simplification comes from the choice of the regulator r_s. Formally, the exact renormalization group flow described from equation (19) does not depend on the choice of the regulator. However, the approximations required to extract a practicable information from this equation generally depends on this choice. This is especially the case for crude truncations whose method is recalled in the appendix (B) to compare with the EVE method. We expect that effective vertex method discussed in this paper does not suffer for the same pathology, or at least, the dependence on the regularization becomes marginal.

Let us remark that the definition (25) is not supported with a rigorous proof. however, despite the fact that we expected the reliability on the results deduced from our method, the approximation scheme that we will use to extract information, especially for non-Gaussian fixed points is suspected to increase the dependence on the regulator. Due to this difficulty, a rigorous discussion on the reliability of our results, especially on the choice of the regulator function will be considered for a future work, and in this section we only investigate the plot of the using the Litim regulator (204). For the rest of this section, we denote by $p \equiv (\bar{m}^2, \bar{\lambda}_{4,1}, \bar{\lambda}_{4,2}, \bar{\lambda}_{6,1})$ the point in the four dimensional phase space.

5.3.1 Vicinity of the non-Gaussian fixed point

The Gaussian point $p_0 := (0, 0, 0, 0)$ is obviously a fixed point of the system (12), with critical exponents $(-2, -1, 0, 0)$, in accordance with the canonical dimension of the involved couplings. Expanding the flow equations around p_0, and keeping only the leading order contributions, we get :

$$\beta_m \approx -2\bar{m}^2 - 10\pi\left(\pi\bar{\lambda}_{4,1} + \frac{32}{3}\bar{\lambda}_{4,2}\right) \tag{247}$$

$$\beta_{4,1} \approx -4\pi\left(\pi\bar{\lambda}_{4,1} + \frac{16}{3}\bar{\lambda}_{4,2}\right)\bar{\lambda}_{4,1} \tag{248}$$

$$\beta_{4,2} \approx -\bar{\lambda}_{4,2} - 8\pi\lambda_{6,1} \tag{249}$$

$$\beta_{6,1} \approx -12\pi\left(\pi\bar{\lambda}_{4,1} + \frac{16}{3}\bar{\lambda}_{4,2}\right)\bar{\lambda}_{6,1}\,. \tag{250}$$

These equations are very reminiscent to some ones already studied in the literature [50, 57] for ϕ^6-models. Setting $\bar{\lambda}_{4,2} = \bar{\lambda}_{6,1} = 0$, we recover the well known asymptotic freedom of the quartic melonic models : $\beta_{4,1} \approx -4\pi^2\bar{\lambda}_{4,1}^2$, ensuring a well behavior in the UV for perturbative theory. Complementary, for $\bar{\lambda}_{4,1} = 0$, the expected UV behavior of the flow lines is radically different. Indeed, let us consider the flow equations in the invariant plane

$(\bar{\lambda}_{4,1}, \bar{\lambda}_{6,1})$:

$$\beta_{4,2} = -\bar{\lambda}_{4,2} - 8\pi\bar{\lambda}_{6,1} \tag{251}$$
$$\beta_{6,1} = -64\pi\bar{\lambda}_{4,2}\bar{\lambda}_{6,1}\,. \tag{252}$$

The situation is quite different from the pure marginal quartic case. In contrast to him, the sign of the beta function depend on the sign of the couplings, and this dependence drastically change the behavior of the flow lines. When the two couplings are both positive, $\bar{\lambda}_{6,1}, \bar{\lambda}_{4,2} > 0$, a region denoted as I on Figure (33)a, the beta functions are positive as well; and the two couplings decrease in the same time. Nevertheless, so far from p_0, the flow line are incoming on the origin. For the rest of the phase diagram, we have to distinguish two regions, respectively labeled II and III, such that $\beta_{4,2} < 0$ in the region II and $\beta_{4,2} > 0$ in the region III; the two regions being separated with the line $\beta_{4,2} = 0$. In the region II, $\bar{\lambda}_{4,2} < 0$ and $\bar{\lambda}_{6,1} > 0$, then, $\beta_{4,2} < 0$ and $\beta_{6,1} > 0$. As a result, any trajectory starting in this region necessarily goes ultimately far away of the Gaussian fixed point. Finally, in the region III, the situation is still different, $\beta_{4,2}$ and $\beta_{6,1}$ are both positive; and we expect that any trajectory starting in this region is getting closer to the $\bar{\lambda}_{6,1}$-axis and move away from the $\bar{\lambda}_{4,2}$-axis. To be more precise, let us consider the region I.

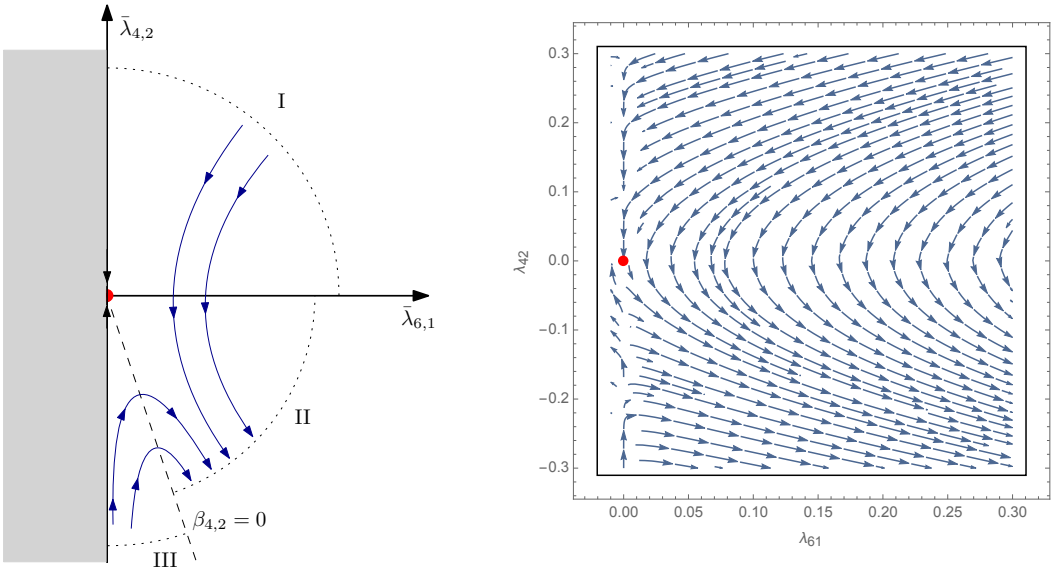


Figure 33: Phase portrait in the plan $(\bar{\lambda}_{4,1}, \bar{\lambda}_{6,1})$, in the vicinity of the Gaussian fixed point. On the left, the qualitative phase space, obtained from an analysis of the differential equations decribing the flow. On the right, the same region obtained from a numerical analysis. In both cases, the red point corresponds to the Gaussian fixed point.

It is easy to show that any trajectory starting in this region (which exclude the vertical axis) have to cross the $\bar{\lambda}_{6,1}$-axis before reaching the Gaussian fixed point, and then is ultimately repelled from it, to the infinity. Indeed, considering a trajectory whose points reach the surface of a disk of radius ϵ around p_0. Excluding the axis, the two coordinates

are both of order ϵ, and then $\beta_{4,2} = \mathcal{O}(\epsilon)$ while $\beta_{6,1} = \mathcal{O}(\epsilon^2)$. As a consequence, for any variation δs of the flow parameter, $\delta\bar{\lambda}_{4,2} \propto \epsilon\delta s$ and $\delta\bar{\lambda}_{6,1} \propto \epsilon^2\delta s$, implying that $\delta\bar{\lambda}_{4,2} \propto \delta\bar{\lambda}_{6,1}/\epsilon$. For any variation $\delta\bar{\lambda}_{6,1}$ in the direction of the $\bar{\lambda}_{4,2}$-axis, the component of the velocity vector in the direction of the horizontal axis becomes arbitrary large. The vector field then becomes more and more vertical, and finally goes through the horizontal axis. It is not so hard to show that around this point corresponds to the minimal distance with the origin of coordinates[15]. The same phenomena is expected in region III, and the qualitative behavior is pictured on Figure (33)a. Figure (33)b is a numerical integration of the same region, which confirm this expected behavior. As a consequence, it seems that the mixing sector is not asymptotically free, due to the presence of pseudo-melons. Solving this difficulty, and a well understanding of the UV completion of the theory then require to have more information about the landscape around the Gaussian fixed point, especially concerning the existence of non-Gaussian UV fixed point to which the outgoing trajectories maybe to ends.

5.3.2 Non Gaussian fixed points

To investigate the non-Gaussian fixed points, we have to solve the complete autonomous system given from proposition (12). However, the complicated structure of these equations require approximations to get solving them. Due to this difficulty, we limit our investigations on the fixed points which can be reach from a perturbative analysis. Our strategy is the following. Increasing the terms keeping in the perturbative expansion of the exact flow equations, we get a list of fixed points which progressively converge to a single one:

$$p_1 \approx (-0.55, 0.003, 0, 0)\,, \tag{253}$$

having one relevant, one irrelevant and two attractive focal directions. Because all the pseudo-melonic couplings vanish, we call this fixed point "melonic". Moreover,it matches with the fixed point already deduced in our previous work [59] in the melonic sector, and with the fixed point called $FP2$ in the Appendix (B) of this paper. This fixed point seems to be a good candidate as UV fixed point, providing an indication in favor of an asymptotic safety scenario. In this respect, the fact that only melonic interactions survives when the trajectories reach this fixed point remains an interesting feature of this theory. However, even if we discard the numerical difficulties, the existence of this fixed point seems to be compromised from the constraint (5) coming from Ward identity. Indeed, a simple numerical calculation show a large deviation at the fixed point p_1, indicating a strong violation of the Ward identity for relevant operators. At this stage, we can not expect that the problem comes from the numerical analysis. Indeed, the same difficulty occurs in the purely melonic sector, where the numerical investigation may be done easily. Moreover, as discussed above, we naively expect that the dependence on the regularization have to be improved with respect to the crude truncations. Nevertheless in both cases the difficulty is the same. A possibility is to consider that this discordance indicates the break down of the validity of the expansion around vanishing mean field, as it is the case

[15] In polar coordinates, denoting by $r(t)$ the distance from the origin, we get easily that $\dot{r}(s) = -r(s)\sin\theta(\sin\theta + 8\pi\cos\theta + 64r(s)\pi\sin\theta\cos\theta)$, vanishing for $\theta = 0$.

in the symmetric phase. More generally, we can expect that the problem come from a crude reduction of the full theory space.

6 Conclusion

In this paper we have built a version of the non-perturbative renormalization group flow including non-trivial dependence of the effective vertices on the relevant and marginal operators in a sector mixing melonics and pseudo-melonics interactions. This allows to use them to solve the renormalization group flow of the full operators in the UV, and close the infinite hierarchy equation coming from the flow equations. The resulting flow equations seems to indicate the existence of a non-trivial UV attractive fixed point including only purely melonic interactions. However, we showed that Ward identity are strongly violated at this fixed point. As a result, our unique fixed point seems to be unphysical, and the possible existence of other non-trivial fixed points far away of our investigation procedure seems to be necessary.

The importance to include the contraint coming from Ward identity in the resolution of the flow equation is not a novelty, and is well known in gauge theory, especially in QCD non-perturbative approach. Note that its not the only limitation of our results. despite the fact that we don't crudely truncate the flow, we have made some approximations whose consistency have to be supported in forthcoming works. In particular our investigations have been limited on the symmetric phase, ensuring convergence of any expansion around vanishing means field. Moreover, we have retained only the first terms in the derivative expansion of the 2-point function, and only considered the local potential approximation, i.e. potentials which can be expanded as an infinite sum of melonic and pseudo melonic local interactions. Some deviations from ultra locality could be introduce non-trivial effects having the same power counting with ultra-locals interactions with higher valences, and then have to contribute with them on the same footing. All these difficulties are not took into account in our conclusions, and will be discussed on some works in progress.

Appendices

A Useful formulas

In this section we provide the proof of the useful sums involved in the flow equations. First of all, let us write

$$\mathcal{A}_{m,n} := \sum_{\vec{p}\in\mathbb{Z}^m} G^n(\vec{p})\,. \tag{254}$$

Due to the Heaviside function $\theta(x)$, the above expression can be decomposed into two different contributions depend respectively on $\theta(e^{2s}-p^2)$ and $\theta(p^2-e^{2s})$. The first one correspond to the integration domain $p^2 \leq e^{2s}$ i.e the IR domain. On the other hand the second integration region $p^2 > e^{2s}$ correspond to UV domain. Now integrating over the

m-ball we get

$$\begin{aligned}\mathcal{A}_{m,n}(p) &= \Big(\frac{\Omega_m(e^{2s}-p^2)^{\frac{m}{2}}}{Z^n e^{2ns}(\bar{m}^2+1)^n}+\frac{m\Omega_m}{Z^n}\int_{\sqrt{e^{2s}-p^2}}^{\infty}\frac{x^{m-1}dx}{(x^2+p^2+e^{2s}\bar{m}^2)^n}\Big)\theta(e^{2s}-p^2)\\ &+ \frac{m\Omega_m}{Z^n}\int_0^{\infty}\frac{x^{m-1}dx}{(x^2+p^2+e^{2s}\bar{m}^2)^n}\theta(p^2-e^{2s}),\end{aligned}\tag{255}$$

where $\Omega_m=\frac{\pi^{\frac{m}{2}}}{\Gamma(\frac{m}{2}+1)}$ is the volume of unit m-sphere. The particular cas of integers m at $p=0$ are given by the following relations:

$$\mathcal{A}_{4,3} = \frac{\pi^2(\bar{m}^2+2)e^{-2s}}{2(\bar{m}^2+1)^2Z^3}+\frac{\pi^2e^{-2s}}{2(\bar{m}^2+1)^3Z^3}\tag{256}$$

$$\mathcal{A}_{3,n} = \frac{4\pi e^{(3-2n)s}}{3Z^n(\bar{m}^2+1)^n}+\frac{4\pi e^{(3-2n)s}}{Z^n}\int_1^{\infty}\frac{x^2dx}{(x^2+\bar{m}^2)^n}\tag{257}$$

$$\mathcal{A}_{2,n} = \frac{\pi e^{(2-2n)s}}{Z^n(\bar{m}^2+1)^n}+\frac{2\pi e^{(2-2n)s}}{Z^n}\int_1^{\infty}\frac{xdx}{(x^2+\bar{m}^2)^n}\tag{258}$$

$$\mathcal{A}_{1,n} = \frac{2e^{(1-2n)s}}{Z^n(\bar{m}^2+1)^n}+\frac{e^{(1-2n)s}}{Z^n}\int_1^{\infty}\frac{dx}{(x^2+\bar{m}^2)^n}\tag{259}$$

Now let us compute the quantity $\sum_{p\in\mathbb{Z}}(\mathcal{A}_{3,2}(p))^n$ and $\sum_{p\in\mathbb{Z}}\mathcal{A}_{3,3}(p)(\mathcal{A}_{3,2}(p))^3$ using (255):

$$\begin{aligned}\mathcal{A}_{3,2}(p) &= \Big[\frac{4\pi(e^{2s}-p^2)^{\frac{3}{2}}}{3Z^2e^{4s}(\bar{m}^2+1)^2}+\frac{4\pi}{e^{2s}Z^2}\int_1^{\infty}\frac{x(e^{2s}x^2-p^2)^{\frac{1}{2}}dx}{(x^2+\bar{m}^2)^2}\Big]\theta(e^{2s}-p^2)\\ &+ \frac{4\pi}{Z^2}\int_0^{\infty}\frac{x^2dx}{(x^2+p^2+e^{2s}\bar{m}^2)^2}\theta(p^2-e^{2s})\end{aligned}\tag{260}$$

Note that the support of the distributions $\theta(e^{2s}-p^2)$ and $\theta(p^2-e^{2s})$ denoted respectively by $\mathcal{D}_1$ and $\mathcal{D}_2$ are such that $\mathcal{D}_1\cap\mathcal{D}_2=\{e^s\}$, which is of nul measure in the Lebesgue sens. Then the integration of the functions of the form $X(p):=(a(p)\theta(e^{2s}-p^2)+b(p)\theta(p^2-e^{2s}))^n$ is therefore:

$$\int dp\,X(p)=\int_{\mathcal{D}_1}dp\,a^n(p)\theta(e^{2s}-p^2)+\int_{\mathcal{D}_2}dp\,b^n(p)\theta(p^2-e^{2s}).\tag{261}$$

To give more explanation about the above relation, let us remark that (261) can be viewed as the following sum

$$\begin{aligned}2\int dp\,X(p) &\equiv \sum_{p\in\mathcal{D}_1}a^n(p)+\sum_{p\in\mathcal{D}_2}b^n(p)+\sum_{\ell=1}^{n-1}\sum_{p\in\mathcal{D}_1\cap\mathcal{D}_2}\frac{n!}{\ell!(n-\ell)!}a^\ell(p)b^{n-\ell}(p)\\ &= \sum_{p\in\mathcal{D}_1}a^n(p)+\sum_{p\in\mathcal{D}_2}b^n(p)+\sum_{\ell=1}^{n-1}\frac{n!}{(n-\ell)!}a^\ell(e^{2s})b^{n-\ell}(e^{2s}),\end{aligned}\tag{262}$$

where in the UV limit i.e. $s\to\infty$ the quantity $a(e^{2s})\equiv e^{-s}Z^\alpha\bar{a}\to 0$ and $b(e^{2s})\equiv e^{-s}Z^\alpha\bar{b}\to 0$, $\alpha\in\mathbb{Z}$. Now applying this result to $\sum_{p\in\mathbb{Z}}(\mathcal{A}_{3;2}(p))^n$ we come to:

$$\sum_{p\in\mathbb{Z}}(\mathcal{A}_{3,2}(p))^n = 2\Big(\frac{4\pi}{Z^2}\Big)^n e^{(1-n)s}\int_1^{\infty}dy\Big(\int_0^{\infty}\frac{x^2dx}{(x^2+y^2+\bar{m}^2)^2}\Big)^n$$

$$+ \quad 2\Big(\frac{4\pi}{Z^2}\Big)^n e^{(1-n)s}\int_0^1 dy\Bigg(\frac{(1-y^2)^{\frac{3}{2}}}{3(\bar{m}^2+1)^2}+\int_1^\infty \frac{x(x^2-y^2)^{\frac{1}{2}}dx}{(x^2+\bar{m}^2)^2}\Bigg)^n. \quad (263)$$

In the same manner

$$\begin{aligned}\sum_{p\in\mathbb{Z}}\mathcal{A}_{3,3}(p)(\mathcal{A}_{3,2}(p))^n &= 2\Big(\frac{4\pi}{Z^2}\Big)^n\frac{4\pi}{Z^3}e^{-(2+n)s}\int_1^\infty dy\Bigg\{\int_0^\infty\frac{x^2dx}{(x^2+y^2+\bar{m}^2)^3}\\ &\times\quad\Bigg(\int_0^\infty\frac{x^2dx}{(x^2+y^2+\bar{m}^2)^2}\Bigg)^n\Bigg\}\\ &+\quad 2\Big(\frac{4\pi}{Z^2}\Big)^n\frac{4\pi}{Z^3}e^{-(2+n)s}\int_0^1 dy\Bigg\{\Bigg(\frac{(1-y^2)^{\frac{3}{2}}}{3(\bar{m}^2+1)^3}+\int_1^\infty\frac{x(x^2-y^2)^{\frac{1}{2}}dx}{(x^2+\bar{m}^2)^3}\Bigg)\\ &\times\quad\Bigg(\frac{(1-y^2)^{\frac{3}{2}}}{3(\bar{m}^2+1)^2}+\int_1^\infty\frac{x(x^2-y^2)^{\frac{1}{2}}dx}{(x^2+\bar{m}^2)^2}\Bigg)^n\Bigg\} \quad (264)\end{aligned}$$

As in the previous paragraph the sum (244) can be integrated in the $d-1$ ball as follows:

$$\begin{aligned}\mathcal{I}_{4,n}(p) &\equiv (d-1)\Omega_{d-1}\frac{\partial_s Z(s)(e^{2s}-p^2)+2Z(s)e^{2s}}{\Big(Z(s)(e^{2s}\bar{m}^2+e^{2s})\Big)^n}\frac{(e^{2s}-p^2)^{\frac{d-1}{2}}}{(d-1)}\\ &- (d-1)\Omega_{d-1}\frac{\partial_s Z(s)}{\Big(Z(s)(e^{2s}\bar{m}^2+e^{2s})\Big)^n}\frac{(e^{2s}-p^2)^{\frac{d+1}{2}}}{(d+1)}. \quad (265)\end{aligned}$$

In the same manner the sum (244) can be integrated in the $d-2$ ball as follows:

$$\begin{aligned}\mathcal{I}_{3,n}(p) &= (d-2)\Omega_{d-2}\frac{\partial_s Z(s)(e^{2s}-p^2)+2Z(s)e^{2s}}{\Big(Z(s)(e^{2s}\bar{m}^2+e^{2s})\Big)^n}\frac{(e^{2s}-p^2)^{\frac{d-2}{2}}}{(d-2)}\\ &- (d-2)\Omega_{d-2}\frac{\partial_s Z(s)}{\Big(Z(s)(e^{2s}\bar{m}^2+e^{2s})\Big)^n}\frac{(e^{2s}-p^2)^{\frac{d}{2}}}{(d)}. \quad (266)\end{aligned}$$

Now we come to the simple expressions of $\mathcal{I}_{4,n}(0)$ and $\mathcal{I}_{3,n}(0)$ as:

$$\mathcal{I}_{4,n}(0)=\frac{\pi^2e^{6s-2ns}}{6Z^{n-1}(\bar{m}^2+1)^n}(\eta+6),\quad \mathcal{I}_{3,n}(0)=\frac{8\pi e^{5s-2ns}}{15Z^{n-1}(\bar{m}^2+1)^n}(\eta+5) \quad (267)$$

$$\mathcal{I}'_{4,n}(0)=-\frac{\pi^2e^{(4-2n)s}}{2Z^{n-1}(\bar{m}^2+1)^n}(\eta+4),\quad \mathcal{I}'_{3,n}(0)=-\frac{4\pi e^{(3-2n)s}}{3Z^{n-1}(\bar{m}^2+1)^n}(\eta+3). \quad (268)$$

B ϕ^6-truncation for mixing -$U(1)$ TGFT

In this section the flow equation for the ϕ^4 model is derived using the usual truncation method of the Weterrich equation. For more detail concerning this process let see the references [51]-[59] and [74]-[78] in the case of matrix models.

B.1 Truncation procedure

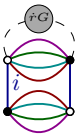
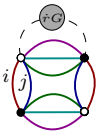
The truncation is a projection of the RG flow into a finite dimensional subspace of the infinite dimensional full theory space. In the case where $d = 5$ we write

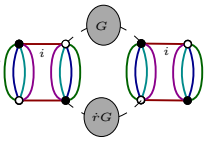
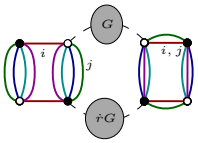
$$\begin{aligned}\Gamma_s &= Z(s)\sum_{\vec{p}} T_{\vec{p}}(\vec{p}^{\,2} + e^{2s}\bar{m}(s)^2)\bar{T}_{\vec{p}} + Z^2(s)\bar{\lambda}_{4,1}(s)V_{4,1} \\ &\quad + Z^2(s)e^s\bar{\lambda}_{4,2}(s)V_{4,2} + Z^3(s)\bar{\lambda}_{6,1}(s)V_{6,1} \end{aligned} \tag{269}$$

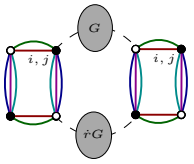
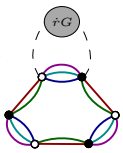
where the renormalized couplings $Z^2(s)\bar{\lambda}_{4,1}(s)$, $Z^2(s)\bar{\lambda}_{4,2}(s)e^s$ and $Z^3(s)\bar{\lambda}_{6,1}(s)$ is used and the functions $V_{4,1}$, $V_{4,2}$ and $V_{6,1}$ are the four and six-point interactions taking into account the two differents sectors: melon and pseudo-melon. The Wetterich flow equation can then be expand as:

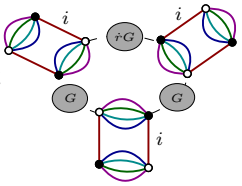
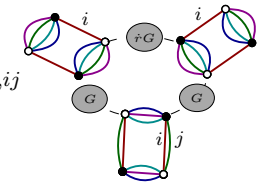
$$\begin{aligned}\partial_s\Gamma_s &= \mathrm{Tr}\,\dot{r}_s G_s^{(0)}\Big(1 - 2\lambda_{4,1}(s)V''_{4,1}G_s^{(0)} - 2\lambda_{4,2}(s)V''_{4,2}G_s^{(0)} - 3\lambda_{6,1}(s)V''_{6,1}(G_s^{(0)})^2 \\ &+ 4(\lambda_{4,1}(s)V''_{4,1}G_s^{(0)})^2 + 4(\lambda_{4,2}(s)V''_{4,2}G_s^{(0)})^2 + 4\lambda_{4,1}(s)V''_{4,1}G_s^{(0)}\lambda_{4,2}(s)V''_{4,2}G_s^{(0)} \\ &+ 6\lambda_{4,1}(s)\lambda_{6,1}(s)V''_{4,1}V''_{6,1}(G_s^{(0)})^3 + 6\lambda_{4,2}(s)\lambda_{6,1}(s)V''_{4,1}V''_{6,1}(G_s^{(0)})^3 \\ &+ 9\lambda_{6,1}^2(s)V''_{6,1}(G_s^{(0)})^4 + \cdots\Big). \end{aligned} \tag{270}$$

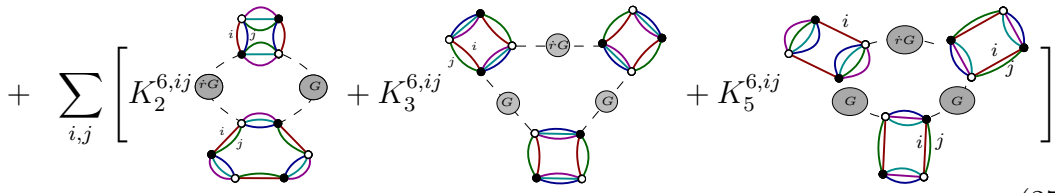
Now separate the contribution to the mass and couplings, the flow equations involves many contractions of lines which can be represented graphically by the following diagrams: (Note that we only considered the leading order contribution taking into account the melons, the pseudo-melons and the intermediate contributions reported in subsection (4.1)).

$$\partial_s\Gamma_s^{(2)} = \sum_i K_1^{2,i}$$  $$+ \sum_{i,j} K_2^{2,ij}$$  , (271)

$$\partial_s\Gamma_s^{(4)} = \sum_i K_1^{4,i}$$  $$+ \sum_{i,j} K_2^{4,ij}$$ 

$$+ \sum_{ij} K_3^{4,ij}$$  $$+ K_4^{4,ij}$$  , (272)

$$\partial_s\Gamma_s^{(6)} = \sum_i K_1^{6,i}$$  $$+ \sum_{i,j} K_4^{6,ij}$$ 



(273)

In (271) the first term correspond to the melonic contribution and the second one to the pseudo-melonic sector. Further, the first line of equation (272) contribute only to the melonic sector and the second line to the pseudo-melonic one. On the other hand the first two graphs in the first line of equation (273) contribute to the melonic sector, the first two graphs of the second line contribute to the pseudo-melonic sector and the last one to the intermediate leading order contribution. Note that only the pseudo-melonic sector will be taking into account in the flow equation of the coupling $\lambda_{6,1}(s)$. The coefficients $K_n^{m,i}$ and $K_n^{m,ij}$ are the combinatorial factors and will be given with detail.

Now using the results of the section (4), which provided the full expressions of the four and six-point functions, and because of the choice of the truncation, we have the following relations:

$$m^2(s) = \Gamma_s^{(2)}(\vec{0}), \tag{274}$$

$$Z(s) = \frac{d\Gamma_s^{(2)}(\vec{p})}{dp_1^2}\Big|_{\vec{p}=\vec{0}}, \tag{275}$$

$$\partial_s \Gamma^{(4)}_{\text{melo}}(\vec{0},\vec{0},\vec{0},\vec{0}) = 4\partial_s \lambda_{4,1}(s), \tag{276}$$

$$\partial_s \Gamma^{(4)}_{\text{pseudo–melo}}(\vec{0},\vec{0},\vec{0},\vec{0}) = 4\partial_s \lambda_{4,2}(s), \tag{277}$$

$$\partial_s \Gamma^{(6)}_{s\,,\text{pseudo-melo}}(\vec{0},\vec{0},\vec{0},\vec{0},\vec{0},\vec{0}) = 36\partial_s \lambda_{6,1}(s). \tag{278}$$

Then using the above expressions and expand in detail the relations (271), (272) and (273), we get the following flow equations in which the dimensionless parameters $\bar{m}$, $\bar{\lambda}_{4,1}$, $\bar{\lambda}_{4,2}$ and $\bar{\lambda}_{6,1}$ are used :

$$\begin{cases} \beta_m = -(2+\eta)\bar{m}^2 - 10\,\bar{\lambda}_{4,1}\bar{\mathcal{I}}_{4,2} - 40\bar{\lambda}_{4,2}\bar{\mathcal{I}}_{3,2} \\ \beta_{4,1} = -2\eta\bar{\lambda}_{4,1} + 4\bar{\lambda}_{4,1}^2\bar{\mathcal{I}}_{4,3} + 16\bar{\lambda}_{4,1}\bar{\lambda}_{4,2}\bar{\mathcal{I}}_{3,3} \\ \beta_{4,2} = -(1+2\eta)\bar{\lambda}_{4,2} - 3\bar{\lambda}_{6,1}\bar{\mathcal{I}}_{3,2} + 4\bar{\lambda}_{4,2}^2\bar{\mathcal{I}}_{3,3} \\ \beta_{6,1} = -3\eta\bar{\lambda}_{6,1} + 12\bar{\lambda}_{4,2}\bar{\lambda}_{6,1}\bar{\mathcal{I}}_{3,3} - 8\bar{\lambda}_{4,2}^3\bar{\mathcal{I}}_{3,4} \end{cases}, \tag{279}$$

In the computation of the anomalous dimension $\eta := \partial_s Z/Z$ we use the fact that

$$\partial_s Z = -2\lambda_{4,1}\frac{d}{dp_1^2}\sum_{\vec{p}_\perp}\partial_s r_s(\vec{p}_\perp)G_s^2(\vec{p}_\perp)\Big|_{\vec{p}=\vec{0}} - 8\lambda_{4,2}\frac{d}{dp_1^2}\sum_{\vec{p}_{\perp'}}\partial_s r_s(\vec{p}_{\perp'})G_s^2(\vec{p}_{\perp'})\Big|_{\vec{p}=\vec{0}}, \tag{280}$$

and now solve the linear equation of the form $\partial_s Z = L(\partial_s Z)$, which leads to

$$\eta \;=\; \frac{12\pi(\pi\bar{\lambda}_{4,1} + 8\bar{\lambda}_{4,2})}{3(\bar{m}^2+1)^2 - \pi(3\pi\bar{\lambda}_{4,1} + 32\bar{\lambda}_{4,2})}. \tag{281}$$

FP	$\bar{m}^2$	$10^4\bar{\lambda}_{4,1}$	$10^4\bar{\lambda}_{4,2}$	$10^6\bar{\lambda}_{6,1}$	η	$\theta^{(1)}$	$\theta^{(2)}$	$\theta^{(3)}$	$\theta^{(4)}$
FP_1	-0.64	0	-5.6	-4.1	0.513	12+13i	12-13i	-14+13i	-14-13i
FP_2	-0.52	28	0	0	0.553	2.5	-3	1+0.6i	1-0.6i
FP_3	1.36	0	-370	-70	-0.545	3.08	-0.41	-0.75	-1.4

Table 1: Summary of the non-Gaussian fixed points.

.

B.2 Fixed points in the UV regime

Solving numerically the system (279), we find some discrete non-Gaussian fixed points, whose relevant characteristics are summarized in the Table (1) below. Also we give the critical exponents $\theta^{(i)}$, $i = 1, 2, 3, 4$ of these different fixed points, corresponding to the opposite signs of the eigenvalues of the *stability matrix* $:\beta_{ij} := \partial_i\beta_j \, i \in \{m^2, \lambda_1, \lambda_2, \lambda_3\}$.

Let's remember that the fixed point are chosen in the domain $\{D > 0\}$ where D is the denominator of the anomalous dimension η i.e.

$$D = 3(\bar{m}^2 + 1)^2 - \pi(3\pi\bar{\lambda}_{4,1} + 32\bar{\lambda}_{4,2}). \tag{282}$$

This denominator introduces a singularity in the phase space of the flow. But further away from the GFP, i.e. the non Gaussian fixed points D may vanish, creating in the plan $(\lambda_i, \bar{m}^2)$, $i \in \{(4,1),(4,2),(6,1)\}$, a singularity hyper-surface with equation $D = 0$. The area below this line where $D < 0$ is thus disconnected from the region $D > 0$ connected to these fixed points. Then, we ignore for our purpose the fixed points in the disconnected region, for which $D < 0$. Note that we get such a singularity surface with the EVE method, get close to the one discussed here for small enough couplings. Numerically we get the fixed point given in table (1). In this table, let us remark that $FP2$ corresponds to what we obtained by taking into account only the melonic contributions which is investigated in our previous work [59]. Now let us discuss the behavior of our model along these non-Gaussian fixed points. For more explanation see [82]. Note that we have four dimensionless couplings, thus the theory space is 4-dimensional. The signs of the eigenvalues determine whether we approach or go away from the fixed point where the linearization is performed. Consider the UV limits, i.e. $k \to \infty$. According to the table (1), we have:

1. For the fixed point FP1, two pair of complex conjugate critical exponents, with reals parts have opposite signs. The fixed point is then focused attractive in the plan defined from two eigenvectors, and focused repulsive in the complementary plan, spanned from the two remaining eigenvectors.

2. For the fixed point FP2, we have one relevant direction, one irrelevant direction, and a focusing attractive behavior in the complementary plan.

3. For the fixed pint FP2, we get one revelant and four irrelevant directions.

References

[1] C. Rovelli, "Loop quantum gravity," Living Rev. Rel. **1**, 1 (1998) doi:10.12942/lrr-1998-1 [gr-qc/9710008].

[2] C. Rovelli and P. Upadhya, "Loop quantum gravity and quanta of space: A Primer," gr-qc/9806079.

[3] J. Ambjorn, Z. Burda, J. Jurkiewicz and C. F. Kristjansen, "Quantum gravity represented as dynamical triangulations," Acta Phys. Polon. B **23**, 991 (1992).

[4] J. Ambjorn, "Quantum gravity represented as dynamical triangulations," Class. Quant. Grav. **12**, 2079 (1995). doi:10.1088/0264-9381/12/9/002

[5] J. Ambjørn, A. Görlich, J. Jurkiewicz and R. Loll, "Quantum Gravity via Causal Dynamical Triangulations," doi:10.1007/978-3-642-41992-8-34 arXiv:1302.2173 [hep-th].

[6] D. Oriti, "Group field theory and simplicial quantum gravity," Class. Quant. Grav. **27**, 145017 (2010) doi:10.1088/0264-9381/27/14/145017 [arXiv:0902.3903 [gr-qc]].

[7] A. Connes and J. Lott, "Particle Models and Noncommutative Geometry (Expanded Version)," Nucl. Phys. Proc. Suppl. **18B**, 29 (1991). doi:10.1016/0920-5632(91)90120-4

[8] J. Aastrup and J. M. Grimstrup, "Intersecting connes noncommutative geometry with quantum gravity," Int. J. Mod. Phys. A **22**, 1589 (2007) doi:10.1142/S0217751X07035306 [hep-th/0601127].

[9] D. Oriti, "A Quantum field theory of simplicial geometry and the emergence of spacetime," J. Phys. Conf. Ser. **67**, 012052 (2007) doi:10.1088/1742-6596/67/1/012052 [hep-th/0612301].

[10] M. de Cesare, A. G. A. Pithis and M. Sakellariadou, "Cosmological implications of interacting Group Field Theory models: cyclic Universe and accelerated expansion," Phys. Rev. D **94**, no. 6, 064051 (2016) doi:10.1103/PhysRevD.94.064051 [arXiv:1606.00352 [gr-qc]].

[11] S. Gielen and L. Sindoni, "Quantum Cosmology from Group Field Theory Condensates: a Review," SIGMA **12**, 082 (2016) doi:10.3842/SIGMA.2016.082 [arXiv:1602.08104 [gr-qc]].

[12] S. Gielen and D. Oriti, "Cosmological perturbations from full quantum gravity," arXiv:1709.01095 [gr-qc].

[13] C. Rovelli, "Quantum gravity," Scholarpedia **3**, no. 5, 7117 (2008). doi:10.4249/scholarpedia.7117

[14] C. Rovelli, "Zakopane lectures on loop gravity," PoS QGQGS **2011**, 003 (2011) [arXiv:1102.3660 [gr-qc]].

[15] C. Rovelli, "Loop quantum gravity: the first twenty five years," Class. Quant. Grav. **28**, 153002 (2011) doi:10.1088/0264-9381/28/15/153002 [arXiv:1012.4707 [gr-qc]].

[16] D. Oriti, J. P. Ryan and J. Thurigen, "Group field theories for all loop quantum gravity," New J. Phys. **17**, no. 2, 023042 (2015) doi:10.1088/1367-2630/17/2/023042 [arXiv:1409.3150 [gr-qc]].

[17] R. Gurau, "Colored Group Field Theory," Commun. Math. Phys. **304**, 69 (2011) doi:10.1007/s00220-011-1226-9 [arXiv:0907.2582 [hep-th]].

[18] V. Rivasseau, "Constructive Tensor Field Theory," arXiv:1603.07312 [math-ph].

[19] V. Rivasseau, "Random Tensors and Quantum Gravity," arXiv:1603.07278 [math-ph].

[20] V. Rivasseau, "The Tensor Theory Space," Fortsch. Phys. **62**, 835 (2014) doi:10.1002/prop.201400057 [arXiv:1407.0284 [hep-th]].

[21] V. Rivasseau, "The Tensor Track, III," Fortsch. Phys. **62**, 81 (2014) doi:10.1002/prop.201300032 [arXiv:1311.1461 [hep-th]].

[22] V. Rivasseau, "The Tensor Track, IV," arXiv:1604.07860 [hep-th].

[23] V. Rivasseau, "The Tensor Track: an Update," arXiv:1209.5284 [hep-th].

[24] R. Gurau, "The complete 1/N expansion of colored tensor models in arbitrary dimension," Annales Henri Poincare **13**, 399 (2012) doi:10.1007/s00023-011-0118-z [arXiv:1102.5759 [gr-qc]].

[25] R. Gurau, "The 1/N expansion of colored tensor models," Annales Henri Poincare **12**, 829 (2011) doi:10.1007/s00023-011-0101-8 [arXiv:1011.2726 [gr-qc]].

[26] R. Gurau, "The 1/N Expansion of Tensor Models Beyond Perturbation Theory," Commun. Math. Phys. **330**, 973 (2014) doi:10.1007/s00220-014-1907-2 [arXiv:1304.2666 [math-ph]].

[27] D. Oriti, "Levels of spacetime emergence in quantum gravity," arXiv:1807.04875 [physics.hist-ph].

[28] L. Freidel, R. Gurau and D. Oriti, "Group field theory renormalization - the 3d case: Power counting of divergences," Phys. Rev. D **80**, 044007 (2009) doi:10.1103/PhysRevD.80.044007 [arXiv:0905.3772 [hep-th]].

[29] S. Carrozza, D. Oriti and V. Rivasseau, "Renormalization of Tensorial Group Field Theories: Abelian U(1) Models in Four Dimensions," Commun. Math. Phys. **327**, 603 (2014) doi:10.1007/s00220-014-1954-8 [arXiv:1207.6734 [hep-th]].

[30] S. Carrozza, "Tensorial methods and renormalization in Group Field Theories," doi:10.1007/978-3-319-05867-2 arXiv:1310.3736 [hep-th].

[31] S. Carrozza, D. Oriti and V. Rivasseau, "Renormalization of a SU(2) Tensorial Group Field Theory in Three Dimensions," Commun. Math. Phys. **330**, 581 (2014) doi:10.1007/s00220-014-1928-x [arXiv:1303.6772 [hep-th]].

[32] J. Ben Geloun, "Renormalizable Models in Rank $d \geq 2$ Tensorial Group Field Theory," Commun. Math. Phys. **332**, 117 (2014) doi:10.1007/s00220-014-2142-6 [arXiv:1306.1201 [hep-th]].

[33] V. Lahoche and D. Oriti, "Renormalization of a tensorial field theory on the homogeneous space SU(2)/U(1)," arXiv:1506.08393 [hep-th].

[34] V. Lahoche, D. Oriti and V. Rivasseau, "Renormalization of an Abelian Tensor Group Field Theory: Solution at Leading Order," JHEP **1504**, 095 (2015) doi:10.1007/JHEP04(2015)095 [arXiv:1501.02086 [hep-th]].

[35] J. Ben Geloun and E. R. Livine, "Some classes of renormalizable tensor models," J. Math. Phys. **54**, 082303 (2013) doi:10.1063/1.4818797 [arXiv:1207.0416 [hep-th]].

[36] D. Ousmane Samary and F. Vignes-Tourneret, "Just Renormalizable TGFT's on $U(1)^d$ with Gauge Invariance," Commun. Math. Phys. **329**, 545 (2014) doi:10.1007/s00220-014-1930-3 [arXiv:1211.2618 [hep-th]].

[37] J. Ben Geloun and D. Ousmane. Samary, "3D Tensor Field Theory: Renormalization and One-loop β-functions," Annales Henri Poincare **14**, 1599 (2013) doi:10.1007/s00023-012-0225-5 [arXiv:1201.0176 [hep-th]].

[38] J. Ben Geloun and V. Rivasseau, "A Renormalizable 4-Dimensional Tensor Field Theory," Commun. Math. Phys. **318**, 69 (2013) doi:10.1007/s00220-012-1549-1 [arXiv:1111.4997 [hep-th]].

[39] V. Lahoche, D. Oriti and V. Rivasseau, "Renormalization of an Abelian Tensor Group Field Theory: Solution at Leading Order," JHEP **1504**, 095 (2015) doi:10.1007/JHEP04(2015)095 [arXiv:1501.02086 [hep-th]].

[40] V. Rivasseau and F. Vignes-Tourneret, "Constructive tensor field theory: The T_4^4 model," arXiv:1703.06510 [math-ph].

[41] L. Lionni and V. Rivasseau, "Intermediate Field Representation for Positive Matrix and Tensor Interactions," arXiv:1609.05018 [math-ph].

[42] J. Ben Geloun and R. Toriumi, "Renormalizable Enhanced Tensor Field Theory: The quartic melonic case," arXiv:1709.05141 [hep-th].

[43] J. Ben Geloun and V. Bonzom, "Radiative corrections in the Boulatov-Ooguri tensor model: The 2-point function," Int. J. Theor. Phys. **50**, 2819 (2011) doi:10.1007/s10773-011-0782-2 [arXiv:1101.4294 [hep-th]].

[44] D. Oriti, "Disappearance and emergence of space and time in quantum gravity," Stud. Hist. Phil. Sci. B **46**, 186 (2014) doi:10.1016/j.shpsb.2013.10.006 [arXiv:1302.2849 [physics.hist-ph]].

[45] F. Markopoulou, "Conserved quantities in background independent theories," J. Phys. Conf. Ser. **67**, 012019 (2007) doi:10.1088/1742-6596/67/1/012019 [gr-qc/0703027].

[46] S. A. Wilkinson and A. D. Greentree, "Geometrogenesis under Quantum Graphity: problems with the ripening Universe," Phys. Rev. D **92**, no. 8, 084007 (2015) doi:10.1103/PhysRevD.92.084007 [arXiv:1506.07588 [gr-qc]].

[47] J. Ben Geloun, "Two and four-loop β-functions of rank 4 renormalizable tensor field theories," Class. Quant. Grav. **29**, 235011 (2012) doi:10.1088/0264-9381/29/23/235011 [arXiv:1205.5513 [hep-th]].

[48] D. Ousmane Samary, "Beta functions of $U(1)^d$ gauge invariant just renormalizable tensor models," Phys. Rev. D **88**, no. 10, 105003 (2013) doi:10.1103/PhysRevD.88.105003 [arXiv:1303.7256 [hep-th]].

[49] V. Rivasseau, "Why are tensor field theories asymptotically free?," EPL **111**, no. 6, 60011 (2015) doi:10.1209/0295-5075/111/60011 [arXiv:1507.04190 [hep-th]].

[50] S. Carrozza, "Discrete Renormalization Group for SU(2) Tensorial Group Field Theory," Ann. Inst. Henri Poincaré Comb. Phys. Interact. 2 (2015), 49-112 doi:10.4171/AIHPD/15 [arXiv:1407.4615 [hep-th]].

[51] J. B. Geloun, R. Martini and D. Oriti, "Functional Renormalisation Group analysis of Tensorial Group Field Theories on $\mathbb{R}^d$," arXiv:1601.08211 [hep-th].

[52] J. B. Geloun, R. Martini and D. Oriti, "Functional Renormalization Group analysis of a Tensorial Group Field Theory on $\mathbb{R}^3$," Europhys. Lett. **112**, no. 3, 31001 (2015) doi:10.1209/0295-5075/112/31001 [arXiv:1508.01855 [hep-th]].

[53] D. Benedetti and V. Lahoche, "Functional Renormalization Group Approach for Tensorial Group Field Theory: A Rank-6 Model with Closure Constraint," arXiv:1508.06384 [hep-th].

[54] D. Benedetti, J. Ben Geloun and D. Oriti, "Functional Renormalisation Group Approach for Tensorial Group Field Theory: a Rank-3 Model," JHEP **1503**, 084 (2015) doi:10.1007/JHEP03(2015)084 [arXiv:1411.3180 [hep-th]].

[55] J. Ben Geloun, T. A. Koslowski, D. Oriti and A. D. Pereira, "Functional Renormalization Group analysis of rank 3 tensorial group field theory: The full quartic invariant truncation," Phys. Rev. D **97**, no. 12, 126018 (2018) doi:10.1103/PhysRevD.97.126018 [arXiv:1805.01619 [hep-th]].

[56] S. Carrozza and V. Lahoche, "Asymptotic safety in three-dimensional SU(2) Group Field Theory: evidence in the local potential approximation," Class. Quant. Grav. **34**, no. 11, 115004 (2017) doi:10.1088/1361-6382/aa6d90 [arXiv:1612.02452 [hep-th]].

[57] V. Lahoche and D. Ousmane Samary, "Functional renormalization group for the U(1)-T^6_5 tensorial group field theory with closure constraint," Phys. Rev. D **95**, no. 4, 045013 (2017) doi:10.1103/PhysRevD.95.045013 [arXiv:1608.00379 [hep-th]].

[58] S. Carrozza, V. Lahoche and D. Oriti, "Renormalizable Group Field Theory beyond melonic diagrams: an example in rank four," Phys. Rev. D **96**, no. 6, 066007 (2017) doi:10.1103/PhysRevD.96.066007 [arXiv:1703.06729 [gr-qc]].

[59] V. Lahoche and D. Ousmane Samary, "Unitary symmetry constraints on tensorial group field theory renormalization group flow," arXiv:1803.09902 [hep-th].

[60] J. Ben Geloun, "Ward-Takahashi identities for the colored Boulatov model,"**44**, 415402 (2011) doi:10.1088/1751-8113/44/41/415402 [arXiv:1106.1847 [hep-th]].

[61] C. I. Pérez-Sánchez, "The full Ward-Takahashi Identity for colored tensor models," doi:10.1007/s00220-018-3103-2 arXiv:1608.08134 [math-ph].

[62] D. Ousmane Samary, "Closed equations of the two-point functions for tensorial group field theory," Class. Quant. Grav. **31**, 185005 (2014) doi:10.1088/0264-9381/31/18/185005 [arXiv:1401.2096 [hep-th]].

[63] D. Ousmane Samary, C. I. Pérez-Sánchez, F. Vignes-Tourneret and R. Wulkenhaar, "Correlation functions of a just renormalizable tensorial group field theory: the melonic approximation," Class. Quant. Grav. **32**, no. 17, 175012 (2015) doi:10.1088/0264-9381/32/17/175012 [arXiv:1411.7213 [hep-th]].

[64] V. Bonzom, "New 1/N expansions in random tensor models," JHEP **1306**, 062 (2013) doi:10.1007/JHEP06(2013)062 [arXiv:1211.1657 [hep-th]].

[65] V. Bonzom, T. Delepouve and V. Rivasseau, "Enhancing non-melonic triangulations: A tensor model mixing melonic and planar maps," Nucl. Phys. B **895**, 161 (2015) doi:10.1016/j.nuclphysb.2015.04.004 [arXiv:1502.01365 [math-ph]].

[66] V. Bonzom, R. Gurau and V. Rivasseau, "Random tensor models in the large N limit: Uncoloring the colored tensor models," Phys. Rev. D **85**, 084037 (2012) doi:10.1103/PhysRevD.85.084037 [arXiv:1202.3637 [hep-th]].

[67] S. Gielen and D. Oriti, "Quantum cosmology from quantum gravity condensates: cosmological variables and lattice-refined dynamics," New J. Phys. **16**, no. 12, 123004 (2014) doi:10.1088/1367-2630/16/12/123004 [arXiv:1407.8167 [gr-qc]].

[68] K. G. Wilson, "Renormalization group and critical phenomena. 1. Renormalization group and the Kadanoff scaling picture," Phys. Rev. B **4**, 3174 (1971). doi:10.1103/PhysRevB.4.3174

[69] K. G. Wilson, "Renormalization group and critical phenomena. 2. Phase space cell analysis of critical behavior," Phys. Rev. B **4**, 3184 (1971). doi:10.1103/PhysRevB.4.3184

[70] C. Wetterich, "Average Action and the Renormalization Group Equations," Nucl. Phys. B **352**, 529 (1991). doi:10.1016/0550-3213(91)90099-J.

[71] C. Wetterich, "Effective average action in statistical physics and quantum field theory," Int. J. Mod. Phys. A **16**, 1951 (2001) doi:10.1142/S0217751X01004591 [hep-ph/0101178].

[72] D. Schnoerr, I. Boettcher, J. M. Pawlowski and C. Wetterich, "Error estimates and specification parameters for functional renormalization," Annals Phys. **334**, 83 (2013) doi:10.1016/j.aop.2013.03.013 [arXiv:1301.4169 [cond-mat.quant-gas]].

[73] J. Berges, N. Tetradis and C. Wetterich, "Nonperturbative renormalization flow in quantum field theory and statistical physics," Phys. Rept. **363**, 223 (2002) doi:10.1016/S0370-1573(01)00098-9 [hep-ph/0005122].

[74] P. Donà, A. Eichhorn, P. Labus and R. Percacci, "Asymptotic safety in an interacting system of gravity and scalar matter," Phys. Rev. D **93**, no. 4, 044049 (2016) doi:10.1103/PhysRevD.93.044049 [arXiv:1512.01589 [gr-qc]].

[75] P. Donà, A. Eichhorn and R. Percacci, "Consistency of matter models with asymptotically safe quantum gravity," Can. J. Phys. **93**, no. 9, 988 (2015) doi:10.1139/cjp-2014-0574 [arXiv:1410.4411 [gr-qc]].

[76] A. Eichhorn, P. Labus, J. M. Pawlowski and M. Reichert, "Effective universality in quantum gravity," arXiv:1804.00012 [hep-th].

[77] A. Eichhorn and T. Koslowski, "Flowing to the continuum in discrete tensor models for quantum gravity," Ann. Inst. H. Poincare Comb. Phys. Interact. **5**, no. 2, 173 (2018) doi:10.4171/AIHPD/52 [arXiv:1701.03029 [gr-qc]].

[78] A. Eichhorn and T. Koslowski, "Continuum limit in matrix models for quantum gravity from the Functional Renormalization Group," Phys. Rev. D **88**, 084016 (2013) doi:10.1103/PhysRevD.88.084016 [arXiv:1309.1690 [gr-qc]].

[79] N. Tetradis and D. F. Litim, "Analytical solutions of exact renormalization group equations," Nucl. Phys. B **464**, 492 (1996) doi:10.1016/0550-3213(95)00642-7 [hep-th/9512073].

[80] D. F. Litim, "Optimization of the exact renormalization group," Phys. Lett. B **486**, 92 (2000) doi:10.1016/S0370-2693(00)00748-6 [hep-th/0005245].

[81] D. F. Litim, "Derivative expansion and renormalization group flows," JHEP **0111**, 059 (2001) doi:10.1088/1126-6708/2001/11/059 [hep-th/0111159].

[82] S. Nagy, "Lectures on renormalization and asymptotic safety," Annals Phys. **350**, 310 (2014) doi:10.1016/j.aop.2014.07.027 [arXiv:1211.4151 [hep-th]].

[83] J. P. Blaizot, R. Mendez-Galain and N. Wschebor, "Non perturbative renormalisation group and momentum dependence of n-point functions (I)," Phys. Rev. E **74**, 051116 (2006) doi:10.1103/PhysRevE.74.051116 [hep-th/0512317].

[84] J. P. Blaizot, R. Mendez-Galain and N. Wschebor, "Non perturbative renormalization group and momentum dependence of n-point functions. II.," Phys. Rev. E **74**, 051117 (2006) doi:10.1103/PhysRevE.74.051117 [hep-th/0603163].

[85] N. Defenu, P. Mati, I. G. Marian, I. Nandori and A. Trombettoni,"Truncation Effects in the Functional Renormalization Group Study of Spontaneous Symmetry Breaking," JHEP **1505**, 141 (2015) doi:10.1007/JHEP05(2015)141 [arXiv:1410.7024 [hep-th]].